The parametric design and robotic assembly of a timber column

Vrenken, L.C.

Award date:
2023

The parametric design and robotic assembly of a timber column

Master Thesis

L.C. Vrenken
l.c.vrenken@student.tue.nl
Student number: 0946316

Eindhoven University of Technology
Department of the Built Environment
Structural Engineering and Design

Graduation Committee:

ir. A.P.H.W. (Arjan) Habraken
Assistant Professor Innovative Structural Design TU/e

dr.ir. S.P.G. (Faas) Moonen
Associate Professor Innovative Structural Design TU/e

M. (Matthew) Ferguson
Education/Research Officer Concrete Structures & Innovative Structural Design TU/e

May 9, 2023

1 Summary

The construction industry nowadays is facing many challenges to reduce its environmental impact and to become more efficient, sustainable and safe. One way to help tackle these challenges is to use more automation. This thesis focuses specifically on timber construction. The goal of this project is to design, engineer and robotically assemble a parametric timber structure. This goal can be subdivided in two parts: the parametric design and the robotic assembly.

First of all, a design concept is made. The structure is a column that consists of beams stacked two by two on top of each other. By changing the angle at which these beams are stacked, the column form can be changed. Subsequently, an optimization is done on a asymmetric pavilion structure with three of these columns. The column forms in the pavilion are optimized by minimizing the most critical force: tension in the joints. The optimization process reduces the tension by approximately 43%, by balancing wind surface area in every direction and by dividing tension more equally over the joints. The optimization results in a pavilion structure with organic columns that meet the structural requirements, in contrary to a non-optimized structure with straight columns that uses the same amount of material.

Then, the robotic assembly process is worked out to build the optimized timber column. The robotic set up consists of two robots that work together. One robot picks and places timber beams in the correct position with a pneumatic gripper. The other robot connects the timber beams with screws. To do this, a robotic screwing end effector is developed with a pneumatic screw machine, a magnetic screw holder and a capacitive proximity sensor. The robot can pick up and place screws easily due to the magnetic screw holder. To screw, the robot moves downwards with a controlled velocity and stops when the sensor indicates that the screw is deep enough inside the timber. The robots can work safely together by using multi move, careful path planning and collision checks. The full assembly process is tested and fine tuned and the optimized column is constructed.

The end result of the project is a full size, robotically constructed, structurally optimized, parametric timber column. Furthermore, a robotic set up is developed where it is possible to automatically assemble a timber structure with screws.

Contents

List of Tables

List of Figures

2 Introduction

This section covers the problem definition, some examples from the literature research, the objective of the project and the report structure.

2.1 Problem definition and reason

The building sector faces large challenges in the upcoming years. First of all, the Netherlands has set a goal to have a fully circular economy by 2050 (Rijksoverheid, 2021). Secondly, there currently is a housing shortage in the Netherlands, which requires the building of approximately 1 million houses in the next 10 years (NOS Nieuws, 2021). These goals ask for rethinking current construction processes and a more sustainable material use. Automation is one of the methods to help us tackle the challenges, because automation can help with many currently existing issues in the construction industry. Some examples of the benefits of automation are:

- Improved productivity → Known production speed and less uncertainties.
- Improved quality → Robotic accuracy and repeatability.
- Sustainability → More design freedom to make optimized structures with less (raw) materials and construction waste.
- Mass customization → Many design options can be easily programmed and executed, without adding extra complexity.
- Improved safety → A robot can replace humans with more dangerous tasks in construction.
- Deal with skilled labor shortage → A robot can replace some of the (skilled) labor.

This project will focus on the automation of assembling a structure. As a construction material for this project timber is chosen. Timber is a material that is again more and more used in the built environment, because it is seen as a more sustainable building material than for example concrete and steel. Timber has the advantage that the CO_2 emissions are relatively low, it can easily be reused/recycled and it can be regrown.

2.2 Literature research

Automation of construction of timber structures is not entirely new. There are some projects done in this field, such as the double-story timber structure from ETH Zürich (Eversmann, Gramazio, & Kohler, 2017) and the DFAB House (Graser et al., 2020) from NCCR Digital Fabrication, which can be seen in Figure 1a and 1b respectively.

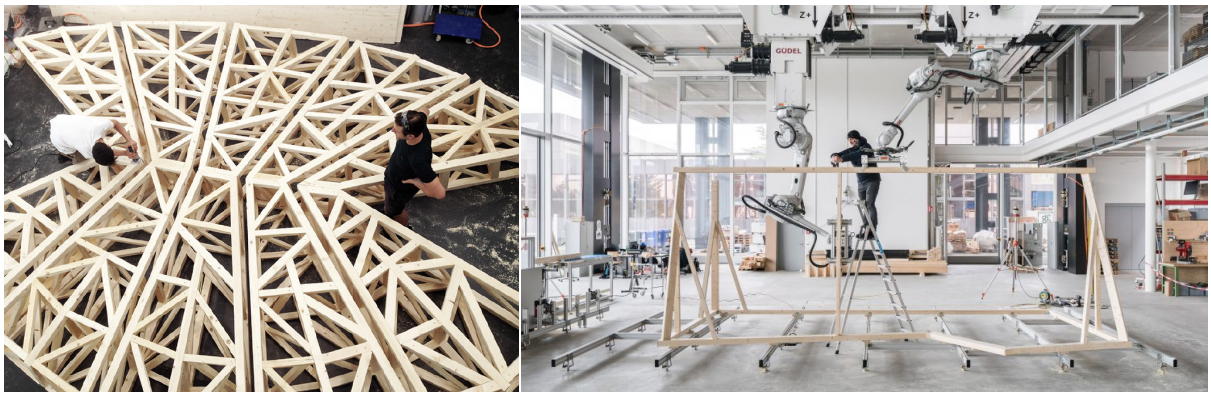

(a) Double storey timber structure (Eversmann et al., 2017)

(b) DFAB House (Graser et al., 2020)

Figure 1: Robotically assembled timber structures (manual joining)

In the double storey timber structure a robotic arm picks up a long solid spruce slat and moves it towards a saw, where it gets cut in the right length and angle. Subsequently, the robot moves the slat to the correct position, where it is fixated manually. In the DFAB house the same procedure is used, however a construction step is added where the robot milled and pre-drilled all of the required holes for the connection. The screwing is still done manually.

There are also a few projects that automated the process of actually joining the timber pieces together, for example by screwing or nailing. Two examples are the wooden re-configurable structure from the University of Southern Denmark (Kunic, Kramberger, & Naboni, 2021) and the Sequential roof (Apolinarska, Bärtschi, Furrer, Gramazio, & Kohler, 2016) from Gramazio & Kohler Research.

(a) Re-configurable structure (Kunic et al., 2021) (b) Sequential roof (Apolinarska et al., 2016)

Figure 2: Robotically assembled timber structures (automated joining)

In the re-configurable structure two collaborative robots are used, equipped with a screwdriver, wrist camera and gripper. One robotic arm first picks and places a timber beam. Then, the same robot detects with the camera where the screwing hole is, corrects the screwing position and screws in a bolt. During screwing torque and force values are monitored. In case of failure, a human can assist and take over control of the robotic arm. The second robotic arm is used to eventually disassemble the structure by detecting the bolt, unscrewing, and removing the beam. The average success rate of assembling and disassembling without human interaction was 86%.

In the sequential roof a large scale robot is equipped with a gripper, which again can move long timber slats towards a cutting table to cut the pieces in the right length. The pieces are moved towards the right location, where a nail gun attached to the robot shoots in nails to join the timber together. When placing the beams on one layer only one nail on each side is implemented. When the layer is completed, the rest of the nails are inserted.

Besides screwing and nailing also other timber joining methods are possible to automate, such as gluing and Japanese joinery. More examples from literature on these different methods are covered in section 4.1.

What can be concluded from the research that has been done in the field of automation of robotic timber construction, is that fully automated construction processes such as for example in the automotive industry are rare. In most cases manual steps are required or human intervention is necessary to correct for failures. Moreover, the projects are often done with extremely expensive and non-standard equipment, making it less accessible to experiment with. Therefore, the focus of this graduation project is to find an accessible solution to fully automate the assembly of a timber structure.

2.3 Objective

The overall goal of the graduation project is to:

Design, engineer and robotically assemble a parametric timber structure.

This main goal can be subdivided in two sub-goals, which both can be divided in several research questions, namely:

1. Design a parametric timber structure.
   (a) What type of structure can be made and what design options are possible with the available robotic set-up?
   (b) What is the structural capacity of the (robotically) screwed connection detail in the chosen column design?
   (c) How can we use parametric design for optimization in structural behaviour and robotic production?
   (d) Is the chosen pavilion structure with structurally optimized columns able to withstand the applied loads?
2. Robotically assemble the timber structure.
   (a) What timber joining methods are possible and which of these methods is the most promising to execute with the available robots?
   (b) What should the robotic screwing set-up look like and what materials, end effectors and other parts are required for this?
   (c) How should the robotic assembly procedure of the chosen column design be programmed?
   (d) Can the robotic screwing set-up be optimized further?

2.4 Report structure

The elaboration on the design can be found in section 3. First of all, the global design concept is worked out and shown in section 3.1. Then, the structural calculations are explained in section 3.2, which includes the structural scheme, loads and load combinations. Subsequently, the details of the connection, the screw locations and the other structural elements are worked out in section 3.3. The optimization process of the design is covered in section 3.4. The results and verification of the structural analysis are given in section 3.5.

The robotic assembly is covered in section 4. First, different timber joining methods are evaluated of which the most optimal method is chosen in section 4.1. Secondly, the robotic set-up including end effectors is worked out in section 4.2. In section 4.3 the assembly procedure is covered. At last, the construction of the final structure can be found in section 4.4. The research questions are covered in their relevant sections, which you can see in Table 1.

The final result of the parametrically designed an robotically constructed column is shown in section 5. The thesis ends with a discussion, conclusion and recommendation in section 6, 7 and 8 respectively.

Table 1: Research questions corresponding section

Research question	**Section**
1a	3.1
1b	3.3
1c	3.4
1d	3.5
2a	4.1
2b	4.2
2c	4.3
2d	4.4

3 Design

In this section the design of the parametric timber structure is covered. First, the global design of the structure is shown. Then, the structure is calculated, analyzed and the details are elaborated upon. Lastly, the optimization process and the final design result of the structure are explained.

3.1 Global design

This section covers research question 1a: *What type of structure can be made and what design options are possible with the available robotic set-up?* There are many structure types and designs possible, for example: column, roof structure, bus stop, pavilion, table etc. In this section all requirements, preferences and constraints of the design are evaluated and from that, a type of structure is chosen and a final design concept is made.

3.1.1 Requirements, preferences and constraints

The main requirement is that the structure can be built by the two robots available in the lab (ABB IRB 1200-5/0.9 and ABB IRB 1600-10/1.45). These robots need to be able to pick up the timber elements, place them in the correct position and join them together.

To pick and place a timber element, a gripper end effector is available, which can be seen in section 4.2.1. The gripper is mainly useful to hold (somewhat) rectangular elements. Constructing a special gripper that could hold other types of elements lays outside the scope of this project. Therefore, the requirement is set that the structure should consist only out of rectangular elements. These rectangular elements could be modified/cut off at certain positions, as long as the gripper can still clamp it sufficiently.

It is not possible to robotically cut the elements due to safety and sound issues in the lab. Therefore, the elements have to be prefabricated in the correct size and shape. Because little to no human interaction is desired, it is beneficial to have only a limited amount of different element sizes/shapes. Then, a number of elements can be easily stocked next to the robot and the robot can continue its process until the stock is empty. A requirement is set to have a maximum of 4 different elements.

To join the timber parts together, screws will be used (see section 4.1). Screwing will exert a force on the structure, so the structure should be able to handle this. All timber structures can be subdivided into the category 'stacked assembly' or 'spatial assembly'. In a stacked assembly all timber parts are stacked next to or on top of each other, so that the connections are all in one direction. In a spatial assembly the timber parts can be connected to each other in various angles to create a spatial structure. An example of both categories can be seen in Figure 3 and 4 respectively. It is chosen to create a stacked assembly, because the screwing force exerted on the structure will be easier to handle. Furthermore, stacked assemblies can consist of simple rectangular elements, while spatial assemblies generally require more complex joints (thus element modifications).

Figure 3: Stacked assembly
(Archello, 2009)

Figure 4: Spatial assembly
(Hughes, Österlund, & Larsen, 2021)

Furthermore, there are some design constraints due to the limitations of the facilities. The structure has to be built by two robotic arms which have a maximum arm reach of 0.9 m and 1.45 m respectively. Therefore, it is only possible to make a small structure, a scale model or a bigger structure which consists of multiple smaller parts that can be manually assembled together. Because the goal of the project is to automate a process which can be used in real life construction, it is chosen to build in full size and to not make a scale model.

The robotic arm which will pick and place the elements has a weight limit of 5 kg including the end effector. The weight of the gripper end effector is about 1 kg, so the elements cannot weigh more than 4 kg.

Moreover, it is set as a preference to have as little screws as possible in the structure, due to sustainability reasons. This can be achieved by limiting the internal forces in the joints.

A summarizing list of all requirements, preferences and constraints of the design can be seen in Table 2.

Table 2: Design requirements, preferences and constraints

Requirements
· Rectangular timber elements · Maximum of 4 different elements · Stacked assembly · Elements and screws must be full size (no scale model)
Preferences
· Original/innovative · As little as possible use of screws
Constraints
· The maximum reach of the available robotic arms are 0.9 m and 1.45 m. · Maximum element weight of 4 kg

3.1.2 Final design concept

Many parametric design concepts are made in Rhinoceros together with Grasshopper (GH), which can be seen in Appendix A. Because the size of the structure is a big limitation, it is chosen to design and assemble a column. A column is usually a slender structure with a relatively small foot print, so parts of the column could be constructed in full size. These parts can be manually stacked and assembled on top of each other to create the desired height.

In the chosen column concept equally sized timber beams are stacked two by two on top

of each other and connected with a vertical screw. By rotating the beams and stacking them in a different angle, various column forms can be created. It can be argued that in this case the timber is not used in the most efficient way, because the highest forces in the column are perpendicular to the grain direction. However, because of the limited arm reach of the robots and the uncertainty of the assembly process, this concept is still chosen as the most suitable. The column will be part of a pavilion structure, where multiple columns are placed underneath one Cross Laminated Timber (CLT) roof. This pavilion structure is nature-inspired as it resembles a collection of trees of which the leaves merge into one roof, see Figure 5. The design concept is shown in Figure 6.

The form of the column will be parametrically optimized, so that the strongest and therefore the most material efficient column combination is found. One of the optimized columns is then chosen to be robotically constructed.

Figure 5: Inspiration pavilion structure

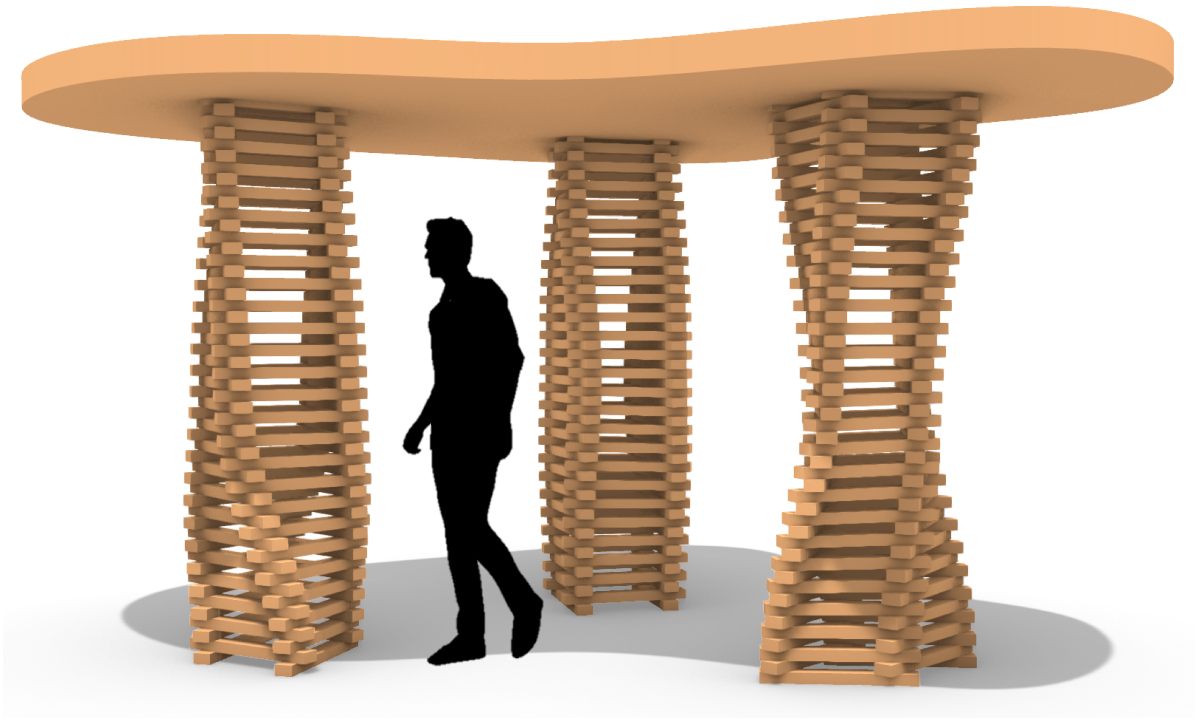

Figure 6: Final design concept

In the variation of the column form, the length of the beams always remains constant. The calculation procedure is visualized in Figure 7. Two variable coordinates of the structure are known: ($x1$,$y1$) and ($x2$,$y2$). By calculating distance X and Y, the angle (α) and the distance from the center (A) on which the beams should be stacked on top of each other to remain constant length are found.

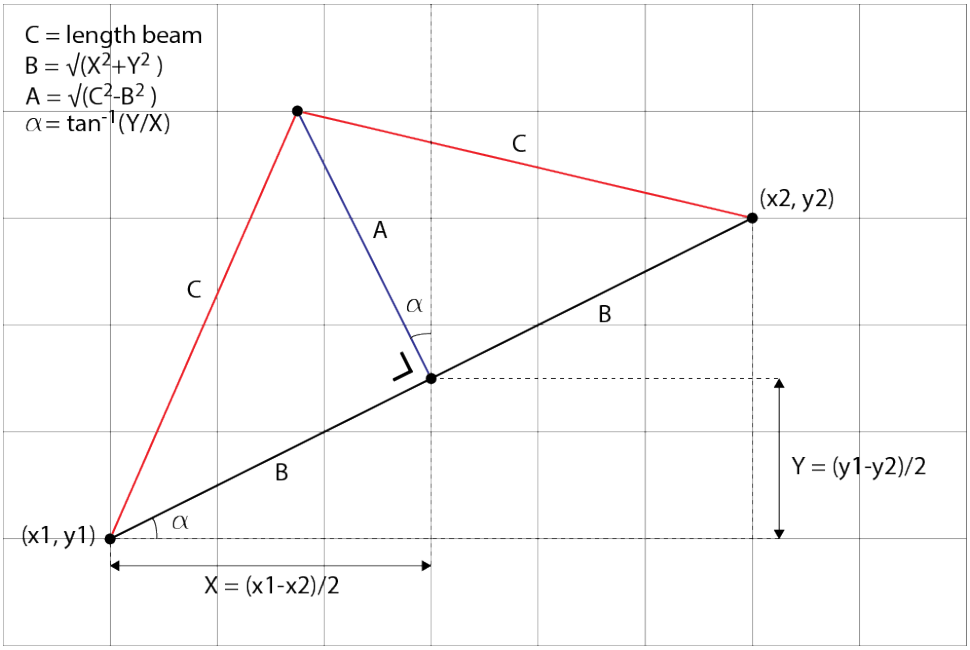

Figure 7: Calculation of beam location and orientation with constant beam length

3.2 Calculation

In this section the structural calculations on the column are done. First, the structural scheme is explained and later the applied loads and load combinations are worked out.

3.2.1 Structural scheme

The structural scheme as used for the calculations can be seen in Figure 8. The timber beams are represented by their center lines, to which the cross section of the beam and an orthotropic material (C24 timber) are assigned. The direction of the timber fiber is parallel to the direction of the center line. The material properties that are used for the calculations can be found in Appendix B.

The connections between the beams are represented by a "connection line". This line vertically connects the intersection points of two beam center lines on top of each other. The connection lines are fixed to the beam center lines, only in the middle of the connection line the rotation around the vertical (z) axis is free. This represents a joint with one screw, which can rotate around the axis of the screw. The connection line is given a cross section with the same width as the beams, which resembles the touching surface between the beams. The same orthotropic C24 material properties are used, only this time the direction of the fiber is perpendicular to the direction of the connection lines. The vertical connection lines represent the 90 degrees fiber direction of the beam, so the strength and stiffness properties in parallel and perpendicular direction are switched. Also, the connection lines have no mass, as this mass is already included in the beam center lines.

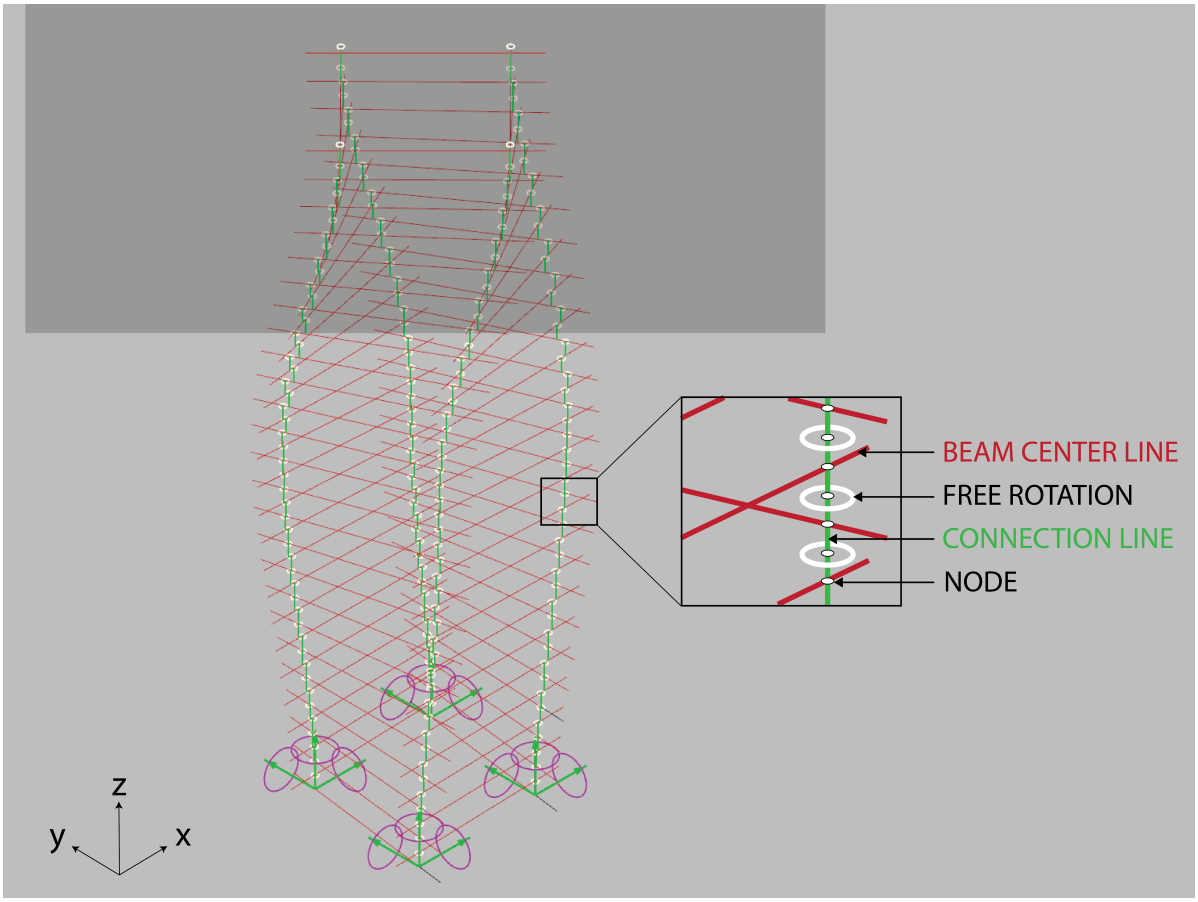

Figure 8: Structural scheme of one column

For the connection to the ground and the roof, several support conditions are evaluated, which can be seen in Figure 10. In Grasshopper Karamba the fixed connection at the bottom is created by adding a fixed support to every column corner, resembling the bottom two beams being completely fixed to the foundation. The fixed connection at the top is created by having four connections with free rotation around the vertical z axis, one at every column corner. This connection again resembles a vertical screwed connection. Together the four connections form a moment resistant (fixed) connection with the roof.

The hinged connections at the top and bottom are modeled by adding an infinitely stiff square frame with diagonals which is fixed to the timber beams. The point of intersection between the diagonals is connected to the roof/ground with a hinge (free rotation x, y, z). This can be seen in Figure 9.

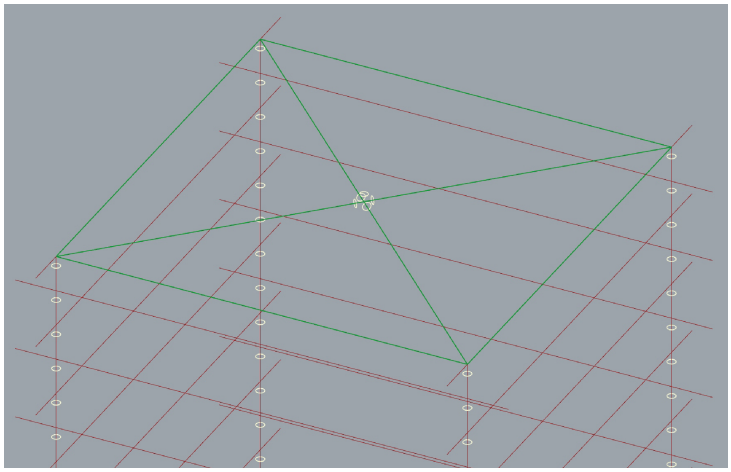

Figure 9: Hinged connection with steel frame (shown in green)

The different variants are calculated with loads according to section 3.2.2. The results of the maximum internal forces can be seen in Table 3. The variant with the lowest maximum tensile force (N_{max}) is option A, in which the bottom and top of the column are fixed and the roof is infinitely stiff. This result can be explained by the fact that the maximum moment due to a horizontal load in the column with fixed connections is approximately a factor two lower than in a structure with a hinged connection, see Figure 11. Therefore, the maximum tension in the screw connection is also about two times lower. Furthermore, a fixed connection to a weak roof has a similar effect as a hinged connection, because the roof can bend which enables the joint to rotate. Therefore a weak roof is not desirable. In conclusion, support variant A is the most optimal configuration and is therefore applied in the final structure.

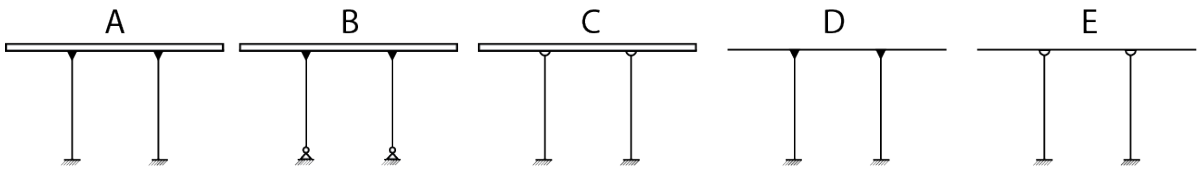

Figure 10: Variants support conditions

Table 3: Internal forces in screw joint and displacements of the top for different support conditions

	Internal forces [kN]						**Displacement [mm]**		
	N_c	N_t	$V_{z,min}$	$V_{z,max}$	$V_{y,min}$	$V_{y,max}$	**x**	**y**	**z**
A	-7.46	2.78	-0.67	0.17	-0.69	0.69	6.0	6.8	-6.2
B	-10.20	5.87	-0.71	0.17	-0.72	0.72	21.0	23.1	-6.3
C	-9.18	4.96	-0.66	0.52	-0.68	0.68	14.5	16.0	-6.5
D	-7.98	3.35	-1.86	2.26	-1.86	1.86	8.0	9.8	-44.8
E	-9.23	4.94	-0.66	0.50	-0.68	0.68	14.6	16.0	-63.9

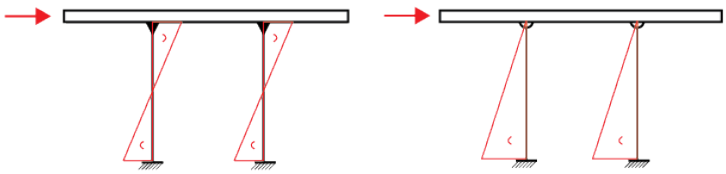

Figure 11: Moment line in columns due to horizontal load

3.2.2 Loads

The different types of loads applied to the structure are:

- Gravity
- Imposed load
- Wind load
- Snow load

The different loads are briefly elaborated in this section. More detailed explanations and calculations can be found in Appendix C.

Gravity

The gravity load is added by giving the timber beams and roof the correct characteristic density and applying a gravity load on all elements in Grasshopper. The used densities can be found in Appendix B.

Imposed load

The design is a roof structure which is not accessible other than for maintenance and the roof angle is 0°. The imposed loads on the roof are given in Table 4 (Appendix C). The distributed load is applied on a maximum area of 10 m^2. Because the roof is approximately this size, the distributed load is applied on the full roof area. The point load is applied to the centroid of the roof. The placement of the imposed loads can be seen in Figure 12.

Table 4: Imposed loads

	Symbol	**Value**	**Area**
Distributed load	q	1.0 kN/m^2	10 m^2
Point load	Q	1.5 kN	0.1*0.1 m^2

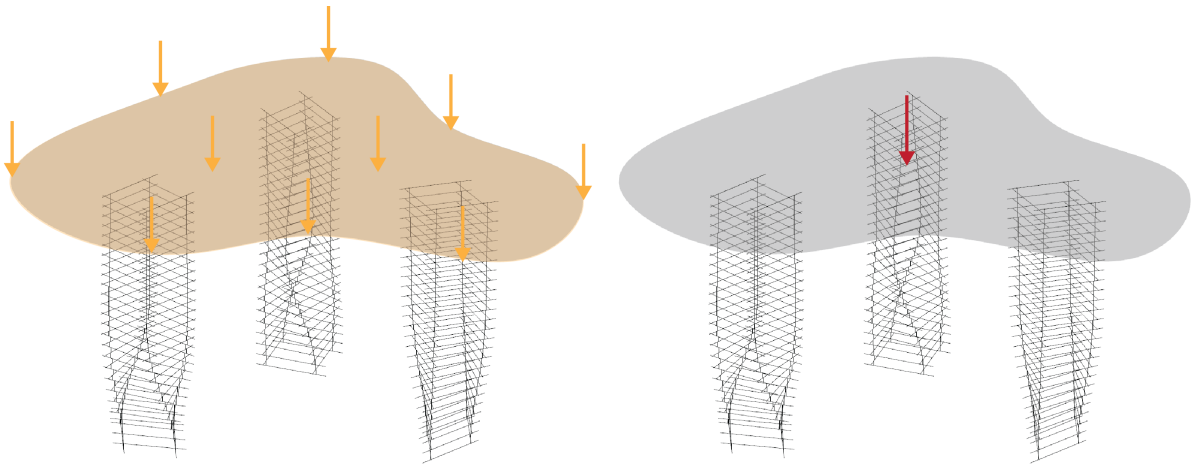

(a) Distributed load q

(b) Point load Q

Figure 12: Imposed loads

Wind load

The structure can be located in an open area in the region of Eindhoven, the Netherlands. Eindhoven lays in wind area III and the height of the structure is less than 4 m, so the extreme wind pressure (q_p) is 0.49 kN/m^2 over the full height of the structure (Appendix C).

The total wind load consists of horizontal wind pressure and suction on the column and roof edges, vertical wind pressure and suction on the roof and wind friction, which are elaborated upon below.

First of all, the horizontal wind pressure and suction are calculated. Because the column structure is open, horizontal wind pressure and suction is applied on every timber element individually. The external pressure and suction coefficients (c_{pe}) are respectively +1,0 and -0.7 (Appendix C). The external wind loads (w_e) that are applied on the column are calculated according to Equation 1. The same wind pressure and suction is applied on the edge of the roof. The length of the roof edge varies, which can be seen in Figure 14. Because no loads can be applied on the side of a mesh, the loads on the side of the roof are applied as a point load in the centroid of the roof.

$$w_e = q_p c_{pe} \tag{1}$$

Secondly, the vertical wind pressure and the suction on the roof are calculated. The roof can be categorized as an empty, free standing canopy. Because the column structure is open, it can be assumed that there are no obstructions underneath the roof. The roof is subdivided in different areas that have different pressure coefficients, which are shown in Figure 13. The coefficients can be seen in Table 5 (see Appendix C). The wind load is then again calculated according to Equation 1.

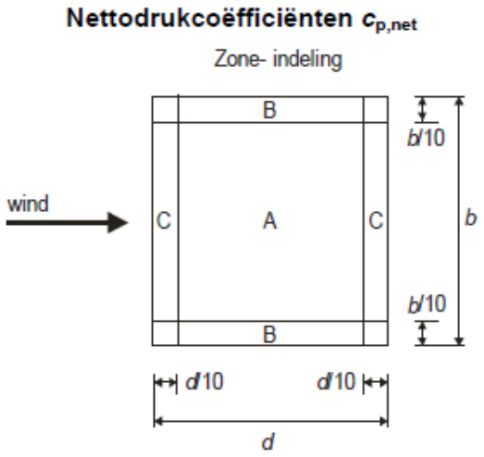

Figure 13: Roof areas (NEN-EN 1991-1-4:2005, section 7.3)

Table 5: Pressure and suction coefficients roof

$c_{p,net}$	**A**	**B**	**C**
Pressure	+0.5	+1.8	+1.1
Suction	-0.6	-1.3	-1.4

The pressure and suction areas of the free standing canopy are approximated by looking at the local tangent of the roof edge. When the angle between the roof tangent and the wind direction is less than 45°, the roof edge belongs to region B. When the angle is more than 45°, the roof edge is categorized as region C. The same procedure is done for calculating the length of the roof edges on which there is horizontal pressure and suction. As a result, the magnitude of the wind load on the roof is different in every direction. The approximation of the wind load in x direction is shown in Figure 14.

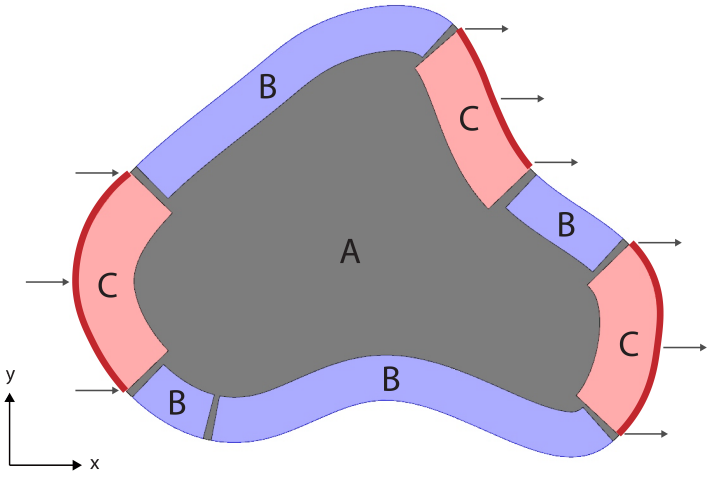

Figure 14: Wind load roof approximation (x direction)

Lastly, wind friction is calculated. Wind friction on the column can be neglected, because the area of the column parallel to the wind is equal to the area perpendicular to the wind (NEN-EN 1991-1-4:2005, section 5.3). The friction on the roof (F_{fr}) cannot be neglected and is calculated according to Equation 2. The wind friction is applied as a point load in the centroid of the roof.

$$F_{fr} = c_{fr} q_p A_{fr} = 0.23\,kN \tag{2}$$

In which:
c_{fr} = friction coefficient = 0.01 (NEN-EN 1991-1-4:2005, Table 7.10)
A_{fr} = friction area = 2 $\cdot A_{roof}$ = 22.0 m^2

The application of the different wind loads can be seen in Figure 15. The wind load is applied and checked in eight wind directions, namely: x, xy, y, $-xy$, $-x$, $-x-y$, $-y$ and $x-y$ (see Figure 16).

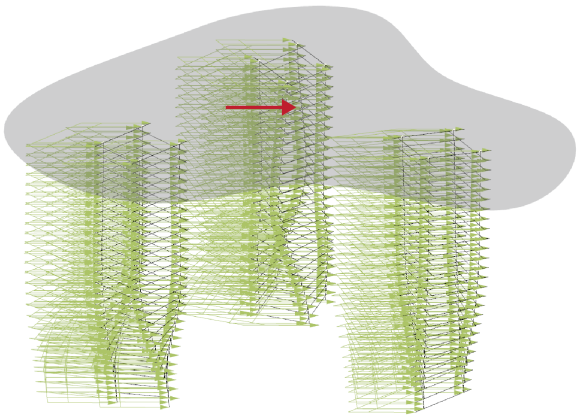

(a) Horizontal wind pressure and suction on columns and roof edges

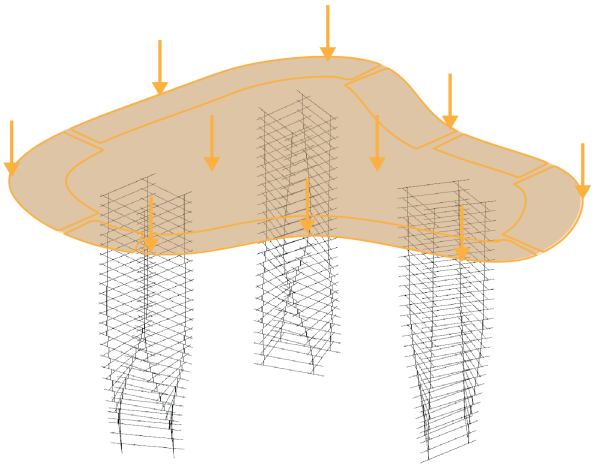

(b) Vertical wind pressure and suction roof (varies per zone)

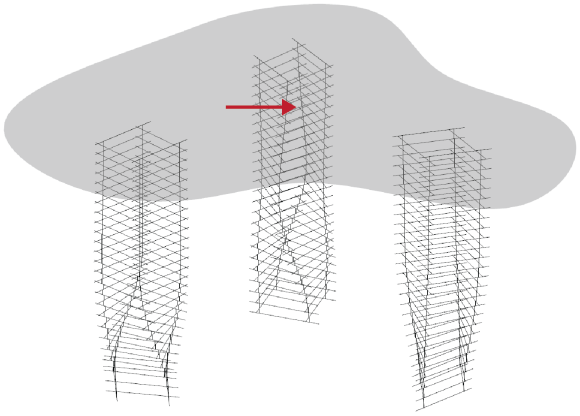

(c) Wind friction

Figure 15: Wind loads

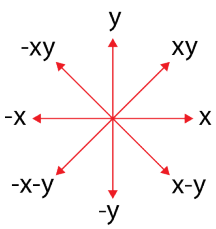

Figure 16: Wind directions

Snow load

The snow load (s) on the roof of the structure is given by Equation 3 (NEN-EN 1991-1-3:2003, section 5.2). The snow load is applied equally on the full roof area, which can be seen in Figure 17.

$$s = \mu_i c_e c_t s_k = 0.56\, kN/m^2 \tag{3}$$

In which:
μ_i = load shape coefficient = 0.8 (NEN-EN 1991-1-3:2003, Table 5.2)
c_e = exposure coefficient = 1.0
c_t = thermal coefficient = 1.0
s_k = characteristic snow load = 0.7 kN/m^2 (NEN-EN 1991-1-3:2003, section 4.1)

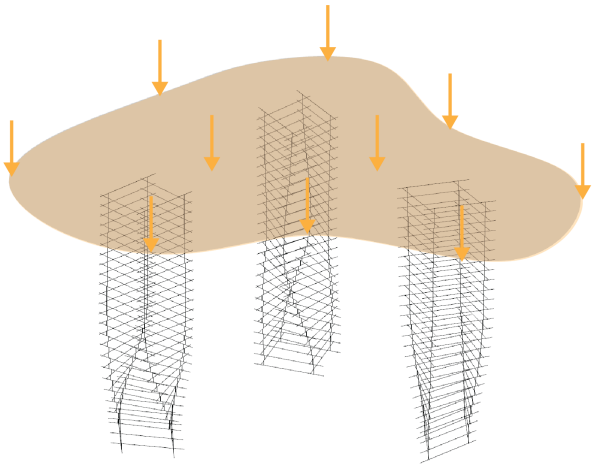

Figure 17: Snow load

3.2.3 Load combinations

The various loads are applied in different load cases (LC), namely:

- LC0 – Gravity
- LC1 – Imposed loads
  - a = Distributed load q
  - b = Point load Q
- LC2 – Wind load
  - a = Horizontal wind load + vertical wind pressure roof + wind friction
  - b = Horizontal wind load + vertical wind suction roof + wind friction
- LC3 – Snow load

The load cases are combined conform to NEN-EN 1990:2002, of which the elaboration can be found in Appendix C. The small pavilion structure is categorized in Consequence Class 1 (CC1), because there is a low consequence for loss of human life and social, economic or environmental consequences are small or negligible (NEN-EN 1990:2002, Table NB.23 – B1). The resulting load combinations of the Ultimate Limit State (ULS) and the Serviceability Limit State (SLS) can be seen in Table 6 and 7 respectively. Both the ULS and SLS load combinations including load factors are implemented in the structural model in Grasshopper Karamba. As stated before, the load combinations with wind are checked for all eight wind directions.

Table 6: Load combinations ULS

Number	Combination ULS	LC0	LC1	LC2	LC3
1	1.1*LC0 + 1.35*LC1a	1.1	1.35		
2	1.1*LC0 + 1.35*LC1b	1.1	1.35		
3	1.1*LC0 + 1.35*LC2a	1.1		1.35	
4	0.9*LC0 + 1.35*LC2b	0.9		1.35	
5	1.1*LC0 + 1.35*LC3	1.1			1.35

Table 7: Load combinations SLS

Number	Combination SLS	LC0	LC1	LC2	LC3
	Characteristic				
1	1*LC0 + 1*LC1a	1	1		
2	1*LC0 + 1*LC1b	1	1		
3	1*LC0 + 1*LC2a	1		1	
4	1*LC0 + 1*LC2b	1		1	
5	1*LC0 + 1*LC3	1			1
	Frequent				
6	1*LC0 + 0.2*LC2a	1		0.2	
7	1*LC0 + 0.2*LC2b	1		0.2	
8	1*LC0 + 0.2*LC3	1			0.2
	Quasi-permanent				
9	1*LC0	1			

3.3 Detailing

In this section the structural capacity of the joints and the placement of screws is elaborated upon, which covers research question 1b: *What is the structural capacity of the (robotically) screwed connection detail in the chosen column design?*. Subsequently, the other structural elements in the design covered. All hand calculations are done in Matlab, of which the code can be seen in Appendix K.

3.3.1 Structural capacity joints

Because the robotically assembled detail is a regular screw connection, it can be calculated according to the guidelines from the Eurocode. The screw joint is calculated for tension and shear.

Tension

In tension, the screw is checked for the pull-out strength of the threaded part, the pull-through strength of the screw head and the tension strength of the screw. The lowest value is the governing tension strength of the screw joint.

The pull-out strength ($F_{ax,k,Rk}$) is calculated according to Equation 4 (NEN-EN 1995-1-1:2005, section 8.7.2).

$$F_{ax,k,Rk} = \frac{n_{ef} f_{ax,k} d l_{ef} k_d}{1.2 cos^2(\alpha) + sin^2(\alpha)} = 1.91\,kN \tag{4}$$

In which:
n_{ef} = number of screws = 1
$f_{ax,k}$ = characteristic pull-out strength = 14 N/mm^2 (Appendix E)
d = screw diameter = 5.0 mm
l_{ef} = penetration depth of screw = 36 mm
k_d = factor for screw diameter = 0.63 (Appendix E)

α = angle between screw and direction of fiber = 90 °

The pull-through strength ($F_{ax,k,Rk}$) is calculated according to Equation 5 (NEN-EN 1995-1-1:2005, section 8.7.2).

$$F_{ax,k,Rk} = n_{ef} f_{head,k} d_h^2 (\frac{\rho_k}{\rho_a})^{0.8} = 1.63\,kN \tag{5}$$

In which:
$f_{head,k}$ = characteristic pull-through strength = 17.3 N/mm^2 (Appendix E)
d_h = screw head diameter = 9.7 mm
ρ_k = characteristic density = 350 kg/m^3 (Appendix B)
ρ_a = associated density = 350 kg/m^3

The tension strength of the screw ($F_{t,Rk}$) is calculated according to Equation 6 (NEN-EN 1995-1-1:2005, section 8.7.2).

$$F_{t,Rk} = n_{ef} f_{tens,k} = 4.90\,kN \tag{6}$$

In which:
$f_{tens,k}$ = characteristic strength screw = 4900 N (SPAX, 2017)

The lowest and thus governing tensile strength is the value of the pull-through strength of the screw head, which is 1.63 kN. That value is used in the structural checks in section 3.5.

Shear
The shear capacity of the screw is calculated according to Equation 7 (NEN-EN 1995-1-1:2005, section 8.2.2).

$$F_{v,Rk} = min \begin{cases} f_{h,1,k} t_1 d & (a) \\ f_{h,2,k} t_1 d & (b) \\ \frac{f_{h,1,k} t_1 d}{1+\beta} (\sqrt{\beta + 2\beta^2(1 + \frac{t2}{t1} + (\frac{t2}{t1})^2) + \beta^3 (\frac{t2}{t1})^2} - \beta(1 + \frac{t2}{t1})) + \frac{F_{ax,Rk}}{4} & (c) \\ 1.05 \frac{f_{h,1,k} t_1 d}{2+\beta} (\sqrt{2\beta(1+\beta) + \frac{4\beta(2+\beta) M_{y,Rk}}{f_{h,1,k} d t_1^2}} - \beta) + \frac{F_{ax,Rk}}{4} & (d) \\ 1.05 \frac{f_{h,1,k} t_2 d}{1+2\beta} (\sqrt{2\beta^2(1+\beta) + \frac{4\beta(1+2\beta) M_{y,Rk}}{f_{h,1,k} d t_2^2}} - \beta) + \frac{F_{ax,Rk}}{4} & (e) \\ 1.15 \sqrt{\frac{2\beta}{1+\beta}} \sqrt{2 M_{y,Rk} f_{h,1,k} d} + \frac{F_{ax,Rk}}{4} & (f) \end{cases} \tag{7}$$

In which:
$f_{h,i,k}$ = characteristic embedment strength = (1) 17.7 N/mm^2, (2) 17.7 N/mm^2 (Appendix E)
t_i = penetration depth = (1) 44 mm, (2) 36 mm
β = ratio embedment strengths = 1
$M_{y,Rk}$ = characteristic yield moment = 23.6e3 Nmm (Appendix E)

The lowest and thus governing value is 1.94 kN, which is the value of failure mode d (see Figure 18).

Figure 18: Failure mode screw in shear (NEN-EN 1995-1-1:2005, Figure 8.2)

3.3.2 Screw locations

First of all the screw locations must meet the Eurocode standards of the minimum distance between screws and the minimum distance to the timber edges and ends. The screw holes are not predrilled and the characteristic timber density is below 420 kg/m^3. Therefore the minimum distances (a_i) can be calculated according to Figure 19 and Equation 8 (NEN-EN 1995-1-1:2005, Table 8.2).

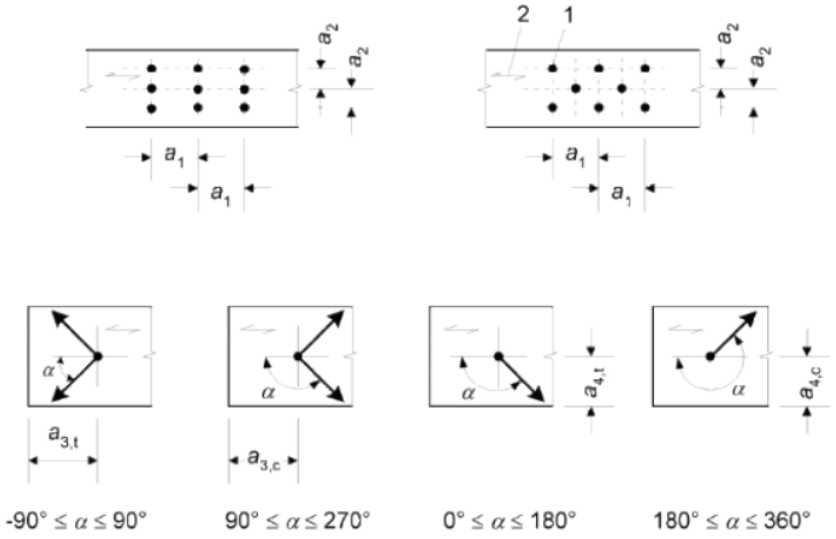

Figure 19: Minimum distances screws in timber (NEN-EN 1995-1-1:2005, Figure 8.7)

$$
\begin{aligned}
a_1 &= (5 + 7 * (\cos(\alpha))) * d = 60\,mm \\
a_2 &= 5 * d = 25\,mm \\
a_{3t} &= (10 + 5 * (\cos(\alpha))) * d = 75\,mm \\
a_{3c} &= 10 * d = 50\,mm \\
a_{4t} &= (5 + 5 * (\sin(\alpha))) * d = 25\,mm \\
a_{4c} &= 5 * d = 25\,mm
\end{aligned}
\tag{8}
$$

To make sure the minimum distances are met in the column structure, each screw is shifted half the distance a_2 from the middle line of the timber beam. Therefore every screw has at least a_2 distance between neighbouring screws. This concept is illustrated in Figure 20. The minimum timber beam width to meet the required distance to the edge is $a_{4t} + a_{4c} + a_2 = 75$ mm. Lastly, the timber beams are extended at the end with distance $a_{3t} + 0.5a_2 = 87.5$ mm, so that every end distance is at least a_{3t}. The distance $0.5a_2$ is added to this last calculation, because it is possible that the screw moved this distance towards the beam end during the screw shift.

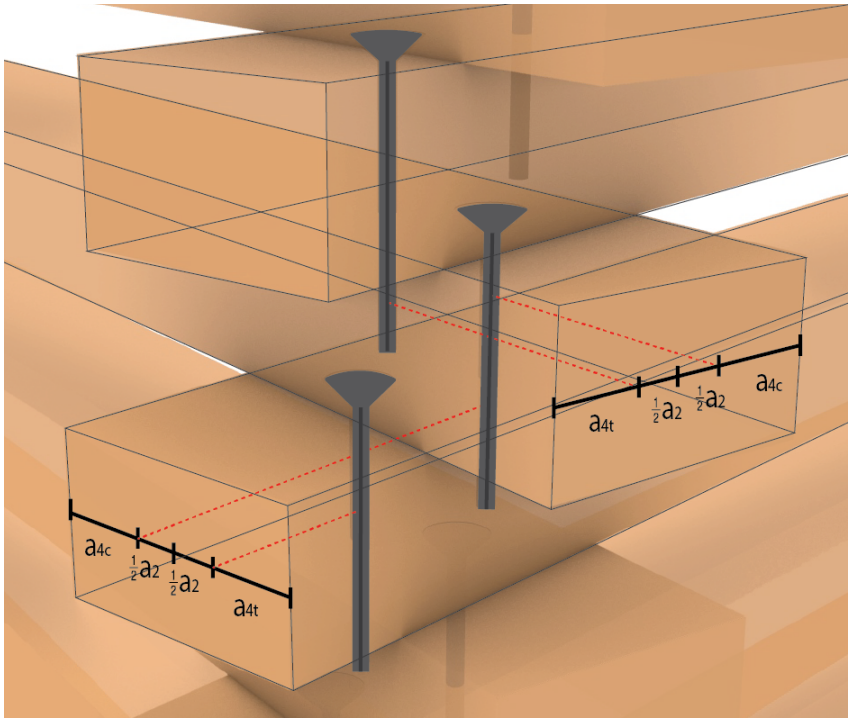

Figure 20: Screw locations

3.3.3 Roof

To limit the tension stresses in the screw joints of the column, it is desired to have a roof which properties approach an infinitely stiff roof (see section 3.2.1). Therefore, a relatively stiff 130 mm thick and 5-layered CLT panel is used, with the largest overhang in the strong direction. The configuration of the layers can be seen in Table 8.

Table 8: CLT roof layers

Layer	E_{mean} $[MPa]$	**h** $[mm]$
1	11000	30
2	370	20
3	11000	30
4	370	20
5	11000	30

The effective bending stiffness (EI_{eff}) of the CLT roof is calculated according to Equation 9 (FPInnovations, 2019).

$$EI_{eff} = \sum_{i=1}^{n} E_i b_i \frac{h_i^3}{12} + \sum_{i=1}^{n} E_i A_i z_i^2 = 5.20e12\, Nmm^2 \tag{9}$$

In which:
E_i = Young's modulus of layer
b_i, h_i, A_i = width, height and area of layer
z_i = distance middle roof to middle of layer

From this, the characteristic effective Young's modulus (E) and shear modulus (G) in both directions of the roof are derived, following rules of thumb, given in Equation 10 to 13 (FPInnovations, 2019). The design values of the stiffness that are used in the structural

calculations are calculated by dividing the characteristic stiffness by material factor γ_M of 1.25 (Glulam).

$$E_{eff} = \frac{EI_{eff}}{b\frac{h^3}{12}} = 9471\,MPa \tag{10}$$

$$E_{eff,90} = \frac{E_{eff}}{30} = 316\,MPa \tag{11}$$

$$G_0 = \frac{E_{eff}}{16} = 592\,MPa \tag{12}$$

$$G_{90} = \frac{G_0}{10} = 59\,MPa \tag{13}$$

To check whether the used CLT roof approaches an infinitely stiff roof, the tension and compression forces in the screw joint are checked for various roof stiffness values (Figure 21). The design roof stiffness is around 7577 MPa. At that point the tension and compression forces barely change when the roof becomes more stiff, which means it indeed approaches an infinitely stiff roof. Even when the CLT stiffness is corrected with a deformation factor k_{def} of 2.0 (CLT, Climate Class 3), the roof approaches an infinitely stiff roof (E = 3157 MPa).

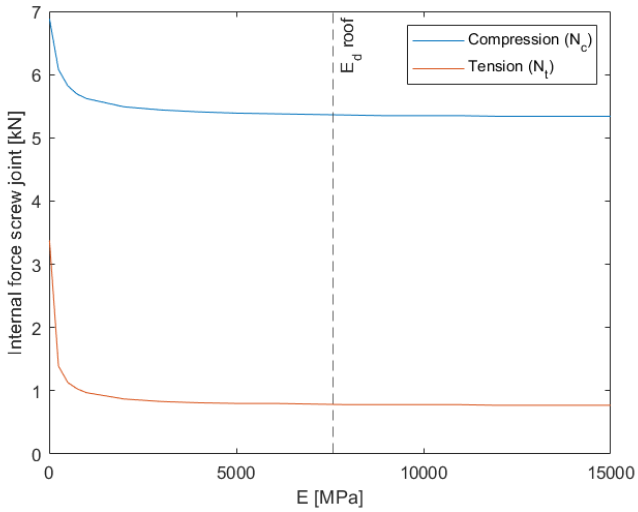

Figure 21: Maximum tension and compression force in screw joint over the roof stiffness

3.3.4 Tension cable

In the calculations on the structure it was found that the tension force in the screw joints was still too high, even after the structural optimization of the column. Several options to limit this tension force further could be:

- Using thicker or more screws in the connection
- Predrilling the screw holes
- Adding additional mass on roof or increasing the roof thickness
- Perforate the roof to limit upward wind suction
- Adding tension cable inside the column

Using thicker or more screws would mean that the timber beams should increase significantly in width, which is undesirable because it requires a lot more timber and the structure would lose its slender look. The same goes for adding mass to the roof. Predrilling and perforating the roof only has minimal effect, which proved to not be enough to limit the tension force sufficiently. Therefore, it is chosen to add tension cables inside the column, which is a relatively elegant yet effective solution and only costs minimal extra material.

The cable used is a 5x19 Fibre Core (FC), with a diameter of 8 mm and tensile strength of 1770 N/mm^2, see Figure 22.

Figure 22: Cross section tension cable
(Eurocable, n.d.)

A prestress is applied in the cable by adding a permanent initial strain load in Grasshopper Karamba. The value of the initial strain is chosen so that the maximum Unity Check of the combination between tension and shear in the screw is exactly 1.00 (see section 3.5) for the final column structure. The prestress (P) applied in one cable can be calculated according to Equation 14. The material properties of the cable can be found in Appendix B.

$$P = \varepsilon EA = 11.3\,kN \tag{14}$$

In which:
ε = initial strain = -2.65 mm/m

In theory, with enough prestress the cable would be able to take all tension out of the screw joints. However, it is chosen to add the cable as an additional system to the structure, that together with the optimization of the column reduces the value of the tension inside the screw joint to an acceptable value. This is done, so the possibilities and improvements of the structural optimization could still be shown and the prestress in the tension cable would be limited.

The creep in the timber due to the tension cable is not taken into account, as this lies outside the scope of this project. If the structure would be built, the effect of creep should be looked into, because the prestress in the tension cable would reduce over time. It would be necessary to retighten the cable at certain moments in time, to make sure the tension remains within limits.

3.4 Optimization

This section covers research question 1c: *How can we use parametric design for optimization in structural behaviour and robotic production?* What can be seen when the pavilion structure is calculated, is that the most critical force in the structure is the tension force in the screw joint. Therefore, the goal of the optimization process is to limit this tension force, so that minimal material has to be used. At first, some input parameters are optimized, such as beam dimensions. Subsequently, the form of the column is optimized.

3.4.1 Optimization of parameters

To minimize the internal tension force in the screw joint in the column, first some standard parameters are optimized, namely the beam and screw dimensions. To find the most optimal beam length, the length is varied while monitoring the effect on the tension and compression force in the joint. The result of this can be seen in Figure 23. The forces decrease with larger beam lengths, because the moment arm of the column increases. However, with larger beam

lengths the surface area of the wind also increases. Therefore, there is an optimal beam length where the internal forces are the lowest somewhere around 0.68 m. Because the C24 beams are bought in 3.6 m length, a beam size is chosen of 0.60 m. This way precisely six beams can be sawn from one full beam, so there is no waste material. The beam width is chosen as 75 mm, because this is the minimal width required to meet the minimal Eurocode distances for the screws (section 3.3.2). The beam height is 44 mm, which is based on the available C24 dimensions in the construction markets in the area.

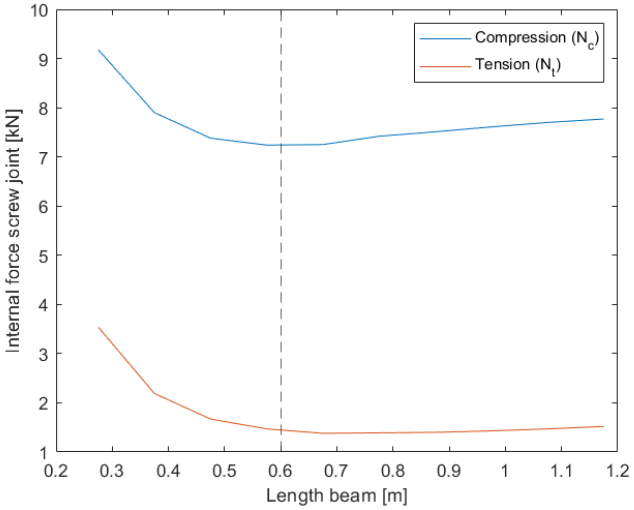

Figure 23: Maximum compression and tension force in joint per beam length

The maximum screw length is two times the beam thickness (88 mm), so the standard screw length of 80 mm is chosen. In this length screws with 5 mm diameter or more are available. The screwing machine is successfully tested for screws up until a diameter of 6 mm. When screws of 6 mm are used, the minimum timber width would increase to 90 mm. This increase in screw and beam dimensions, give an improvement on the tension and shear strength (approximately +25%), but this increases the material use significantly and it is expected that the robotic arms that will be used to construct the column will have trouble handling beams of that size. Therefore it is chosen to use screws with a diameter of 5 mm and a length of 80 mm.

Another parameter that is optimized is the so called column shift. The column shift is the shift of the bottom part of the column along the y-axis, which can be seen in Figure 24. The effect of the column shift can be seen in Figure 25. It can be concluded that the tension force can be reduced with about 8%, at a shift of -0.2 m. However, in can also be concluded that the shear force with this column shift increases with about 23%, which introduces a new problem that the shear force becomes the most critical force. Therefore, it is chosen to not shift the column.

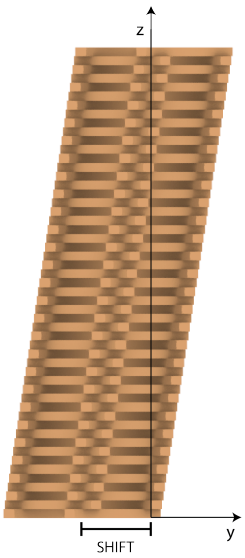

Figure 24: Column shift

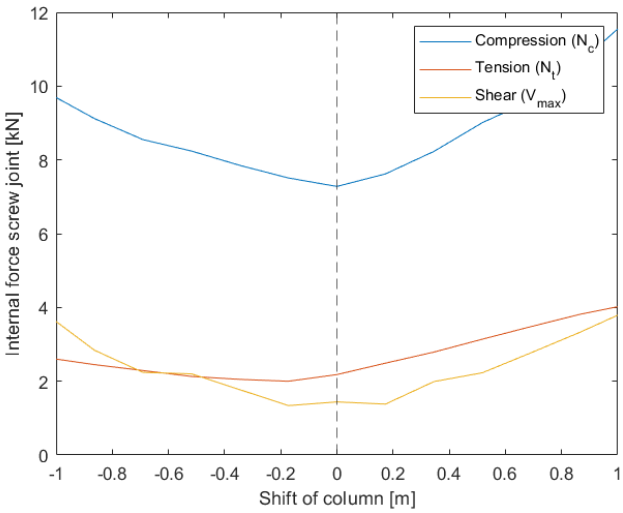

Figure 25: Maximum compression and tension force in joint per column shift

3.4.2 Form optimization

Then, the form of the column is optimized. As stated before, the goal of the optimization is to reduce the tension force in the screw joint, as this force is the most critical. The tension forces are highest during wind load with wind suction on the roof (ULS load combination 4, Table 6). Therefore, this load case is used during the optimization process. The optimization is done in the Grasshopper plugin Octopus.

The variables of the optimization can be seen in Figure 26. At the top, middle and bottom of the column two variables can be varied: rotation (R) and diameter in one direction (D), which leads to six variables per column.

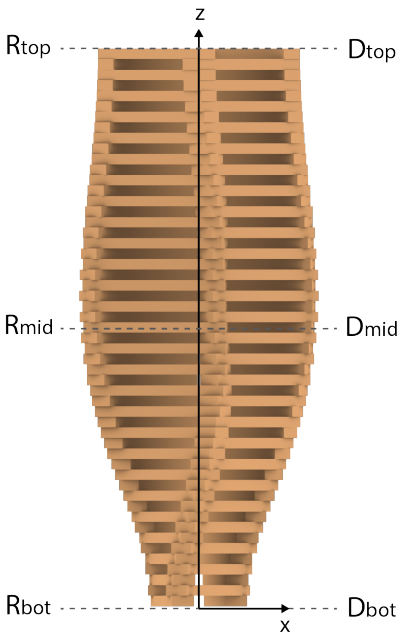

Figure 26: Optimization variables

The form optimization process is done in three steps with increasing complexity, namely:

1. **Optimization of one column in one direction**
   The first step is done to be able to clearly see the effects of what the optimization process does and how the form of the column adapts to a load.

2. **Optimization of symmetrical structure**
   This step is done to see if the optimization process works for a structure with multiple columns and more complex load cases. The goal is to verify the optimization process and to see whether the optimized result indeed performs better than a non-optimized result for all ULS load combinations (thus not only in one direction).

3. **Optimization of asymmetrical structure**
   The last step is done to see if the optimization in an asymmetric structure with asymmetric loading leads to more room for improvement and more interesting column forms. Therefore, the optimization is done on the final design concept: an organic, non symmetrical pavilion.

The structural calculations and results from the three optimization steps are covered subsequently in this section. In every step, the optimized result is compared to a structure with straight columns positioned in two different ways: 0° and 45° rotated (see Figure 27).

(a) 0° (b) 45°

Figure 27: Straight column orientation

Step 1: Optimization of one column in one direction

As a first step in the optimization, a single column is optimized for a wind force in only one direction ($x/-x$). The used support condition can be seen in Figure 28. By adding a roller support underneath the roof, this support condition approaches the situation where the column is put inside a structure with multiple columns. The used load cases for optimization can be seen in Table 9. In this step only the horizontal wind on the column is yet taken into account. The wind friction and suction on the roof are left out.

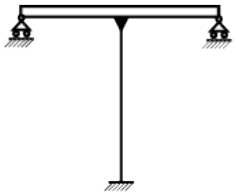

Figure 28: Support condition optimization single column

Table 9: Optimization load combinations single column

Number	Combination	Comment
1.1	0.9*LC0 + 1.35*LC2(x)	Gravity + Wind x (only horizontal load on column)
1.2	0.9*LC0 + 1.35*LC2(-x)	Gravity + Wind -x (only horizontal load on column)

The result of the optimization can be seen in Figure 29. The wind surface area of the single column for every wind direction can be seen in Table 10. The reaction forces at the support on every column corner (1-4) for the optimized column (Opt) and the straight columns (0° and 45°) can be seen in Table 11. Furthermore, the normal forces in the screw joint for every column form is shown in Figure 30.

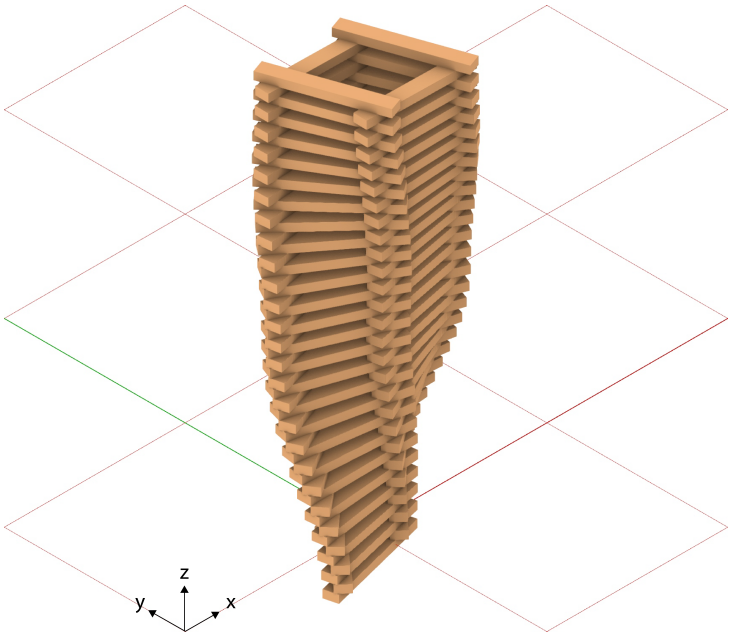

Figure 29: Result optimization single column

Table 10: Comparison wind surface area columns single column

	Wind surface area $[m^2]$				
	x	**xy**	**y**	**-xy**	**Total**
0	1.32	1.90	1.37	1.90	6.50
45	1.90	1.32	1.90	1.37	6.50
Optimized	1.02	1.76	2.32	1.74	6.84

Table 11: Reaction forces optimization single column (Load Combination 1.1)

	Reaction force [kN]												
	1			**2**			**3**			**4**			**Total**
	x	**y**	**z**	**x**	**y**	**z**	**x**	**y**	**z**	**x**	**y**	**z**	**x**
0	-0.39	0.00	1.75	-0.39	0.00	1.75	-0.38	0.00	-0.84	-0.38	0.00	-0.84	-1.54
45	-0.54	0.01	0.50	-0.53	0.00	2.96	-0.54	0.00	-2.10	-0.53	-0.01	0.43	-2.14
Opt	-0.30	-0.04	1.08	-0.31	0.04	-0.49	-0.28	0.01	1.58	-0.26	-0.01	-0.50	-1.14

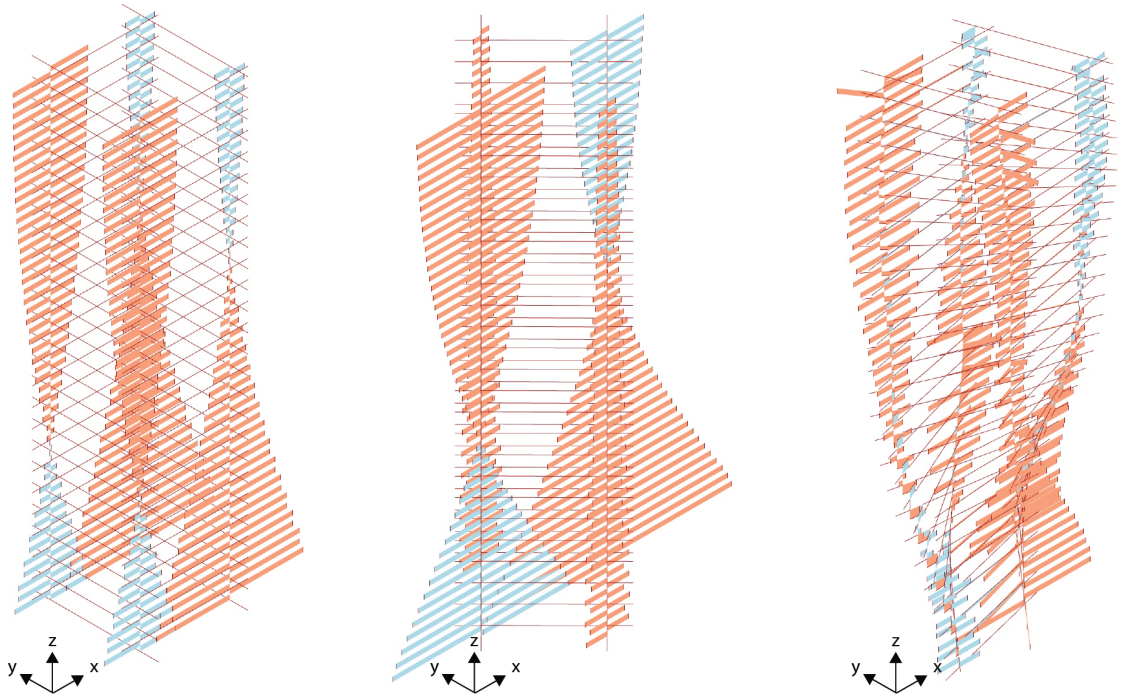

(a) 0 (b) 45 (c) Opt

Figure 30: Comparison internal tension (blue) and compression (red) in screw joint (Load Combination 1.1)

From the resulting form, reaction forces and internal forces the following can be concluded:

- The wind area of the column in the x direction is reduced (-25%) compared to the 0° straight column, which means that also the maximum wind load is reduced with this amount. This is supported by the total reaction force in the x direction in Table 11 (highlighted in blue), which absolute value is indeed 25% less for the optimized column than for the 0° straight column.
- The bottom and top rotate so that the tension force is divided over more than one column corner (and thus more than one screw). This is supported by looking at the maximum

vertical tensile reaction forces in Table 11 (highlighted in red) and the distribution of the internal forces in Figure 30. In the 45° straight column, all tension is taken by one column corner, which results in a high peak value. In the 0° straight column and the optimized column, the tension is divided over two corners, so the maximum value is significantly lower.

Step 2: Optimization of symmetrical structure

In the second step of the optimization process, a symmetric structure is optimized and analyzed. The loads on the symmetric structure are slightly modified compared to the asymmetric structure, which can be seen in Appendix D.

The original column in this structure is mirrored in the xz-plane, the yz-plane and in a vertical line in the middle of the structure, so in total there are four of the same columns underneath a square roof (see Figure 31). The load combinations used for the optimization can be seen in Table 12. In this optimization also the wind friction and wind suction on the roof are included. The wind is only applied in x, xy and y direction, because the other wind directions give the same results due to symmetry.

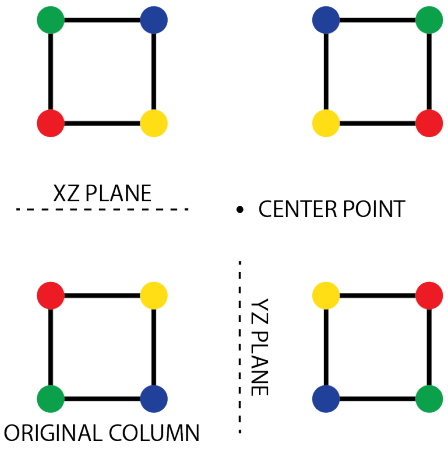

Figure 31: Mirror planes symmetric structure

Table 12: Optimization load combinations symmetric structure

Number	Combination	Comment
2.1	0.9*LC0 + 1.35*LC2b(x)	Gravity + Wind x
2.2	0.9*LC0 + 1.35*LC2b(xy)	Gravity + Wind xy
2.3	0.9*LC0 + 1.35*LC2b(y)	Gravity + Wind y

The optimized result of the symmetric structure can be seen in Figure 32. The maximum internal forces in the screw joint of the full structure in the ULS are then compared with the straight columns, which can be seen in Table 13. The wind surface area for every direction and reaction forces are also analyzed and can be seen in Appendix F.

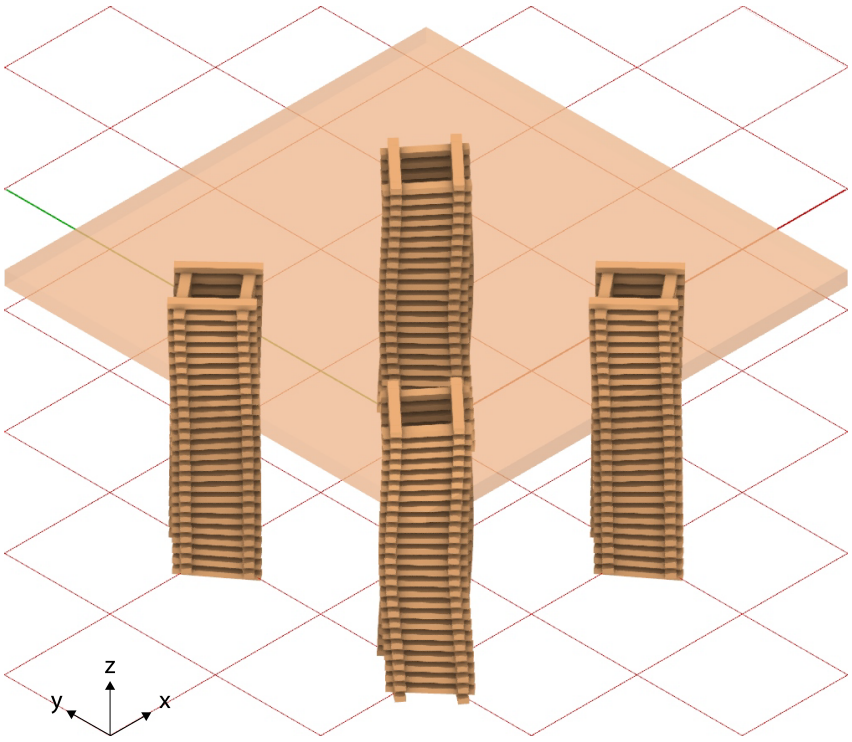

Figure 32: Result optimization symmetric structure

Table 13: Internal forces in screw joint for all ULS load cases

	N_c $[kN]$	N_t $[kN]$	$V_{z,min}$ $[kN]$	$V_{z,max}$ $[kN]$	$V_{y,min}$ $[kN]$	$V_{y,max}$ $[kN]$	M_t $[kNm]$	M_y $[kNm]$	M_z $[kNm]$
0	-6.29	1.13	-0.43	0.43	-0.45	0.45	0.00	0.02	0.04
45	-8.31	1.12	-0.59	0.58	-0.63	0.63	0.00	0.03	0.04
Opt	-8.31	1.08	-1.10	1.31	0.67	0.67	0.00	0.04	0.03

From these results the following conclusions can be drawn:

- The maximum tension force in the screw joint is lowest in the optimized structure. Thus, the optimization process with the used optimization load combinations (Table 12) indeed results in less tension in the joint in the ULS. This means that the optimization process works for structures with more columns and more complex load combinations.
- The optimal shape is almost straight. This is due to the fact that there are only symmetrical load cases on a symmetric structure. When the column changes in shape, it becomes more optimal in one direction, but less optimal in the other direction. Because the columns are mirrored, the improvement of changing the form of one column is cancelled out by the mirrored columns. The fact that the result is almost straight verifies the optimization procedure.
- The column itself is not 100% symmetrical, because beams are stacked two by two and one side has 25 beam layers and the other side has 26 beam layers. Therefore, the optimal shape is slightly asymmetric and there is some optimization possible. This minor asymmetry leads to the fact that the tension force can be reduced slightly (-4%).
- The shear forces seem to increase in the optimized columns. The internal shear is not yet governing, but should be closely watched.

Step 3: Optimization of asymmetrical structure

In the last step of the optimization process the final design concept is optimized. In this asymmetric structure, the roof has an organic form and three columns are randomly positioned underneath this roof. Each column has six variables, so each column generates its uniquely optimized form.

The load cases for the optimization can be seen in Table 14. Because the structure is not symmetrical in any direction, all eight wind directions are taken into account. Again, in every optimization load case there is wind suction on the roof, as this results in the highest tension in the screws.

Table 14: Optimization load combinations asymmetric structure

Number	Combination	Comment
3.1	0.9*LC0 + 1.35*LC2b(x)	Gravity + Wind x
3.2	0.9*LC0 + 1.35*LC2b(xy)	Gravity + Wind xy
3.3	0.9*LC0 + 1.35*LC2b(y)	Gravity + Wind y
3.4	0.9*LC0 + 1.35*LC2b(-xy)	Gravity + Wind -xy
3.5	0.9*LC0 + 1.35*LC2b(-x)	Gravity + Wind -x
3.6	0.9*LC0 + 1.35*LC2b(-x-y)	Gravity + Wind -x-y
3.7	0.9*LC0 + 1.35*LC2b(-y)	Gravity + Wind -y
3.8	0.9*LC0 + 1.35*LC2b(x-y)	Gravity + Wind x-y

The final result of the asymmetric optimization can be seen in Figure 33.

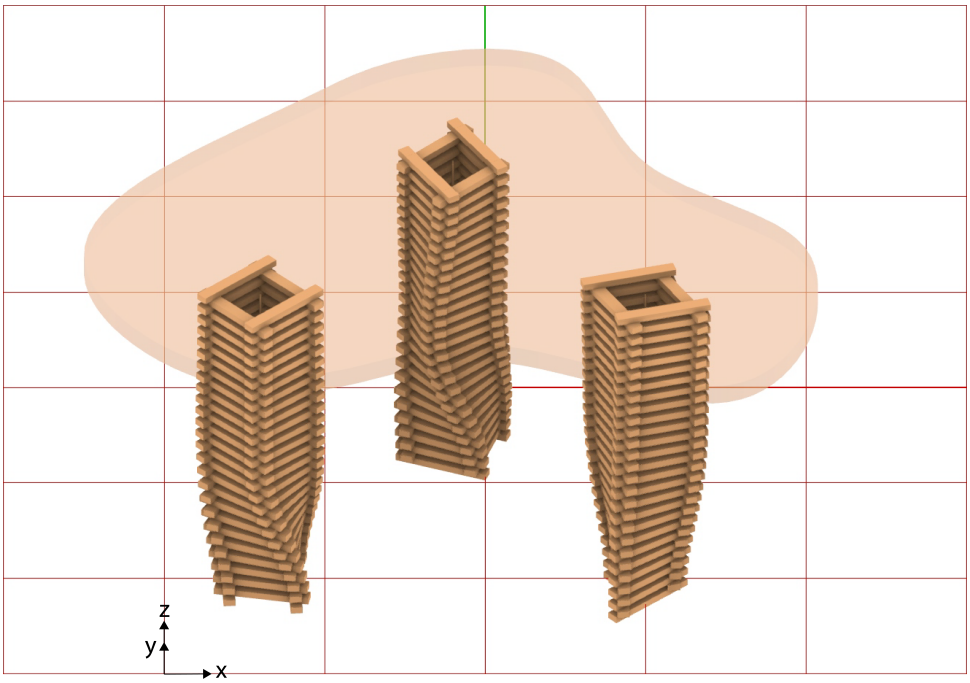

Figure 33: Final result asymmetric optimization

First, the wind area of the three asymmetric columns together is calculated for every wind direction, which can be seen in Figure 15. As can be seen is that the maximum wind area (highlighted in red) is less in the optimized structure, than for the structure with straight columns. The wind area of the optimized structure is divided more equally over all wind directions and thus has a lower peak value.

Table 15: Comparison wind surface area columns asymmetric structure

	Wind surface area $[m^2]$				
	x	**xy**	**y**	**-xy**	**Total**
0	4.12	5.71	3.96	5.71	19.50
45	5.71	3.96	5.71	4.12	19.50
Optimized	5.60	4.78	5.17	4.99	20.53

The reaction forces in the asymmetric structure per column (C1, C2 & C3) are given in Table 16. It can be seen that the total horizontal reaction force (highlighted in blue) is lower when the wind surface area is lower. So, the maximum wind load in the most critical wind direction is lower for the optimized structure than for the straight structures. Furthermore, a similar conclusion is found as with the optimization of a single column, namely that the maximum tension force (highlighted in red) is lower when it is divided over more column corners. In the straight column structures, all column corners are oriented in the same direction. Therefore, there are critical wind directions where the tension is only divided over one corner per column, which leads to a peak tension value. In the optimized structure, this tension is more equally divided in every wind direction, so the maximum value is lower. This phenomenon is visualized in Figure 34.

Table 16: Reaction forces asymmetric structure (Load Combination 3.1)

		Reaction force [kN]												
		1			**2**			**3**			**4**			**Total**
		x	**y**	**z**	**x**	**y**	**z**	**x**	**y**	**z**	**x**	**y**	**z**	**x**
0	**C1**	-0.23	0.01	0.85	-0.23	0.01	0.83	-0.23	0.00	-0.70	-0.23	0.00	-0.71	-0.92
	C2	-0.23	-0.01	0.70	-0.23	-0.01	0.71	-0.23	-0.01	-0.85	-0.23	-0.01	-0.83	-0.93
	C3	-0.22	0.00	0.75	-0.22	0.00	0.73	-0.22	0.00	-0.75	-0.22	0.00	-0.74	-0.87
	Total													-2.72
45	**C1**	-0.32	0.01	0.12	-0.32	0.01	1.59	-0.32	0.01	-1.41	-0.32	0.01	0.05	-1.28
	C2	-0.32	-0.01	-0.08	-0.32	-0.01	1.40	-0.32	-0.01	-1.59	-0.32	-0.01	-0.09	-1.28
	C3	-0.30	0.00	0.02	-0.30	0.00	1.44	-0.30	0.00	-1.44	-0.30	0.00	-0.02	-1.21
	Total													-3.78
Opt	**C1**	-0.31	0.00	0.53	-0.28	-0.01	-1.15	-0.25	0.00	1.37	-0.28	0.00	-0.34	-1.13
	C2	-0.33	0.00	0.83	-0.31	0.01	1.02	-0.28	-0.01	-1.24	-0.37	-0.02	-1.02	-1.29
	C3	-0.30	-0.02	-1.30	-0.33	0.02	0.70	-0.35	0.01	-0.70	-0.31	0.01	1.30	-1.29
	Total													-3.70

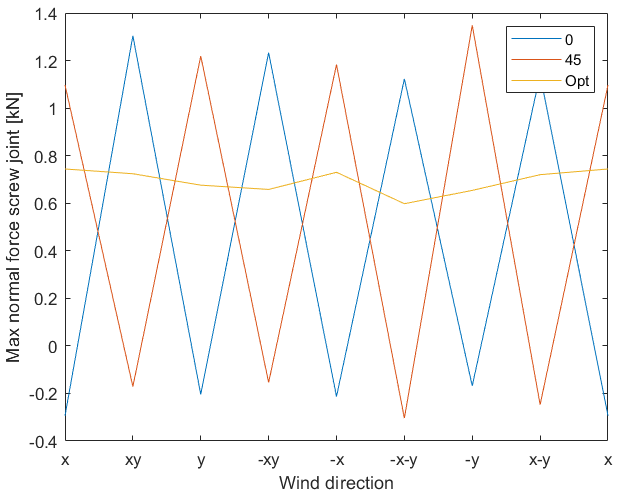

Figure 34: Maximum normal force in screw connection per wind direction

3.5 Result

This section covers research question 1d: *Is the chosen pavilion structure with structurally optimized columns able to withstand the applied loads?* First the results in the Ultimate Limit State (ULS) and Serviceability Limit State (SLS) are checked for the final asymmetric pavilion. Then the results of the optimized columns are compared to the straight columns. Again, all hand calculations are done in Matlab (see Appendix K).

3.5.1 ULS

For the analysis of the Ultimate Limit State, the ULS load cases are used as given in Table 7, with the wind loads in eight directions as shown in Figure 16. The Young's modulus (E) of the timber and CLT are reduced according to Equation 15 (NEN-EN 1995-1-1:2005, section 2.3.2).

$$E_{mean,fin} = \frac{E_{mean}}{1 + \psi_2 k_{def}} \tag{15}$$

In which:
ψ_2 = partial factor (Figure 68)
k_{def} = deformation factor = 0.8 (sawn timber, CC2), 2.0 (CLT, CC3)

The structural elements of the pavilion structure that are checked are: the column beams, the screwed connection, the prestressed cable and the CLT roof. The elements are checked by performing Unity Checks (UC) with the internal design forces found in Grasshopper Karamba and the design strength (X_d) according to Equation 16 (NEN-EN 1995-1-1:2005, section 2.4).

$$X_d = k_{mod} \frac{X_k}{\gamma_M} \tag{16}$$

In which:
k_{mod} = modification factor = 1.1 (instantaneous), 0.8 (short), 0.5 (permanent)
γ_M = partial factor = 1.3 (solid timber), 1.25 (CLT)

The maximum stress in the face of the CLT roof ($\sigma_{face,roof}$) and the maximum shear stress (t_{roof}) are calculated according to Equation 17 and 18 respectively.

$$\sigma_{face,roof} = \frac{M_{Ed} z E_{face}}{EI_{eff}} = 2.05\, N/mm^2 \tag{17}$$

$$t_{roof} = \frac{3V_{Ed}}{2A} = 0.32\, N/mm^2 \tag{18}$$

In which:
z = distance roof middle to face = 65 mm
EI_{eff} = effective bending stiffness = 5.20e12 Nmm^2
A = area cross section roof = 0.26 m^2

The results of the maximum internal design forces found in the structure in the ULS can be seen in Table 17. All calculations of the individual Unity Checks can be found in Appendix G. The summarized results of the checks can be seen in Table 18. All Unity Checks are equal or below 1, which means that the structure is validated. As can be seen, the most critical force in the structure is the combination of tension and shear in the screw joint.

Table 17: Maximum internal forces ULS

	N_c [kN]	N_t [kN]	V_z [kN]	V_y [kN]	M_t [kNm]	M_y [kNm]	M_z [kNm]
Beam	0.84	0.65	5.24	0.88	0.02	0.09	0.02
Joint	5.45	0.74	1.38	0.77	0.00	0.06	0.04
Cable	-	7.56	-	-	-	-	-
	N_c [kN/m]	N_t [kN/m]	V [kN/m]		M [kNm/m]		
Roof	1.22	1.14	56.30		1.86		

Table 18: Unity Checks

Element	Check	Unity Check
Beam	Compression 0°	0.02
	Compression 90°	0.54
	Tension 0°	0.02
	Bending y	0.22
	Bending z	0.17
	Torsion	0.00
	Shear	0.51
	Combination compression + bending y	0.22
	Combination compression + bending z	0.17
	Combination tension + bending y	0.24
	Combination tension + bending z	0.19
Joint	Tension	0.54
	Shear	0.84
	Combination tension + shear	1.00
Cable	Tension	0.26
Roof	Bending	0.44
	Shear	0.38

Furthermore, buckling is checked in the column by calculating the model with second order beam theory in Grasshopper Karamba. With that output, the buckling mode and Buckling Load Factor (BLF) can be calculated. The first buckling mode can be seen in Figure 35. The calculated BLF of the full structure is 35.3. In this calculation no extra safety factors are taken into account. However, because the BLF is significantly above the critical value of 1, it is assumed that the columns in the structure will most likely not buckle under the applied loads.

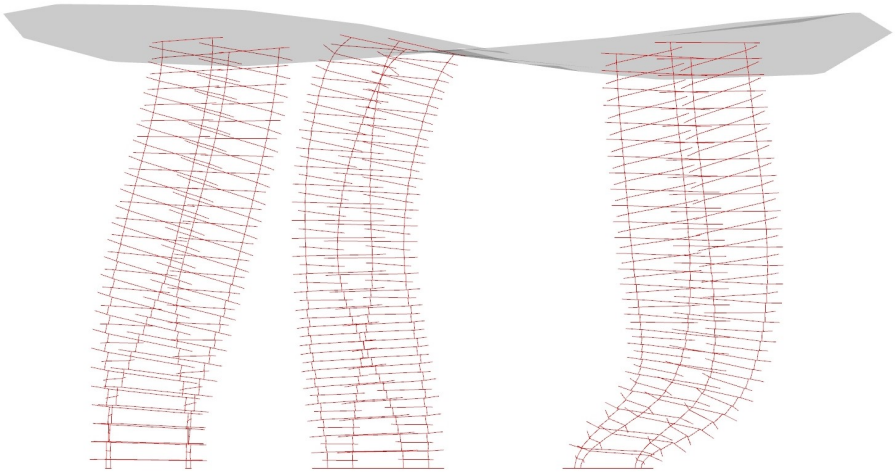

Figure 35: First buckling mode of full structure (1.5 x deformation)

3.5.2 SLS

For the analysis of the Serviceability Limit State, the SLS load cases are used as given in Table 7. Furthermore, the Young's modulus of the timber and CLT are reduced according to Equation 19 (NEN-EN 1995-1-1:2005, section 2.3.2).

$$E_{mean,fin} = \frac{E_{mean}}{1 + k_{def}} \tag{19}$$

The instantaneous maximum deformation can be seen in Table 19. The final deformation (u_{fin}) is calculated with Equation 20 (NEN-EN 1995-1-1:2005, section 2.2.3). The maximum allowable vertical deformation is taken as the roof span/250, which is 12.1 mm. It can be concluded that the vertical deformation is within these limits.

Table 19: Maximum instantaneous deformation with SLS load combinations

	Deformation [mm]		
	x	**y**	**z**
Gravity, prestress (G)	-0.18	-0.42	-3.53
Applied load (Q)	-0.14	-1.03	-0.75
Wind (Q)	8.31	-1.03	-0.15
Snow (Q)	-0.04	-0.57	-0.43

$$u_{fin,z} = u_{inst,G}(1 + k_{def}) + u_{inst,Q,1}(1 + \phi_{2,1}k_{def}) + \sum u_{inst,Q,i}(\phi_{0,i} + \phi_{2,i}k_{def}) = 11.3\,mm \tag{20}$$

In which:
$u_{inst,G}$, $u_{inst,Q}$ = instantaneous deformation for load G (permanent) and Q (variable)

3.5.3 Comparison before and after optimization

The comparison between the optimized structure and the structure with straight columns can be seen in Table 20. As can be seen, the maximum tension force in the screw connections of the optimized structure is reduced with almost 43% compared to the straight column 0°. The maximum Unity Check of the optimized structure is reduced by almost 5%. This reduction is a bit less extreme than the reduction in tension force. That is due to the fact that the shear force in the optimized structure slightly increases, which causes an increase in the most governing Unity Check (tension and shear in the screw). However, it can be concluded that the optimized structure is the only structure that suffices the structural criteria, while in all three structures exactly the same amount of material is used. Therefore, the optimization proves to be successful.

Table 20: Comparison before and after optimization

	Max N_t [kN]	**Difference [%]**	**Max UC**	**Difference [%]**
0	1.30	0.0	1.05	0.0
45	1.35	3.4	1.09	3.8
Optimized	0.74	-42.9	1.00	-4.8

4 Assembly

This section covers the robotic assembly of the parametric timber structure. At first, the method of joining the timber is chosen. Subsequently, the robotic set-up and procedure are explained. At last, the actual construction is shown.

4.1 Timber joining method

This section covers research question 2a: *What timber joining methods are possible and which of these methods is the most promising to execute with the available robots?* Research is done on the different methods to (robotically) join timber parts. In total four possible methods are found:

1. Screws
2. Nails
3. Adhesive
4. Japanese joinery

The different assembly techniques are explained and evaluated in section 4.1.1 to 4.1.4 and from that the most promising method is chosen in section 4.1.5.

4.1.1 Screws

The most widely used connection method in timber is screwing. Screws can create a very strong yet relatively simple joint in wood, which makes it so favourable. To make this connection robotically a screw machine/mechanism should be added to the end of one robot arm. This mechanism should be able to place a screw in the correct position and turn it with enough torque so the screw completely goes into the timber. For placing the screw in the correct position several options are available, such as: picking up a screw with magnetism or vacuum, grabbing a screw or having an automatic screw feeding mechanism. Overall, a relatively complex end effector is needed. Furthermore, it should be noted that with screwing there is a significant risk of splitting of the timber. To prevent this it is possible to (robotically) predrill the timber or use special self tapping screws that limit this risk of splitting. In short, screwing is a common and strong method to join timber. However, it is quite a difficult procedure to automate and it requires complex end effectors. An example of a screwing end effector which can pick up screws can be seen in Figure 36.

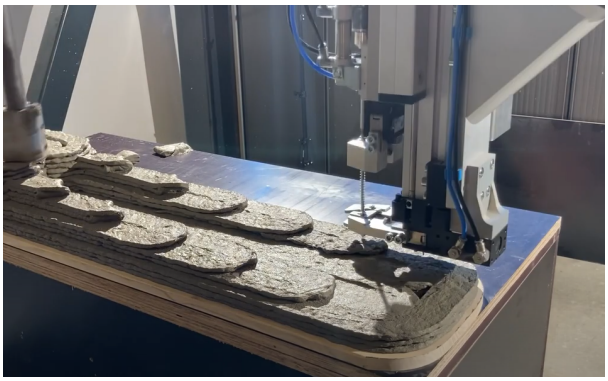

Figure 36: Robotically placed reinforcement using the automated screwing device (Hass & Bos, 2022)

4.1.2 Nails

Another method to join timber is with nails. These nails can be shot in the timber (with for example a nail gun) or they can be pushed in while holding the timber in place, which reduces

the impact on the structure. Nailed connections are also quite common in timber structures, but mostly in applications such as connecting panels rather than in timber framework. The connection can be relatively simple and strong, but it is commonly less strong than a screwed connection and it requires more nails than it would require screws. To automate a nailed connection the robot should be able to place the nails in the correct position. Furthermore, a nail gun or nail push mechanism should be added to the robot arm, which is again fairly complex. Furthermore, shooting nails with a robotic arm has the safety issue that nails can be shot in a wrong direction. Extra safety measurements should be taken to make sure this could not lead to damage. An example of a robotic nailing end effector can be seen in Figure 37.

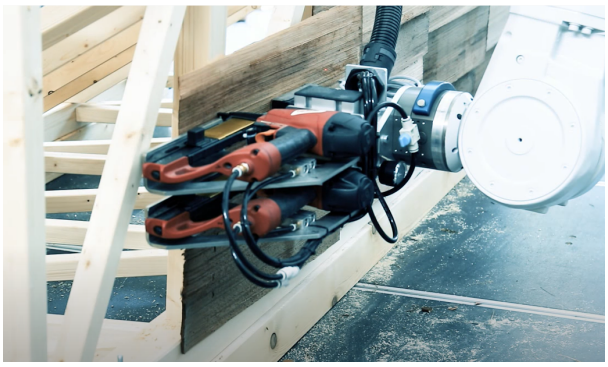

Figure 37: Robotic nailing end effector used in paneling of the two storey timber structure (Eversmann et al., 2017)

4.1.3 Adhesive

A glue/adhesive can also be used to make a timber joint. This method is less common than screws or nails, but is still sometimes used in timber structures. The joint can reach an okay strength and is fairly simple. However, the failure mode of adhesives is commonly very sudden, which is not desirable in a structure. The adhesive should be applied with a special end effector/nozzle which controls the amount of adhesive. Then, the robots should keep the timber parts in place until the adhesive is dry enough, which could be a slow process. Overall the procedure is a bit simpler, but the result has less potential than screwed or nailed connections. A robotic assembly method with adhesive (where a manual step is required) can be seen in Figure 38.

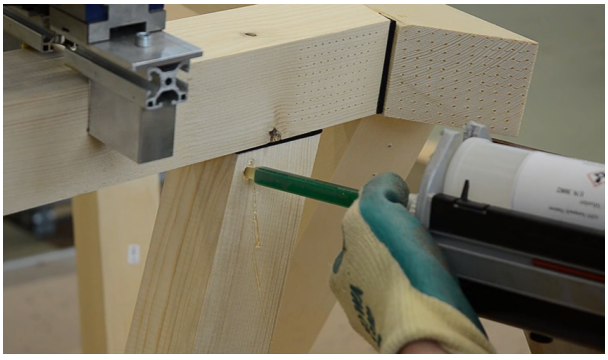

Figure 38: Robotic assembly of timber structure with adhesive (NRP 66 Research Project, 2017)

4.1.4 Japanese joinery

The last method to join timber is by Japanese joinery, where timber parts are fitted together like a puzzle without the use of other materials. This method is used, but not common in modern

structures. The connection can be strong, but is often quite complex. The timber parts itself need to be milled or sawn very precisely in order to create a strong connection. The assembly procedure itself does not require complex end effectors, only grippers. However, often the parts need to be fitted together with quite some force, which could be a problem for the robots. Also, the movements of the robots would be very complex and require extreme accuracy. An example of a robotic assembly of a Japanese joinery structure can be seen in Figure 39.

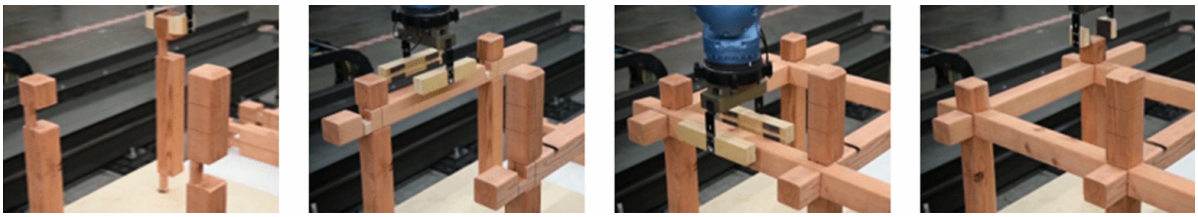

Figure 39: Robotic assembly of Japanese joinery structure
(Koerner-Al-Rawi, Park, Phillips, Pickoff, & Tortorici, 2020)

4.1.5 Evaluation

The assembly methods are evaluated in multiple individual criteria, namely:

- Can the construction method can be used in real life structures?
- How strong is the connection?
- How simple is the connection?
- How simple is the assembly process to execute by robots? Does it require complex end effectors or not? Is significant precision required or is it fail proof?
- Is the assembly method sustainable? Does it require a lot of extra (less sustainable) materials?
- Is disassembly possible?

The results of the evaluation can be seen in Table 21. Each criteria is given a weight factor between 1 to 3 to take its importance into account. The scores can vary from very bad (- -) to very good (++). From the Multi Criteria Decision Analysis it is clear that screwing is the assembly method with the most potential. Therefore, this method is chosen to work out in further detail.

Table 21: Multi Criteria Decision Analysis

	Weight factor	**Screws**	**Nails (shoot)**	**Nails (push)**	**Adhesive**	**Japanese joinery**
Applicable in real structures	3	++	+	+	0	0
Strength connection	3	++	+	+	0	+
Simplicity connection	2	++	++	++	++	-
Simplicity procedure	2	- -	+	0	0	-
Sustainability	2	-	- -	- -	0	++
Safety	2	+	- -	+	+	+
Disassembly possible	1	++	0	0	-	++
Total [+]		**14**	**4**	**8**	**7**	**7**

4.2 Robotic assembly set-up

This section covers research question 2b: *What should the robotic screwing set-up look like and what materials, end effectors and other parts are required for this?*

There are several tasks that have to be automated, namely:

- Pick and place timber beam
- Pick and place screw
- Screwing

Each task is individually worked out in section 4.2.1 to 4.2.3.

4.2.1 Pick and place timber beam

Picking and placing of the timber beams is done with a gripper end effector, which can be seen in Figure 40. This pneumatic gripper has two aluminium brackets that can move towards each other and can therefore clamp an object. New aluminium parts are made so that they can pick up beams of the correct width. The position of the aluminium brackets can also be modified slightly, so the beams can be picked up with varying force.

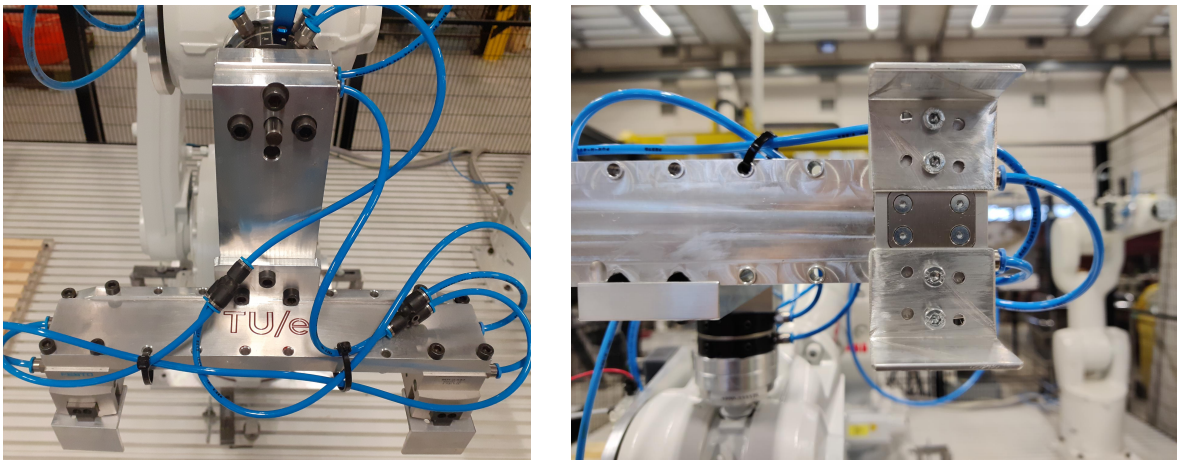

(a) Full gripper (b) Aluminium brackets

Figure 40: Gripper end effector

The required amount of beams are placed in a square pile on top of each other, as shown in Figure 41. The gripper end effector has a stroke of 3 mm on each side, which means that the beams should be placed with a maximum error of less than 3 mm. This is done by placing the beams on a template fixed to the ground table and by using blocks in between the beams to assure the correct distance between them.

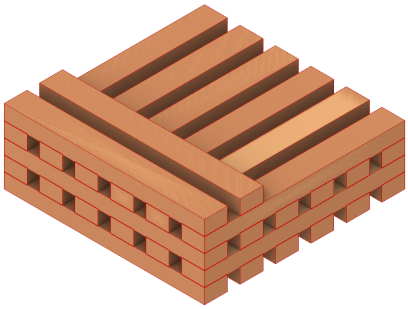

Figure 41: Beam stock

4.2.2 Pick and place screw

Research is done on the different ways to pick and place a screw. In total five possible options are found:

1. **Gripper**
   A gripper is a mechanism that can clamp a screw and release it. The gripper mechanism can be powered, for example as in the automated screwing device (see Figure 36), or it can be unpowered as can be seen in Figure 42a.
   A powered gripper is a fairly complex mechanism which requires an extra power supply and motors. Furthermore, no existing powered screw gripper end effectors are found for sale, which means a new prototype would have to be made for this application. An unpowered gripper is simpler, but it would be challenging to always get the screw correctly inside the gripper.

2. **Magnet**
   A magnet can pick up and move a screw to the correct position. A regular magnetic bit can be used, or a special bit with a ring magnet such as in Figure 42b.
   A magnet is a fairly simple and cheap solution that does not need any other accessories. However, it is a challenge to automate the process of picking up the screw correctly on the bit without damaging it.

3. **Vacuum**
   Another possibility to pick up screws is by adding a vacuum pick up suction head. This application can be seen in Figure 42c.
   The vacuum pick up suction head needs an extra air tube connection and air control, which makes it relatively complex and expensive.

4. **Automatic screw feeder through air tube**
   In the automatic screw feeder, screws are sorted in a machine and fed through a pressured air tube to the bit head, which can be seen in Figure 42d.
   An automatic screw feeder is very reliable and already widely used in for example the automotive industry. However, the downside is that the application has to be tailored specifically to one screw size and the screw length/width is limited. Furthermore, it needs an external tubing that can obstruct the robotic arms and it is by far the most expensive solution.

5. **Autofeed screw gun**
   An autofeed screw gun can take screws from screw strips that are guided along a rails towards the bit head. An example can be seen in Figure 42e.
   An autofeed screw gun is relatively simple, widely available and relatively cheap. The downside is that these machines are difficult to attach to a robot arm and that they are quite heavy. Furthermore, special screw strips have to be used, which have to be refilled every ± 50 screws.

(a) Gripper
(WERA, n.d.)

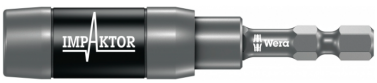

(b) Magnet
(WERA, n.d.)

(c) Vacuum
(Sumake Industrial, n.d.)

(d) Automatic screw feeder through air tube
(Sumake Industrial, n.d.)

(e) Autofeed screw gun
(Makita, n.d.)

Figure 42: Options to pick and place screws

All in all, the magnetic screw holder with ring magnet is chosen as the pick and place tool, because it is a simple and cheap yet promising solution. A magnetic screw holder is found that is especially made for long and heavy screws: the WERA Impaktor (Figure 42b). The corresponding bits have a diamond coating to reduce slip of the bit in the screws.

The screws are stocked inside a screw pick up station, which can be seen in Figure 43. The screw pick up station is laser cut, to achieve great accuracy of the screw positions ($\pm 0.05\ mm$).

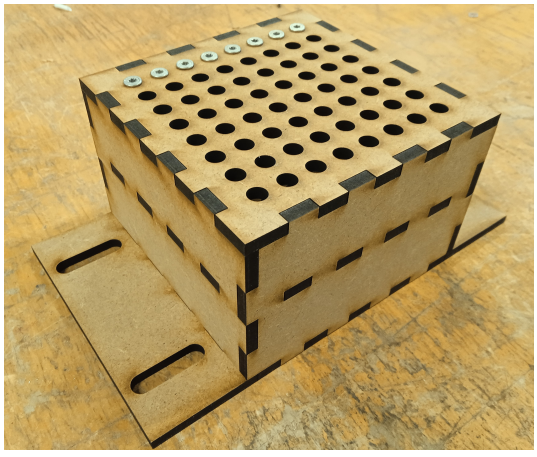

Figure 43: Screw pick up station

4.2.3 Screwing

For screwing a screw machine is used. First of all research is done on which screw machines are available that could be used for this project. A list of the different screw machine options found can be seen in Appendix H. Then, several requirements are set of which the screw machine must comply. In this section these requirements are explained and the most suitable option is chosen.

First of all, there are three types of screw machines available:

- Pneumatic
- Electric (cable)
- Electric (battery)

During an automated process it is undesirable if the power source works for a limited amount of time, like with a battery. Changing the battery when empty causes delay and human interaction. A screw machine with battery is also significantly bigger and heavier in general than the other two options, which makes it less favourable. During assembly the two robots move in a limited space with long pieces of timber, so it is also undesirable to have obstructions of cables. The pneumatic screw machine can be driven through the pneumatic system inside the robot, so no cables will obstruct the movements of the robots. With an electric screw machine the cable cannot simply be routed through the robot. The cable must be routed outside the robot or the electric circuit of the machine should be modified. Also, very little suitable electric screw machines with cable are found on the market. All in all, the pneumatic screw machine is the most preferable option. The maximum air pressure that can flow through the ABB IRB 1200 and the ABB IRB 1600 are respectively 5 bar (ABB, 2022a) and 8 bar (ABB, 2022b). All pneumatic screw machines found require an air pressure of more than 6 bar, so the screw machine should be mounted on the ABB IRB 1600.

Then, it is required that the screw machine can be turned on and off during the assembly process. To do this several methods are possible:

- Control air flow with switch
- Create mechanism to push in lever
- Screw machine with push start

The first possibility would be to add an air flow switch so that the air flow can be controlled remotely. However, the air flow switch that is currently attached to the robot is not capable to control the high air pressure needed for most pneumatic screw machines. Therefore, it would be needed to modify this. Another possibility is to create a mechanism to push in the lever of the screw machine to turn it on, but this would be a fairly complex solution. The last option is to buy a screw machine with "push start" function, so that it turns on automatically when light pressure is applied on the bit. The push start option requires the least modifications to the current set-up, compared to the other two options. Another great benefit of the push-start mechanism is that there is an axial spring inside the screw machine, which can account for small variations and errors in the vertical movement of the screw during screwing. In conclusion, the push-start mechanism is the most desirable.

The torque range of the screw machine should be sufficient to screw in screws commonly used in timber construction. Therefore, the machine should be able to screw screws with diameters between 3 and 7 mm and lengths up to about 200 mm. A research is found where torque values are measured for different screw types (Jung, Zhang, Harris, & Chang, 2019). For fully threaded screws with a diameter of 7 mm and a length of 295 mm in pre-drilled Glulam, a torque is needed of 6.9 Nm. For partially threaded screws with the same dimensions without predrilling a

torque is needed of 6.8 Nm. In other research it is found that a screw of 5 mm thickness and 40 mm length in pre-drilled plywood requires a tightening torque of 5 Nm (Kumpenza, Schmidt, Sotayo, Ringhofer, & Müller, 2020). From these sources it is determined that the maximum torque should be at least 6 Nm. Moreover, the maximum torque is limited by the torque that the robot arm can handle. In Figure 44 and Table 22 you can see the maximum torque values of the joints in the ABB IRB 1600. When the screw machine is applied in line with the end of the robot arm, the torque of the screw machine will be directed into joint F. Then, the maximum torque may not exceed 6.47 Nm. When the screw machine is placed perpendicular to the end of the arm, the torque will be directed into joint E, so a maximum torque of 13.93 Nm is allowed. The minimum torque should be less than 2 Nm, to be able to also screw in shorter and thinner screws without damaging them.

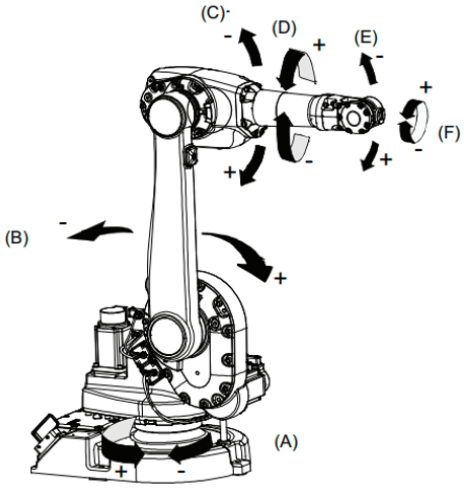

Figure 44: Joints ABB IRB 1600
(ABB, 2022b)

Table 22: Maximum torque joints

Joint	**Torque [Nm]**
D	13.93
E	13.93
F	6.47

Another requirement of the screw machine is that RPM should not be too high. A high RPM can lead more easily to damages, cracks in the timber and slippage of the bit on the screw. Also, with a higher RPM the downward velocity of the robot during screwing has to be higher, which leads to less accuracy and less time to intervene if the screw is not screwing in correctly. Therefore, the requirement is set that the maximum RPM is 750 (or adaptable to a value $\leq$ 750).

The screw machine should have an axial form, so that it can be attached to the robot more easily. Lastly, it should have a standard 1/4" hex drive shape so that normal screw bits can be used. The summarized list of requirements can be seen in Table 23.

Table 23: Screw machine requirements

Requirements
· Pneumatic (max. 8 bar)
· Push start
· Weight $\leq 2\ kg$
· Min torque $\leq 2\ Nm$
· Max torque $\geq 6\ Nm$
· RPM ≤ 750
· Axial form
· Drive shape 1/4" hex

The screw machine that fitted all requirements best is the RODAC RC3460. The machine can be seen in Figure 45 and the specifications are given in Table 24 (Rodac, n.d.). The screw machine should be mounted to the ABB IRB 1600 and cannot be mounted to the ABB IRB 1200, because of the required air pressure and minimum tube diameter.

Figure 45: Rodac RC3460 screw machine

Table 24: Rodac RC3460 specifications

Specifications
· Pneumatic (6.3 bar)
· Push start
· Weight = 0.69 kg
· Min torque = 1.5 Nm
· Max torque = 9.5 Nm
· RPM = 550
· Axial form
· Drive shape 1/4" hex
· Air flow = 550 L/min
· Minimum inner tube diameter = 8 mm

When constructing a timber structure, the robots have to be able to account for inaccuracies. When the robots stack beams on top of each other, the height of the real life structure can differ significantly from the expected height that is programmed into the robot, increasingly with each layer. To ensure that the screws will still always be screwed in at the right depth, a sensor is added. The different sensors that could be used for this application are:

- Laser distance sensor
- (Capacitive) proximity sensor
- Force sensor
- Push button

A proximity sensor is chosen as the best option for this application, because it does not have to come in contact with the material, unlike the force sensor and the push button. Also, it is significantly cheaper and easier to implement than a laser distance sensor. The requirements of the sensor can be found in Table 25.

Table 25: Sensor requirements

Requirements
· Capacitive proximity sensor
· Max error $\leq$ 1 mm
· M8 3-pin connector
· LED indicator

A proximity sensor is found which meets all requirements: the Autosen AC006 (Autosen, n.d.). The maximum error of this sensor (e_s) can be calculated according to Equation 21. A benefit of this sensor is that it can also easily be altered in height, because it is partially threaded.

$$e_s = (e_h + e_r + e_t)s_d = 0.52\,mm \tag{21}$$

In which:
e_h = hysteresis error = 15 %
e_r = reproducibility error = 1 %
e_t = temperature error = 10 %
s_d = switching distance = 2 mm

Figure 46: Sensor AC006
(Autosen, n.d.)

The screwing machine is connected to the robot with a stiff aluminium holder. The sensor is attached to the screwing end effector with a 3D printed bracket inside the holder, which enables the sensor to be close to the bit head. The full screwing end effector can be seen in Figure 47. The sensor can easily be tuned in height by turning the nuts. During testing, the nut at the bottom is removed, so that when the sensor feedback fails, the sensor can be pushed upwards. This prevents damage to the sensor and/or sensor bracket. The CAD file of the bracket can be found in Appendix I.

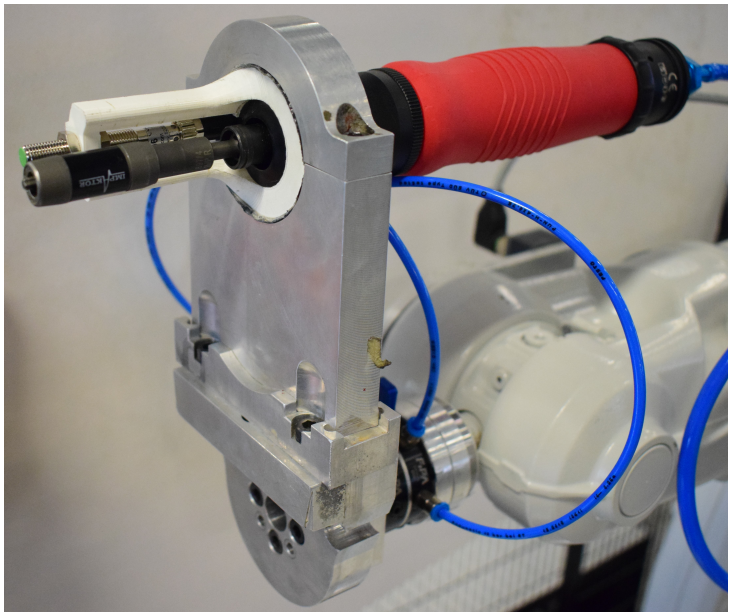

Figure 47: Screwing end effector

4.3 Procedure

This section covers research question 2c: *How should the robotic assembly procedure of the chosen column design be programmed?* First, the path planning of the robots is covered. Then, the screwing procedure is explained in more detail. Subsequently, the multi move programming and the collision checks are explained.

4.3.1 Path planning

The positioning of the robots is carefully determined. The robots are each placed in one corner of the table, so they both approach the column structure from different directions, which minimizes the chance for collisions. Furthermore, it gives them the most possible space to move in, which limits the chance for unexpected movements or movements through singularity points. The optimal positions used can be found in Appendix I. The IRB1600 with screwing end effector is Robot 1 (R1) and the IRB1200 with gripper is Robot 2 (R2).

The bottom two beams of the column part are always aligned so that both robots are located at a column corner. Robot 1 approaches the structure from the x and $-y$ direction and uses fly by points to move around Robot 2. Robot 2 approaches the structure from the $-x$ and y direction. It always passes through its home position between picking up and placing a beam, so that the path is predictable and uses the correct axis configurations. The paths are visualized in Figure 48.

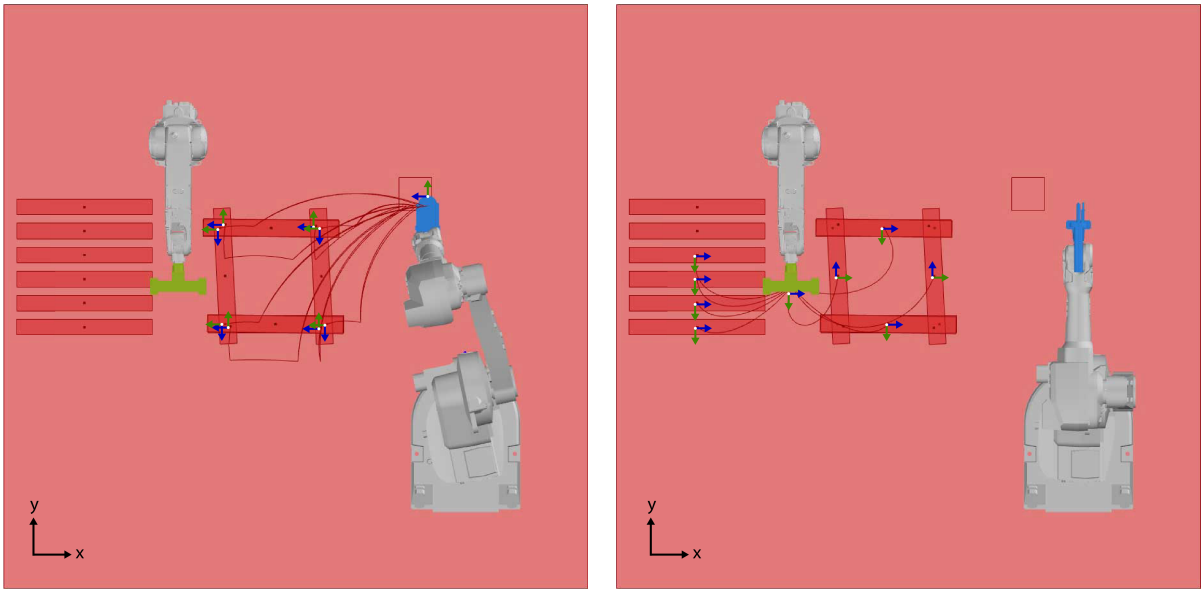

(a) Robot 1 (b) Robot 2

Figure 48: Path planning

The paths consist of joint movements and linear movements. The large movements between picking up and placing are done with joint movements with a relatively high velocity (v = 300 mm/s). When the robot is near the beam, it makes a linear movement downwards with a lower (thus more precise) velocity (v = 100 mm/s). The fly by points in between joint movements have a zone (Z). This zone indicates that the robot does not have to pass the point exactly, but can approach it within the assigned zone, which leads to smoother and faster paths. This procedure is visualized in Figure 49.

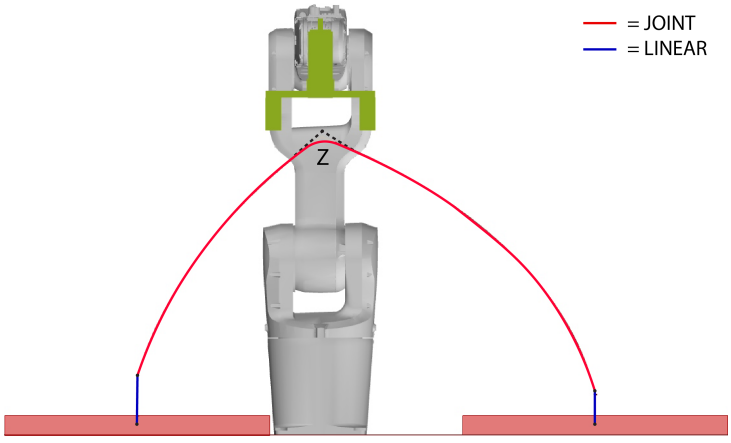

Figure 49: Movements

4.3.2 Screwing

Picking up the screw is done by moving the magnetic screw holder towards the screw. To make sure the bit always clicks correctly into the screw head, the robot rotates around the z-axis above the screw. When the screw is picked up, the robot moves towards the screw position and the screwing procedure starts. The robot moves vertically downwards with a speed (v_{down}) calculated according to Equation 22. The definition of the screw lead can be seen in Figure 50. The downward speed is an approximation, because the screw machine does not always rotate with exactly the same value, due to variations in the required torque in the timber. The spring

inside the screwing machine accounts for these inaccuracies.

$$v_{down} = \frac{RPM}{60} Lead \tag{22}$$

In which:
RPM = rotations per minute screw machine = 550 RPM
$Lead$ = screw lead = 0.90 mm

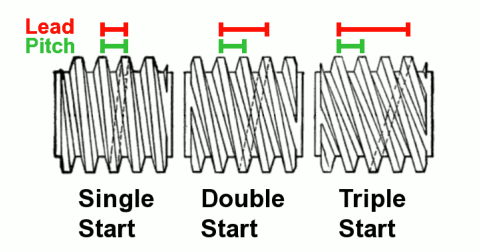

Figure 50: Screw lead
(Oberg, Valentine, & Stable, 1910)

The linear screwing movement stops when the sensor gives a signal that the screw is deep enough inside the timber beam. The sensor is connected to the I/O ports of the robot, so when the sensor detects the timber beam, the sensor signal changes and the robot stops with the downward movement. This is done with a linear search command ($SearchL$) in the RAPID code (programming language to control ABB industrial robots). With this command the tool moves linearly with a fixed velocity to an assigned point, until the sensor signal changes. The code is written in Python blocks in Grasshopper, which can be seen in Appendix J.

4.3.3 Multi move

During construction it is necessary that the two robotic arms work together and wait for each other to perform certain tasks.

First of all, Robot 1 can pick up a screw and Robot 2 can pick up a beam simultaneously. Then, Robot 2 can place the beam at the programmed position in the column. Once the beam is in the correct position, Robot 1 can move the picked up screw towards the correct screw position and screw in the screw. Then, Robot 1 can pick up the second screw and screw this in at the other side of the timber beam. Once both screws are in, Robot 2 can let go of the beam and proceed with picking up and placing the next beam. This procedure (visualized in Figure 51) is repeated until the full column part is constructed.

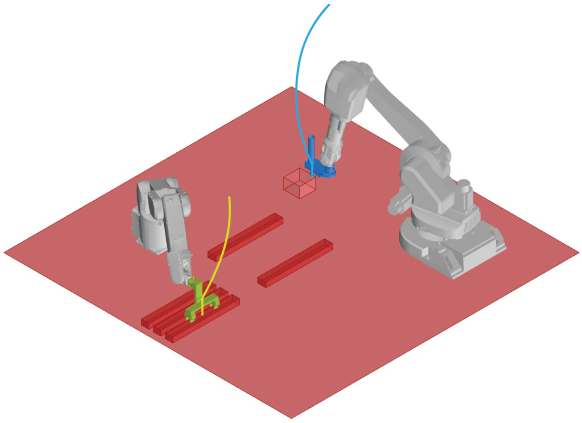

(a) R1 picks up screw & R2 picks up beam

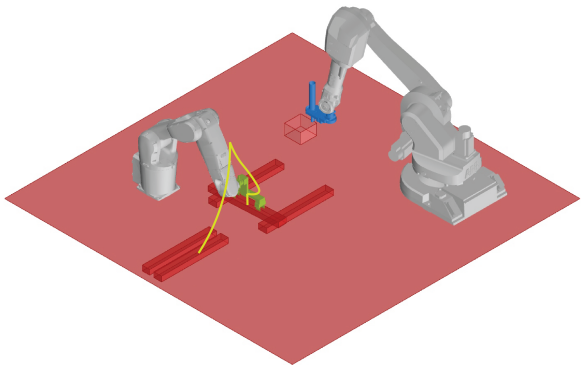

(b) R2 places beam in correct position

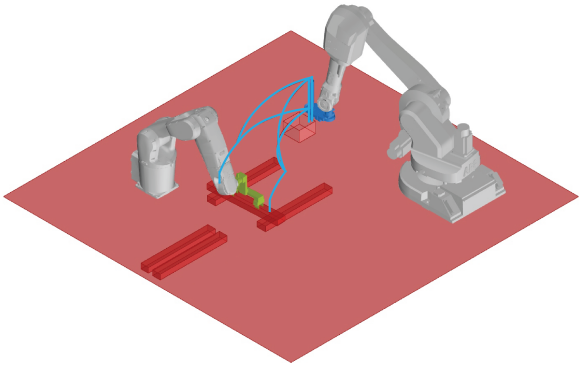

(c) R1 screws in two screws

Figure 51: Construction procedure

This building sequence is realized by using multi move components, which are available in the Grasshopper plugin Robot Components. In the RAPID code two "Wait Sync Task" synchronization points are defined (sync1 and sync2). The robots can only continue with their next task once both robots have reached the specific synchronization point. An example of the RAPID code for one beam placement with two screws can be seen in Figure 52. Further details can again be seen in Appendix J.

Robot 1

```
MoveJ Pick_up_screw_z_R1_0, v300, z0, screwing_tool\WObj:=wobj0;
MoveL Pick_up_screw_R1_0, v100, z0, screwing_tool\WObj:=wobj0;
MoveL Pick_up_screw_rotate_R1_0, v100, z0, screwing_tool\WObj:=wobj0;
MoveL Pick_up_screw_R1_0, v100, z0, screwing_tool\WObj:=wobj0;
MoveL Pick_up_screw_z2_R1_0, v100, z0, screwing_tool\WObj:=wobj0;
WaitSyncTask sync1, my_tasks;
MoveJ Fly_by_point_A_R1_0, v300, z40, screwing_tool\WObj:=wobj0;
MoveJ Fly_by_point_B_R1_0, v300, z40, screwing_tool\WObj:=wobj0;
MoveJ Screw_position_z_R1_0, v300, z0, screwing_tool\WObj:=wobj0;
MoveL Screw_position_R1_0, v40, z0, screwing_tool\WObj:=wobj0;
SearchL \Stop,IRB1600_IO_0_DI1,sp,Screwing_R1_0,Downward_speed_
screwing,screwing_tool\WObj:=wobj0;
WaitTime 0.2;
MoveL Screw_position_z2_R1_0, v300, z0, screwing_tool\WObj:=wobj0;
MoveJ Fly_by_point_B_R1_0, v300, z40, screwing_tool\WObj:=wobj0;
MoveJ Fly_by_point_A_R1_0, v300, z40, screwing_tool\WObj:=wobj0;
MoveJ Pick_up_screw_z_R1_1, v300, z0, screwing_tool\WObj:=wobj0;
MoveL Pick_up_screw_R1_1, v100, z0, screwing_tool\WObj:=wobj0;
MoveL Pick_up_screw_rotate_R1_1, v100, z0, screwing_tool\WObj:=wobj0;
MoveL Pick_up_screw_R1_1, v100, z0, screwing_tool\WObj:=wobj0;
MoveL Pick_up_screw_z2_R1_1, v100, z0, screwing_tool\WObj:=wobj0;
MoveJ Fly_by_point_A_R1_1, v300, z40, screwing_tool\WObj:=wobj0;
MoveJ Fly_by_point_B_R1_1, v300, z40, screwing_tool\WObj:=wobj0;
MoveJ Screw_position_z_R1_1, v300, z0, screwing_tool\WObj:=wobj0;
MoveL Screw_position_R1_1, v40, z0, screwing_tool\WObj:=wobj0;
SearchL \Stop,IRB1600_IO_0_DI1,sp,Screwing_R1_1,Downward_speed_
screwing,screwing_tool\WObj:=wobj0;
WaitTime 0.2;
MoveL Screw_position_z2_R1_1, v300, z0, screwing_tool\WObj:=wobj0;
MoveJ Fly_by_point_B_R1_1, v300, z40, screwing_tool\WObj:=wobj0;
MoveJ Fly_by_point_A_R1_1, v300, z40, screwing_tool\WObj:=wobj0;
WaitSyncTask sync2, my_tasks;
```

Robot 2

```
MoveJ Pick_up_beam_z_R2_0, v300, z0, parallel_gripper\WObj:=wobj0;
MoveL Pick_up_beam_R2_0, v100, z0, parallel_gripper\WObj:=wobj0;
WaitTime 0.5;
SetDO IRB1200_IO_0_DO1, 1;
WaitTime 0.5;
MoveL Pick_up_beam_z_R2_0, v100, z0, parallel_gripper\WObj:=wobj0;
MoveAbsJ Fly_by_point_R2, v300, z80, parallel_gripper\WObj:=wobj0;
MoveJ Beam_position_z_R2_0, v300, z0, parallel_gripper\WObj:=wobj0;
MoveL Beam_position_R2_0, v100, z0, parallel_gripper\WObj:=wobj0;
WaitSyncTask sync1, my_tasks;
WaitSyncTask sync2, my_tasks;
WaitTime 2;
SetDO IRB1200_IO_0_DO1, 0;
WaitTime 1;
MoveL Beam_position_z2_R2_0, v100, z0, parallel_gripper\WObj:=wobj0;
MoveAbsJ Fly_by_point_R2, v300, z80, parallel_gripper\WObj:=wobj0;
```

Joint movement
Linear movement
End effector task
Synchronization point

Figure 52: Example RAPID code

4.3.4 Collision check

A collision check is done for the full building sequence to make sure that the robots, end effectors and building materials do not crash in to each other. The following geometries are modeled and imported into RobotStudio:

- Robot 1 (IRB1600)
- Robot 2 (IRB1200)
- Gripper tool
- Screwing tool (including sensor)
- Beam
- Screw
- Ground table

Then, collision sets are defined, which can detect whether a geometry (nearly) collides with another geometry. A near miss criterion is added, so the geometries cannot be closer than the assigned near miss value to each other. A negative near miss value means they can overlap the maximum of the assigned value, so no warning will be given when the geometries touch. The collision sets can be seen in Table 26. An example of Collision set 1 can be seen in Figure 53. The full assembly procedure is simulated including collision check before construction.

Table 26: Collision sets

Set	**Body A**	**Body B**	**Near miss criterion** $[mm]$
1	Robot 2 + Gripper tool	Robot 1 + Screwing tool + Screw	20
2	Beam	Robot 1 + Robot 2	20
3	Beam	Screwing tool + Table	-1

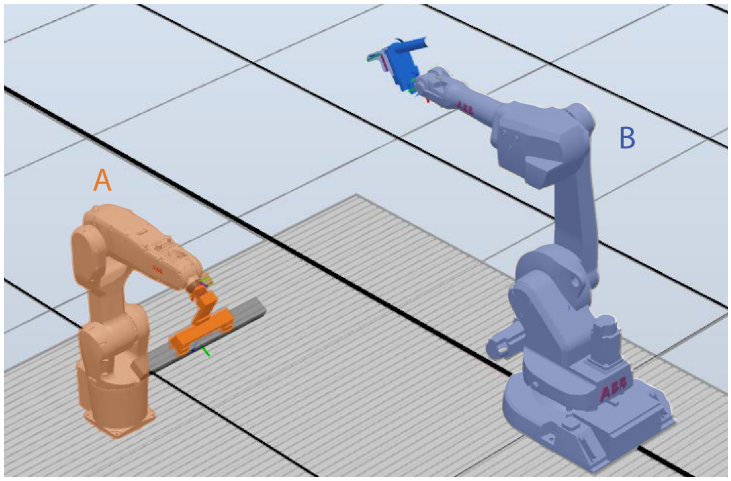

Figure 53: Collision set 1

4.4 Construction

This section covers research question 2d: *Can the robotic screwing set-up be optimized further?* First, the individual processes are tested and during these tests, the optimal settings and movements are found. Then, the final construction process of the column is covered.

4.4.1 Testing and optimization

First of all a range of different screw sizes are tested (without sensor feedback), which can be seen in Table 27. All screw sizes are repeated three times, so in total 27 screws are screwed in. The maximum torque value of the screw machine is experimentally adapted with increasing screw sizes. All screws are screwed in successfully, so it can be concluded that the screwing end effector is at least able to screw in screws with 4-6 *mm* diameter and 40-100 *mm* length. Larger screw sizes are not tested, despite the fact that the specifications of both the screwing machine and the robot would allow it. This choice is made, because in the timber column larger screws will not be used and the risk of damaging the screw machine and/or the robot increases with higher torque values.

Table 27: Screw sizes

Diameter [mm]	**Length [mm]**	**Bit**	**Max torque [Nm]**
4.0	40	T20	2
4.0	50	T20	2
5.0	40	T25	3
5.0	50	T25	4
5.0	60	T25	4
5.0	80	T25	4
5.0	100	T25	4
6.0	80	T30	4
6.0	100	T30	5

During the first screwing test, the depth of the screw head in the timber beam varied a few millimeters, because at some locations the actual height of the timber beam differed from the programmed height of the beam (see Figure 54a). For this reason, the proximity sensor is added. Subsequently, the screwing procedure including the sensor feedback is tested with ten 5x80 *mm* screws. The sensitivity and height of the sensor are fine tuned so that the screw head is screwed fully inside the timber. Again, all screws were screwed in successfully and now also at approximately the same depth. This result can be seen in Figure 54b.

(a) Without sensor (b) With sensor

Figure 54: Screwing test

The second procedure that is tested is picking up screws. A screw pick up station which can handle screws with 4-6 mm diameter and 40-100 mm length is made, which can be seen in Appendix I. Then, screws are tested with the two most common drive types in timber construction: Torx (size T20, T25 & T30) and Pozidriv (size PZ2 & PZ3). It is found that all tested screw types can be picked up successfully.

The screwing tool is calibrated precisely, so that the bit is exactly at the programmed tool plane. Furthermore, the pick up movement to make sure that the bit fits in the screw head is fine tuned, so that it is smooth and successful. A screw pick up test is done with 100 5x80 screws in the screw pick up station that is used during the construction of the column (Figure 43). All 100 screws were picked up correctly with a success rate of 100%.

4.4.2 Construction column

The timber beams that are used in the column have a width of 70 mm, instead of the required 75 mm, to save material and costs. This means that the screws are approximately 2.5 mm too close to the edge of the beam on each side. This is assumed to be acceptable for the demo column, which is constructed to prove the working of the robotic assembly process and will not be used in a real life pavilion. Because the arm reach of the robots is limited, a structure height of approximately 0.6 m can be achieved. Therefore, the full column is constructed in four parts of approximately thirteen layers each. During the construction of the first two beams, no screws are screwed in. These beams are placed by the gripper and then manually fixed to a timber ground plate using corner brackets, which can be seen in Figure 55a. The rest of the layers are fully robotically constructed (Figure 55b).

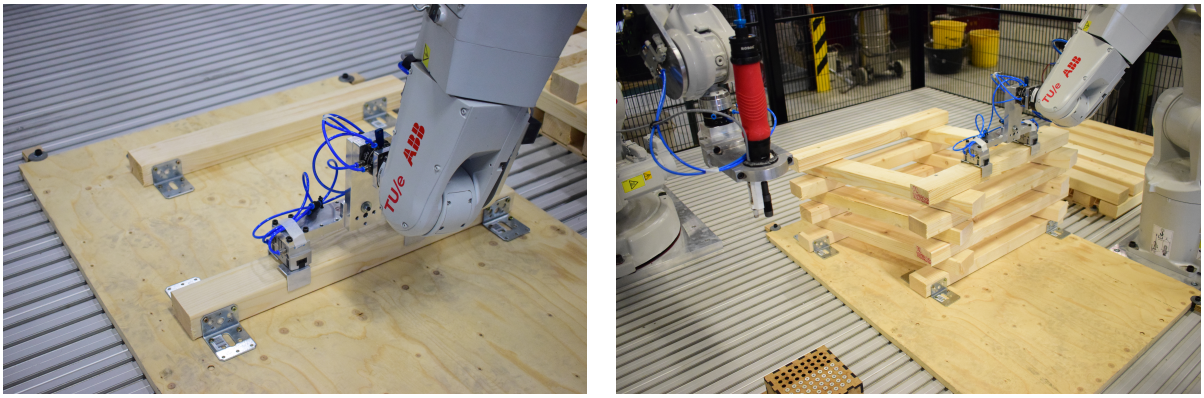

(a) First two beams (b) Rest of beams

Figure 55: Column construction

Every now and then a human intervention was needed. In total six construction errors were found, which can be seen in Figure 56. The amount of times an error occurred for each column part can be seen in Table 28.

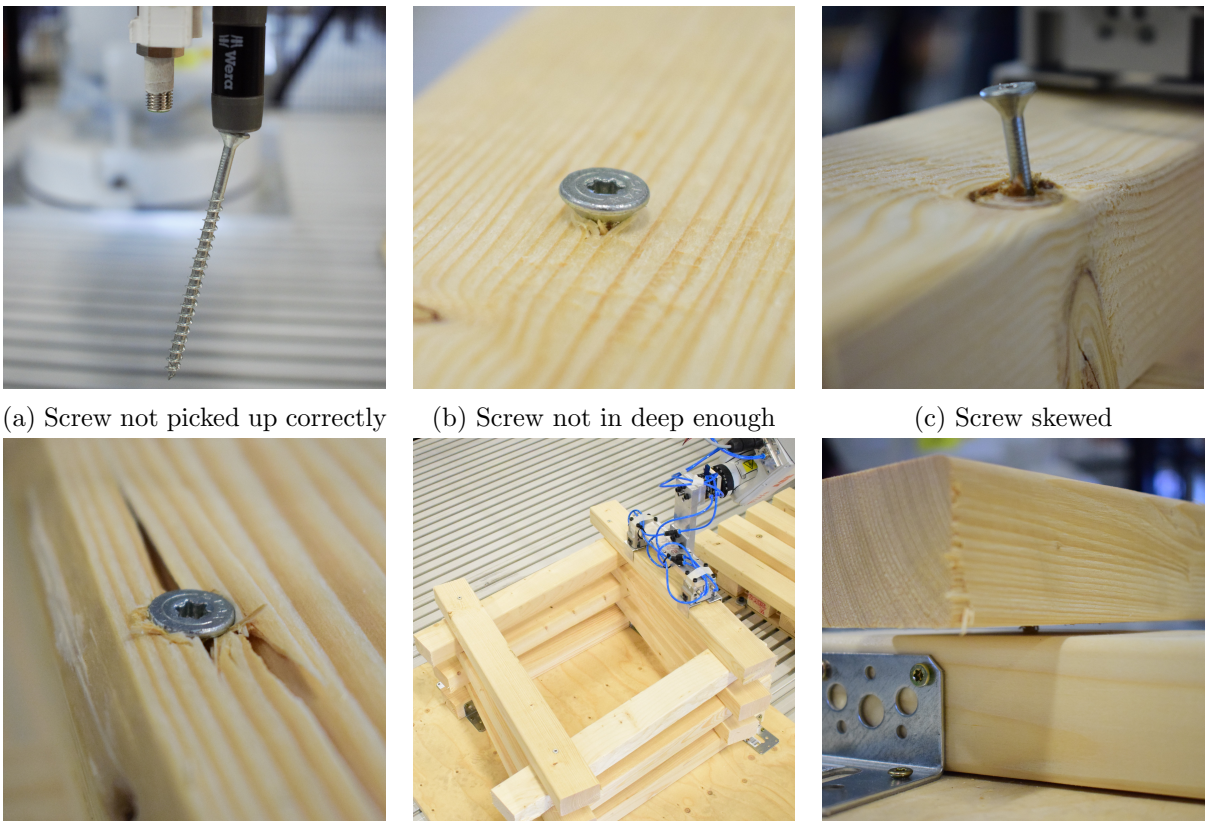

(a) Screw not picked up correctly (b) Screw not in deep enough (c) Screw skewed

(d) Timber split (e) Structure too high (f) Gap between beams

Figure 56: Construction errors which required human intervention

Table 28: Number of construction errors per column part

	Part 1	**Part 2**	**Part 3**	**Part 4**
Screw not picked up correctly	0	0	1	0
Screw not in deep enough	3	0	0	0
Screw skewed	1	1	0	0
Timber split	0	0	1	0
Structure too high	6	1	0	0
Gap between beams	2	3	1	2
Total	**12**	**5**	**3**	**2**

In total one screw is not picked up correctly, due to small inaccuracies in the robot, the calibration of the tool and the location of the screw holder. Furthermore, during construction of the first part, the screws were not always in deep enough. After adjusting the sensor height again, this error is fixed completely.

For all column parts in total two screws were skewed, both due to knots in the timber. Also, one time the timber split, due to an already existing crack in the beam. Both these errors are easily fixed by checking the timber carefully for knots and cracks beforehand.

Another error is that the actual structure was sometimes a few millimeters higher or lower than the programmed values, so the beam is not always pushed down with the same force by the gripper. When the structure is higher than expected, the robotic arm with gripper wants to push too hard down on the structure. This is fixed by adjusting the programmed height by adding a bit of space (on average 0.4 mm) between each layer of beams. However, when the structure is a bit lower than expected, the beam is not pushed down hard enough. When the timber beam is not pushed down, the beam can move upwards during screwing, which leads to a gap between the stacked beams. This error could unfortunately not be easily fixed during the construction of the column.

In total 188 screws and 102 beams are placed. The success rate of the different construction steps can be found in Table 29.

Table 29: Success rate per construction step

Step	**Success rate [%]**
Pick up screw	99.5
Place screw	100.0
Screw	96.8
Pick up beam	100.0
Place beam	85.3
Total	**96.3**

At last, the four column parts are assembled manually with steel corner brackets. Each corner bracket is connected with four 5x40 screws. The shear capacity is 2.13 kN (see Appendix E) and the tension capacity is 3.24 kN (Equation 4-6), which is sufficiently strong.

5 Result

The column that is chosen to be constructed is one of the optimized columns from the asymmetric structure, which can be seen in Figure 57a. The robotically constructed timber column can be seen in Figure 57b and 58. A video is made of the robotic construction process (Vrenken, 2023).

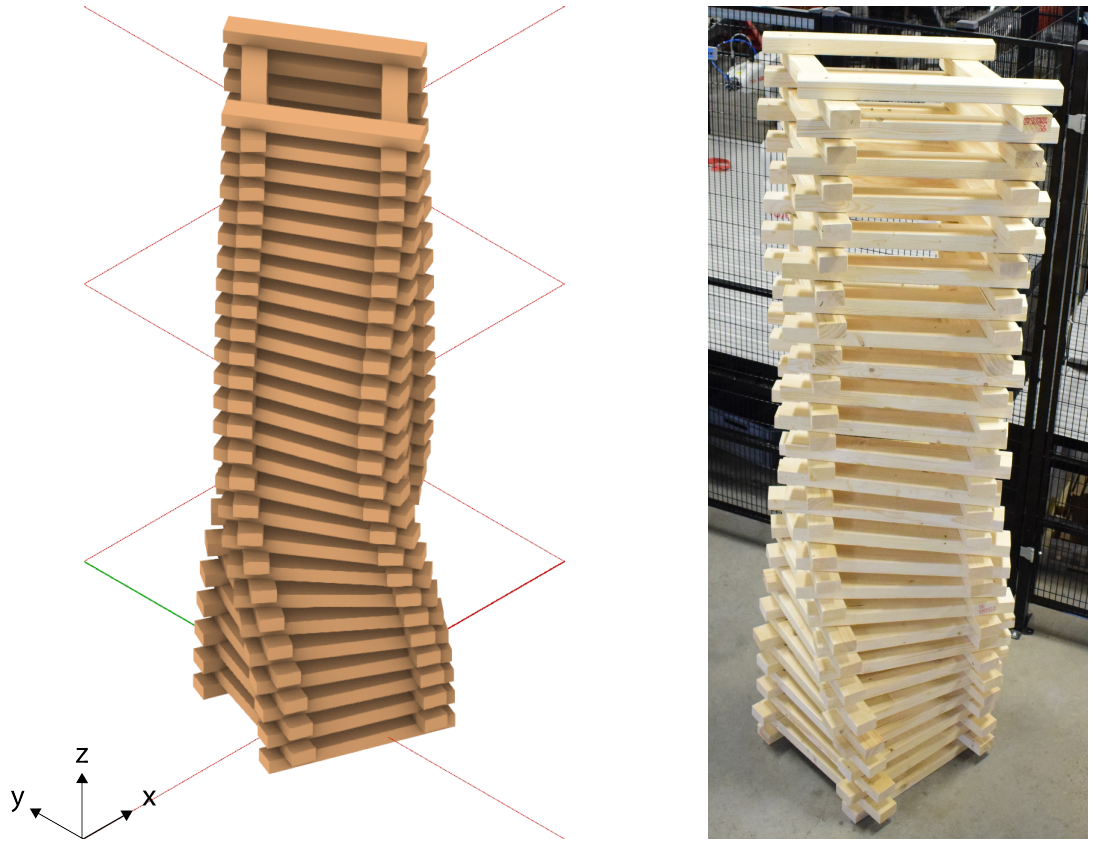

(a) Parametric design

(b) Robotically constructed result

Figure 57: Comparison design versus robotic construction

Figure 58: Photos robotically constructed column

6 Discussion

The discussion is done in two parts: discussion on the parametric design and the discussion on the robotic assembly.

6.1 Design

The global design is kept relatively simple and safe: rectangular beams with the same size that are stacked on top of each other. It can be argued that in this column design, the timber is not used in the most efficient way, because the highest forces are oriented perpendicular to the fiber direction of the beams. A column could be made with less timber when the highest internal forces are in line with the timber fiber direction, for example in a truss structure. However, the current stacked design is chosen because during the design phase there were many uncertainties on how the robotic assembly process would go (what is possible, how much force does screwing exert on the structure, how precise are the robots etc.). Also, because of the limited arm reach of the robots, it was not possible to create a very wide structure, so the beams had to be stacked on top of each other.

With the structural calculations on the column, some assumptions and approximations are made. For example, the rotational stiffness of the screw joints, the stiffness properties of the CLT roof and the wind load on the columns and roof. A different assumption or approximation could lead to significantly different results in the structural verification and optimization. In the time span of the project the properties and loads are substantiated as far as possible. However, when the structure would be built in real life, some extra verification is needed on the stiffness properties of the joints and the wind loading. This can be done by for example testing the properties of the robotically assembled screw joint and putting a (scale) model in a wind tunnel.

Then for the optimization, the main goal is of course to use as little material as possible. However, in the optimization process the amount of material is not minimized, but the most critical internal force (tension in the screw joint), which then indirectly can lead to less material use. This is done because the timber and screws come in limited, discrete sizes, so it is not possible to gradually optimize these. Another possibility would be to optimize the structure according to the lowest Unity Check, so in this case minimizing the combination of tension and shear in the screw joint. This could possibly lead to an even more efficient structure. However, the result of the optimization would become unexplainable, because multiple criteria are minimized simultaneously. Therefore, it is chosen to only focus on limiting one internal force, so that the optimization process could be analyzed more clearly and the result would be explainable.

6.2 Assembly

The original idea was to have no manual construction steps, but this is simply not possible when creating a larger structure. A compromise is found by making a full scale structure in multiple small parts. The manual step can completely be removed when making a smaller structure, when the reach of the robot arms is enlarged, or when the robots can move. However, this could also lead to bigger inaccuracies that have to be taken into account.

Furthermore, some human intervention was needed during the robotic construction. Most errors found during construction could be immediately solved, only the placement of the beams could still be improved further. The main problem is that the height of the structure varies a few millimeters, so the beams are sometimes pushed down too much and sometimes not pushed down enough. One solution could be to add a spring in the gripper end effector, that can account for small inaccuracies in the height. Another solution could be to use the data from the proximity sensor as a correction for the structure height. During screwing, the coordinates at which the sensor detects the timber are stored. These coordinates can be used as a reference height for the beams that are put in the next layer. If the structure height is known more

precisely, the downwards force can be controlled more precisely. Another solution could be to add a force sensor to the gripper, so that the gripper can apply an equal amount of downwards pressure on the beam every time. It is expected that with this improvement a significantly higher success rate can be achieved. Another quick solution to fix the space in between the beams could also be to use partially threaded screws, so the beam is not pushed upwards as much during screwing.

Lastly, in the final column it can be seen that the extension of the beams outside the structure vary quite much. At first, it was thought that this was due to some inaccuracies in the robot and gripper calibration. However, the variation in extension seemed to be a pattern. It is found that the beams that were placed in one direction in the beam stack, were picked up just a few millimeters right from the middle. This caused the extension of the beam to vary every six beams. The expected cause of this imperfection is that the beams were not exactly 600 mm in length, because during sawing a few millimeters of material was removed from each beam. Furthermore, the template for the beam stack is made and tested for a beam width of 69 mm, but the beams ordered for the column were suddenly 70 mm in width. These variations made it more difficult to calibrate the beam stack correctly, which led to a small offset. Unfortunately, this was only discovered after the construction of the full column.

7 Conclusion

The conclusions for the different research questions are individually elaborated below.

- **What type of structure can be made by robotic assembly and what design options are possible?**
  The robotic assembly of the structure creates a lot of design freedom, because designs can have complex angles and variations, without causing extra complex tasks for the robots. However, the robotic assembly also causes some limitations. The size of the structure is very limited by the available reach of the robots. Also, the element forms are limited to (somewhat) rectangular beams by the way they have to be picked up, in this case with a gripper. Furthermore, robotic screwing exerts quite some force on the structure during construction. Because during the design phase the newly developed, robotic assembly process still had many uncertainties, a relatively safe design is chosen. Therefore, the chosen design consists of rectangular elements of the same size stacked on top of each other. By varying the angle on which the beams are stacked, interesting forms can be created.

- **What is the structural capacity of the (robotically assembled) connection detail?**
  The structural capacity of the robotically assembled detail is approximated by the Eurocode formulas of a regular screw joint. The screw joint in the column has a tension capacity of 1.63 kN and a shear capacity of 1.94 kN.

- **How can we use parametric design for optimisation in structural behaviour and robotic production?**
  By creating a parametric design, the features of the structure can be easily tuned. The effect of changing a variable can be calculated immediately, which gives the opportunity to optimize the variables of a structure relatively easy. In this project, an optimized column form is found, which performs better than a simple straight column with the same amount of material: the most critical Unity Check is about 5% lower. The optimized form would be nearly impossible to construct by hand, because of the variation in angles and screw positions. By directly inserting the coordinates and orientation of the materials into a robotic assembly process, any form is possible. The set up of the optimization and assembly process costs some time, but eventually leads to easy mass customization, shorter production times and more sustainable (optimized) structures.

- **Is the structure able to withstand the applied loads?**
  All the structural checks done on the structure in section 3.5 are sufficient. Therefore, it is assumed that the structure is able to withstand the applied loads.

- **What timber joining methods are possible and which of these methods is the most promising to execute with robots?**
  In total four different possible joining methods are found: screwing, nailing, adhesive and Japanese joinery. A Multi Criteria Analysis is done on all methods, with criteria on applicability, strength, simplicity and sustainability. It is concluded that in this case screwing is the most promising option to execute with the robots.

- **What should the robotic assembly set-up look like and what materials, end effectors and other parts are required for this?**
  To assemble a timber structure with screws, the robotic set up needs to be able to: pick and place timber beams, pick and place screws and screw. In this case this is done by two robots that can work together, of which one handles the screwing and one handles the timber beams. For the whole screwing process, a screw end effector is made with a

pneumatic screw machine, a magnetic screw holder and a capacitive proximity sensor. To pick and place the timber a pneumatic gripper is used. At last, something is needed where the timber and the screws can be stocked in reach of the robot arms. In this case this is done by a screw holder and a ground template for the beams.

- **How should the assembly procedure be programmed?**
  In the assembly procedure the path planning is carefully determined, so that the robots can reach their targets without collisions or singularity issues. In this case the two robots are placed on opposite corners of the structure, so that they approach from different directions. Also, fly by points are added, so that the robots move around each other. Furthermore, the robots need to be able to work together. To do this, multi move synchronizations points are added in the robot code, so that the robots wait for each other to perform the next task. The building sequence is programmed as followed: (1) Robot 1 picks up a screw and Robot 2 picks up a beam simultaneously, (2) Robot 2 places the beam in the correct position, (3) Robot 1 screws in two screws. The whole assembly procedure is simulated beforehand with collision checks between all geometries to verify a safe construction.

- **Can the set-up be optimized further?**
  The robotic assembly set up is optimized by adding a capacitive proximity sensor to the screwing end effector, which makes sure that the screw is always screwed in to approximately the same depth. The set up can be optimized even further by adding a solution for the robot with gripper end effector to account for inaccuracies of the structure height (e.g. a spring or a sensor).

All in all, the objective to design, engineer and robotically assemble a parametric timber structure is achieved. A column structure is optimized and structurally improved compared to a simple, straight column. This column is robotically constructed with two robot arms, one with a gripper end effector and one with a screwing end effector. The success rate of all robotic construction steps is currently 96.3%, but has the potential to increase even further.

8 Recommendation

For a future project, a more challenging design could be made where the timber is used in a more efficient way. It is possible to construct with different element sizes and forms, for example in a layered (and scaled) truss structure or even a spatial structure (see examples in Figure 59). Because the robotic set up is now already available, ideas could be tested early in the design process.

Another step that could be done is to improve the current robotic assembly set-up even further. One improvement could be to reduce the need for human intervention. The main problem currently is that the height of the structure varies a few millimeters, so the beams are sometimes pushed down too much and sometimes not pushed down enough. This can be solved by adding a spring or force sensor to the gripper, by using the sensor data of the proximity sensor to correct for the structure height, or by using different screws. Another improvement could be to increase the accuracy in x, y and z by adding a wrist camera, which could be helpful when the location of the beams requires more precision in for example a spatial structure. Furthermore, as a small improvement it is recommended to include a spring in the sensor bracket. This way, when the sensor feedback fails, the sensor is gently pushed upwards with the spring. This prevents damaging to the sensor and/or sensor bracket.

Lastly, a next project could be to add and combine different construction steps to the process. One step could be to add predrilling of the timber. The benefits of this are that the capacity of the screw connection increases, the required distances between screws and edges decrease and the risk of splitting and skewed screws decreases. Another construction step could be to robotically saw the timber in the right length and angle. The benefit of this is that the design freedom increases, because every length and angle can be precisely sawn by the robots. A solution to achieve this is by adding a stationary drill/saw to the setup. Then, the robot that picks and places the beams could move towards the drill/saw and modify the beam before placing it in the correct location.

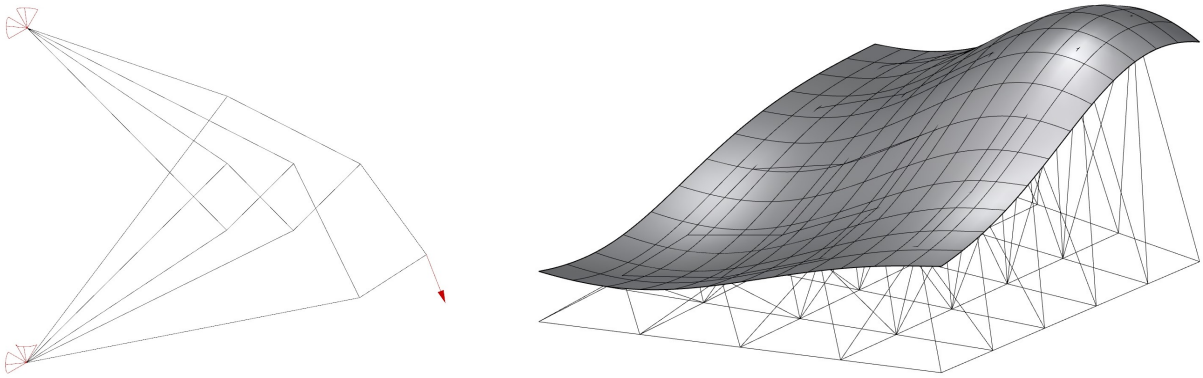

(a) Layered truss structure

(b) Spatial structure

Figure 59: Examples of possible future designs

References

ABB. (2022a, 6). *Product specification ABB IRB 1200.* Retrieved from https://search.abb.com/library/Download.aspx?DocumentID=3HAC046982-001&LanguageCode=en&DocumentPartId=&Action=Launch

ABB. (2022b, 6). *Product specification ABB IRB 1600/1660.* Retrieved from https://search.abb.com/library/Download.aspx?DocumentID=3HAC023604-001&LanguageCode=en&DocumentPartId=&Action=Launch

Apolinarska, A. A., Bärtschi, R., Furrer, R., Gramazio, F., & Kohler, M. (2016). Mastering the "Sequential Roof". *Advances in Architectural Geometry 2016*, 240 - 258. doi: 10.3218/3778-4-17

Archello. (2009). *West Fest Pavilion.* Retrieved from https://archello.com/project/west-fest-pavilion

Autosen. (n.d.). *AC006 Capacitive sensor M8x1 thread Standard Class IP67.* Retrieved from https://autosen.com/en/Position-Sensors/Capacitive-sensors/Standard-Class/Capacitive-sensor-M8x1-thread-Standard-Class-IP67-AC006

Eurocable. (n.d.). Cable constructions. Retrieved from https://www.eurocable.be/assets/cms/catalogue/Eurocable_1-1-7.pdf

Eversmann, P., Gramazio, F., & Kohler, M. (2017, 9). Robotic prefabrication of timber structures: towards automated large-scale spatial assembly. *Construction Robotics*, *1*. doi: 10.1007/s41693-017-0006-2

FPInnovations. (2019). *Canadian CLT Handbook* (SP-532E ed., Vol. I; E. Karacabeyli & S. Gagnon, Eds.).

Graser, K., Baur, M., Apolinarska, A., Dörfler, K., Hack, N., Jipa, A., ... Kohler, M. (2020, 4). DFAB HOUSE - A Comprehensive Demonstrator of Digital Fabrication in Architecture. In *Fabr. 2020 mak. resilient archit.* (pp. 130–139). doi: 10.2307/j.ctv13xpsvw.21

Hass, L., & Bos, F. (2022). Robotically Placed Reinforcement Using the Automated Screwing Device – An Application Perspective for 3D Concrete Printing. *RILEM Bookseries*, *37*, 417 – 423. Retrieved from https://www.scopus.com/inward/record.uri?eid=2-s2.0-85133180798&doi=10.1007%2f978-3-031-06116-5_62&partnerID=40&md5=6d41eabdeb040a204986b6bf780f4a53 doi: 10.1007/978-3-031-06116-5{_}62

Hughes, R., Österlund, T., & Larsen, N. M. (2021, 9). Integrated design-for-manufacturing and AR-aided-assembly workflows for lightweight reciprocal frame timber structures. *Construction Robotics*, *5*. doi: 10.1007/s41693-020-00048-3

Jung, K., Zhang, C., Harris, R., & Chang, W.-S. (2019, 12). Drive-In Torque for Self-Tapping Screws into Timber. *Construction Materials*, *175*. doi: 10.1680/jcoma.18.00087

Koerner-Al-Rawi, J., Park, K. E., Phillips, T. K., Pickoff, M., & Tortorici, N. (2020). Robotic timber assembly. *Construction Robotics*, *4*(3), 175–185. Retrieved from https://doi.org/10.1007/s41693-020-00045-6 doi: 10.1007/s41693-020-00045-6

Kumpenza, C., Schmidt, G.-D., Sotayo, A., Ringhofer, A., & Müller, U. (2020). Study on torque and clamping forces of screw-connected plywood. *Engineering Reports*, *2*(7), e12211. Retrieved from https://onlinelibrary.wiley.com/doi/abs/10.1002/eng2.12211 doi: https://doi.org/10.1002/eng2.12211

Kunic, A., Kramberger, A., & Naboni, R. (2021, 9). Cyber-Physical Robotic Process for Re-Configurable Wood Architecture Closing the circular loop in wood architecture. *Digital fabrication and robotics*, *2*.

Makita. (n.d.). *Assortiment.* Retrieved from https://www.makita.nl/

NOS Nieuws. (2021, 2). *Schreeuwend tekort aan woningen, wat moet eraan gedaan worden?* Retrieved from https://nos.nl/artikel/2369109-schreeuwend-tekort-aan-woningen-wat-moet-eraan-gedaan-worden

NRP 66 Research Project. (2017). *Additive Robotic Fabrication of Complex Timber Structures.* Retrieved from https://gramaziokohler.arch.ethz.ch/web/e/forschung/184.html

Oberg, E., Valentine, A., & Stable, J. M. (1910). Screw thread cutting, 3rd Ed. *The Industrial Press*, 4.

Rijksoverheid. (2021, 10). *Uitvoeringsprogramma Circulaire Economie 2021-2023.* Retrieved from https://open.overheid.nl/repository/ronl-669a180a-7f09-4336-890c-633cf2c3b852/1/pdf/uitvoeringsprogramma-circulaire-economie.pdf

Rodac. (n.d.). *RC3460 Schroevendraaier 550 RPM Push Start.* Retrieved from https://shop.rodac.com/store4u/showFile.aspx?language=NL&fileType=Artikel

SPAX. (2017). *SPAX Design Guide - ETA and EC5* (Tech. Rep.). Retrieved from https://www.spaxpacific.com/en/service/service/catalogues-brochures/

Sumake Industrial. (n.d.). *Products.* Retrieved from https://www.sumake.com/

Vrenken, L. (2023, 3). *Robotic Assembly of a Parametric Timber Column.* [video] YouTube. Retrieved from https://www.youtube.com/watch?v=ZgWgojllBio

WERA. (n.d.). *Producten.* Retrieved from https://www-de.wera.de/nl

Appendix

A Design concepts

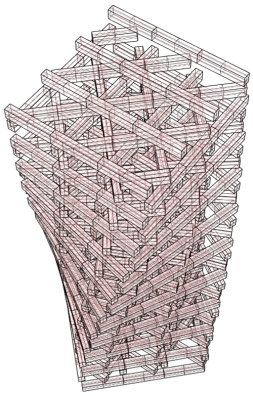

(a) Column with variation of layers

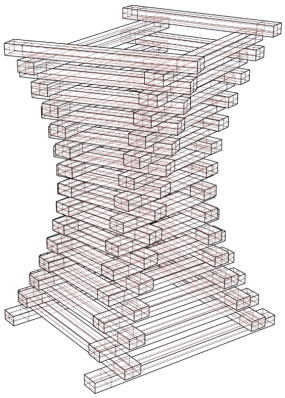

(b) Column with width variation and twist

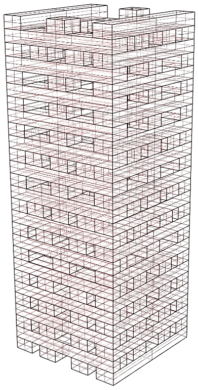

(c) Column with extra small blocks (randomly positioned)

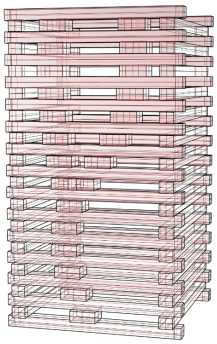

(d) Column with extra small blocks (positioned along curve)

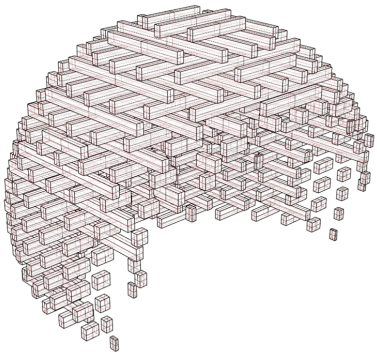

(e) Spherical pavilion with layers in 2 directions

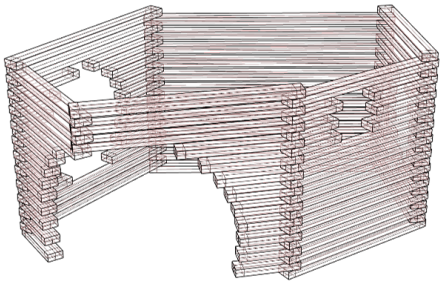

(f) Pavilion with randomly placed round holes

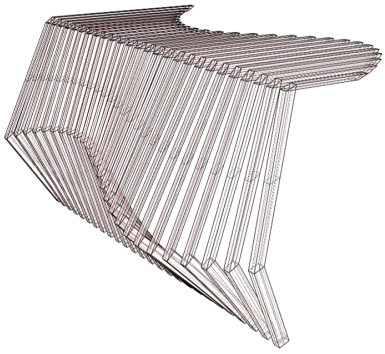

(g) Pavilion which follows curves

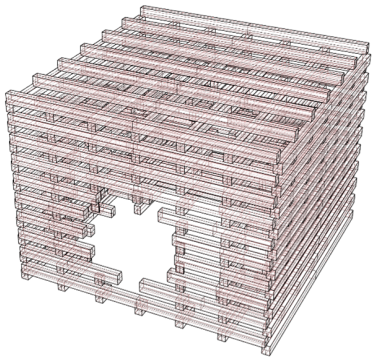

(h) Square pavilion with layers in 2 directions

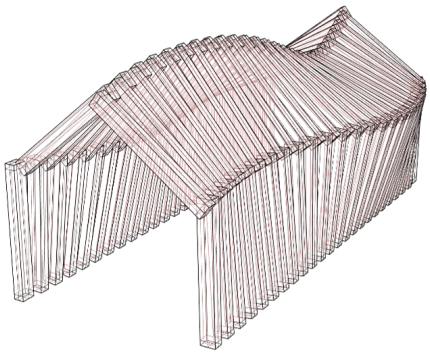

(i) Pavilion with equal beam sizes

Figure 60: Several design concepts

B Material properties

For the timber beams, strength class C24 is chosen, because it is one of the most widely available types. The material properties of C24 can be found in Table 30 (retrieved from NEN-EN 338:2016, Table 1). For the roof GL24h is used, again for its common availability. These material properties can be found in Table 31 (retrieved from NEN-EN 1194:1999, Table 1). The cable used is a 5x19 Fibre Core (FC), with a diameter of 8 mm, of which the properties can be found in Table 32 (Eurocable, n.d.).

Table 30: Material properties C24

Property	**Symbol**	**Value**
Strength		$[N/mm^2]$
Bending	$f_{m,k}$	24
Tension parallel	$f_{t,0,k}$	14.5
Tension perpendicular	$f_{t,90,k}$	0.4
Compression parallel	$f_{c,0,k}$	21
Compression perpendicular	$f_{c,90,k}$	2.5
Shear	$f_{v,k}$	4.0
Stiffness		$[kN/mm^2]$
Mean modulus of elasticity parallel	$E_{m,0,mean}$	11.0
5% modulus of elasticity parallel	$E_{m,0,k}$	7.4
Mean modulus of elasticity perpendicular	$E_{m,90,mean}$	0.37
Mean shear modulus	G_{mean}	0.69
Density		$[kg/m^3]$
5% density	ρ_k	350
Mean density	ρ_{mean}	420

Table 31: Material properties GL24h

Property	**Symbol**	**Value**
Strength		$[N/mm^2]$
Bending	$f_{m,g,k}$	24
Tension parallel	$f_{t,0,g,k}$	16.5
Tension perpendicular	$f_{t,90,g,k}$	0.4
Compression parallel	$f_{c,0,g,k}$	24
Compression perpendicular	$f_{c,90,g,k}$	2.7
Shear	$f_{v,g,k}$	2.7
Stiffness		$[kN/mm^2]$
Mean modulus of elasticity parallel	$E_{0,g,mean}$	11.6
5% modulus of elasticity parallel	$E_{0,g,05}$	9.4
Mean modulus of elasticity perpendicular	$E_{90,g,mean}$	0.39
Mean shear modulus	$G_{g,mean}$	0.72
Density		$[kg/m^3]$
Characteristic density	$\rho_{g,k}$	380
Mean density	$\rho_{g,mean}$	462

Table 32: Material properties 6x19 FC 1770 Cable

f_t $[N/mm^2]$	F_{bl} $[kN]$	E $[MPa]$	ρ $[kg/m]$	A $[mm^2]$
1770	37.0	85.000	0.22	24

C Loads

C.1 Imposed loads

- The design is a roof structure which is not accessible other than for maintenance. Therefore the structure belongs in Category H (NEN-EN 1991-1-1:2002, Table 6.9). The angle of the roof is 0°. The imposed loads on the roof can be seen in Figure 61.

Klasse van belaste oppervlakte	Dakhelling α	q_k kN/m^2	Q_k[b] kN
H (niet toegankelijk) [a]	$0 \leq \alpha < 15°$	1,0	1,5
	$15° \leq \alpha < 20°$	$4 - 0{,}2 \times \alpha$	
	$\alpha \geq 20°$	0	
H (wel toegankelijk)	Zie tabel NB.1 - 6.2		
H (onder maaiveld gelegen ruimten, geen verkeersbelasting)		4	7
[a] De belasting q_k werkt op een oppervlakte A van 10 m^2, binnen de grenzen van nul tot het hele dakoppervlak.[b] Werkend op een oppervlakte van 0,1 m × 0,1 m.			

Figure 61: Imposed loads roof (NEN-EN 1991-1-1:2002, Table NB.4 – 6.10)

C.2 Wind load

- The structure is located in Eindhoven, which lays in wind area III (see Figure 62).

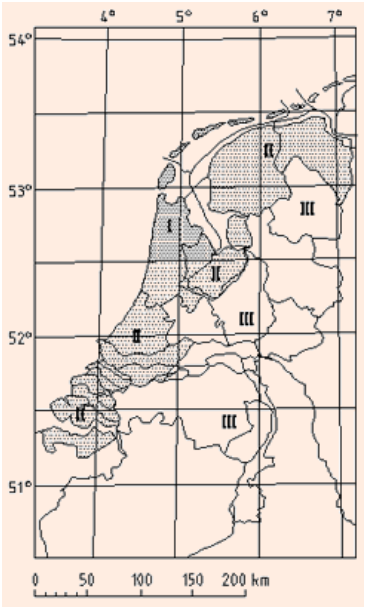

Figure 62: Wind areas in the Netherlands (NEN-EN 1991-1-1:2002, Figure NB.1)

- The extreme wind pressure q_p can be seen in Figure 63.

Hoogte m	Gebied I			Gebied II			Gebied III	
	Kust	Onbebouwd	Bebouwd	Kust	Onbebouwd	Bebouwd	Onbebouwd	Bebouwd
1	0,93	0,71	0,69	0,78	0,60	0,58	0,49	0,48
2	1,11	0,71	0,69	0,93	0,60	0,58	0,49	0,48
3	1,22	0,71	0,69	1,02	0,60	0,58	0,49	0,48
4	1,30	0,71	0,69	1,09	0,60	0,58	0,49	0,48
5	1,37	0,78	0,69	1,14	0,66	0,58	0,54	0,48
6	1,42	0,84	0,69	1,19	0,71	0,58	0,58	0,48
7	1,47	0,89	0,69	1,23	0,75	0,58	0,62	0,48
8	1,51	0,94	0,73	1,26	0,79	0,62	0,65	0,51
9	1,55	0,98	0,77	1,29	0,82	0,65	0,68	0,53
10	1,58	1,02	0,81	1,32	0,85	0,68	0,70	0,56

Figure 63: Extreme wind pressure q_p $[kN/m^2]$ (NEN-EN 1991-1-1:2002, Table NB.4 – 6.10)

- Because the wind is applied on all timber elements individually and these have a load area of less than 1 m^2, $c_{pe,1}$ coefficients are used (no $c_{pe,10}$). The column is seen as a vertical structure with a rectangular floor area. The external wind pressure and suction coefficients are retrieved from Figure 64. The h/d factor of the column is approximately 3.7. As a simplification, this suction coefficient with h/d factor 5 is applied over the full height of the column. The external pressure coefficient (area D) is +1.0. The external suction coefficient (area E) on the top is -0.7. No seperate internal wind load is applied, because the structure is open.

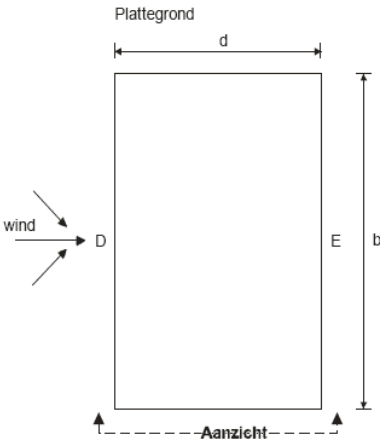

(a) Areas

Zone	A		B		C		D		E	
h/d	$c_{pe,10}$	$c_{pe,1}$	$c_{pe,10}$	$c_{pe,1}$	$c_{pe,10}$	$c_{pe,1}$	$c_{pe,10}$	$c_{pe,1}$	$c_{pe,10}$	$c_{pe,1}$
5	-1,2	-1,4	-0,8	-1,1	-0,5		+0,8	+1,0	-0,7	
≤ 1	-1,2	-1,4	-0,8	-1,1	-0,5		+0,8	+1,0	-0,5	

(b) Coefficients

Figure 64: Wind pressure and suction coefficients on column (NEN-EN 1991-1-4:2005, section 7.2.2)

- The pressure and suction coefficients ($c_{p,net}$) are retrieved from Figure 65. The roof angle is 0° and the obstruction $\varphi = 0$.

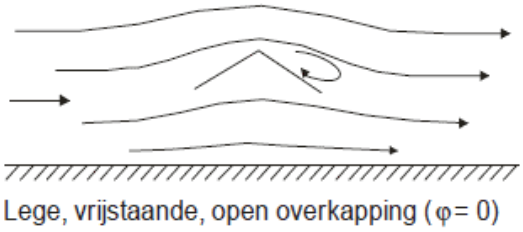

(a) Type

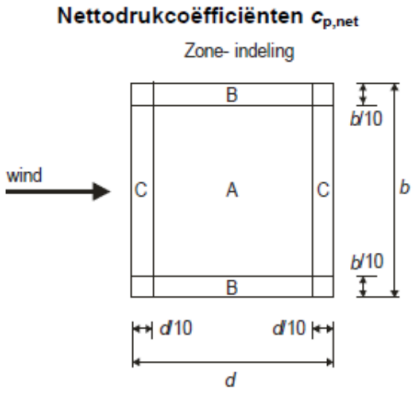

(b) Areas

Dakhelling α	Blokkering φ	Globale krachtcoëfficiënten c_f	Zone A	Zone B	Zone C
0°	Maximaal voor alle φ Minimaal voor φ = 0 Minimaal voor φ = 1	+ 0,2 - 0,5 - 1,3	+ 0,5 - 0,6 - 1,5	+ 1,8 - 1,3 - 1,8	+ 1,1 - 1,4 - 2,2

(c) Coefficients

Figure 65: Wind pressure and suction coefficients on roof (NEN-EN 1991-1-4:2005, section 7.3)

- The friction Area (A_{fr}) is calculated according to Equation 23. Both the top surface and the bottom surface of the roof are taken into account.

$$A_{fr} = 2A_{roof} = 22.0\,m^2 \tag{23}$$

In which:
A_{roof} = area of roof = 11.0 m^2

C.3 Load combinations

The structure is categorized in Consequence Class 1 (CC1), because there is a low consequence for loss of human life and social, economic or environmental consequences are small or negligible (NEN-EN 1990:2002, Table NB.23 – B1). The load combinations of the ULS for CC1 are taken from Figure 66. The load combinations for the SLS (characteristic, frequent and quasi-permanent) are taken from Figure 67. The partial factors (ψ_0, ψ_1 and ψ_2) are taken from Figure 68.

CC	Blijvende en tijdelijke ontwerpsituatie	Blijvende belastingen		Overheersende veranderlijke belasting	Veranderlijke belastingen gelijktijdig met de overheersende	
		Ongunstig	Gunstig		Belangrijkste (indien aanwezig)	Andere
1	(Vgl. 6.10a)	$1{,}2\ G_{k,j,sup}$ [a]	$0{,}9\ G_{k,j,inf}$		$1{,}35\ \Psi_{0,1}\ Q_{k,1}$	$1{,}35\ \Psi_{0,i}\ Q_{k,i}\ (i>1)$
	(Vgl. 6.10b)	$1{,}1\ G_{k,j,sup}$ [b]	$0{,}9\ G_{k,j,inf}$	$1{,}35\ Q_{k,1}$		$1{,}35\ \Psi_{0,i}\ Q_{k,i}\ (i>1)$
3	(Vgl. 6.10a)	$1{,}5\ G_{k,j,sup}$ [a]	$0{,}9\ G_{k,j,inf}$		$1{,}65\ \Psi_{0,1}\ Q_{k,1}$	$1{,}65\ \Psi_{0,i}\ Q_{k,i}\ (i>1)$
	(Vgl. 6.10b)	$1{,}3\ G_{k,j,sup}$ [b]	$0{,}9\ G_{k,j,inf}$	$1{,}65\ Q_{k,1}$		$1{,}65\ \Psi_{0,i}\ Q_{k,i}\ (i>1)$

Figure 66: Load combinations ULS (NEN-EN 1990:2002, Table NB.5)

Combinatie	Blijvende belastingen G_d		Veranderlijke belastingen Q_d	
	Ongunstig	Gunstig	Overheersende	Andere
Karakteristiek	$G_{kj,sup}$	$G_{kj,inf}$	$Q_{k,1}$	$\psi_{0,i}\ Q_{k,i}$
Frequent	$G_{kj,sup}$	$G_{kj,inf}$	$\psi_{1,1}\ Q_{k,1}$	$\psi_{2,i}\ Q_{k,i}$
Quasi-blijvend	$G_{kj,sup}$	$G_{kj,inf}$	$\psi_{2,1}\ Q_{k,1}$	$\psi_{2,i}\ Q_{k,i}$

Figure 67: Load combinations SLS (NEN-EN 1990:2002, Table A1.4)

Belasting	Ψ_0	Ψ_1	Ψ_2
Voorgeschreven belastingen in gebouwen, categorie			
Categorie A: woon- en verblijfsruimtes	0,4	0,5	0,3
Categorie B: kantoorruimtes	0,5	0,5	0,3
Categorie C: bijeenkomstruimtes	0,6/0,4 [a]	0,7	0,6
Categorie D: winkelruimtes	0,4	0,7	0,6
Categorie E: opslagruimtes	1,0	0,9	0,8
Categorie F: verkeersruimte, voertuiggewicht ≤ 25 kN	0,7	0,7	0,6
Categorie G: verkeersruimte [b], 25 kN < voertuiggewicht ≤ 160 kN	0,7	0,5	0,3
Categorie H: daken	0	0	0
Industrieel gebruik waarbij de veranderlijke belasting:			
— niet langdurig aanwezig is	0,5	0,5	0,3
— langdurig aanwezig is	1,0	0,9	0,8
Sneeuwbelasting	0	0,2	0
Belasting door regenwater	0	0	0
Windbelasting	0	0,2	0
Temperatuur (geen brand)	0	0,5	0

[a] De waarde 0,6 geldt voor delen van het gebouw die in geval van een calamiteit zwaar kunnen worden belast door een mensenmenigte (vluchtroutes, trappen enz.); de waarde 0,4 geldt in overige gevallen.

[b] Met verkeersruimte wordt in dit geval een ruimte bedoeld waar voertuigen kunnen rijden, bijvoorbeeld parkeergarages

Figure 68: Partial factors ψ (NEN-EN 1990:2002, Table NB.2 – A1.1)

D Loads on symmetric structure

D.1 Imposed load

The imposed loads are placed at the most unfavorable positions in the structure, see Figure 69. The area of the distributed load is 10 m^2.

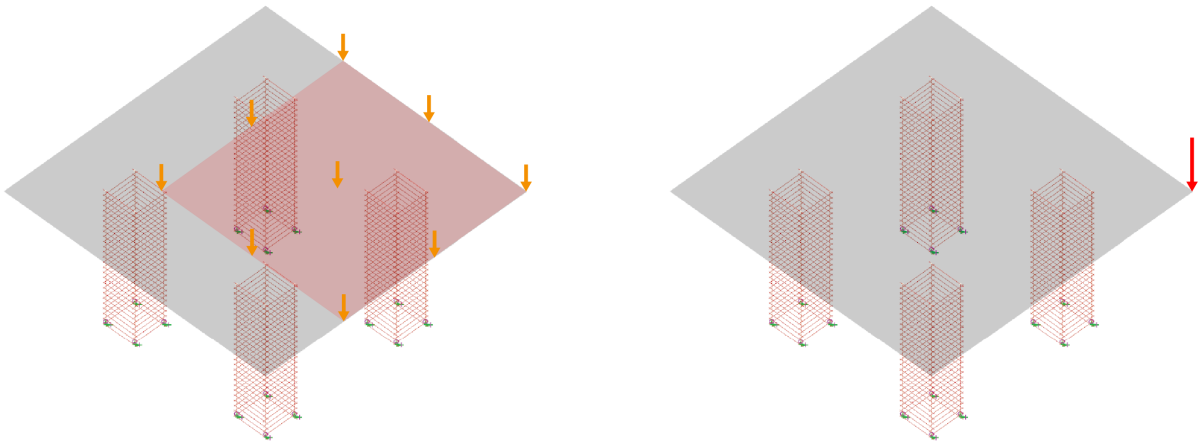

(a) Distributed load q (on 10 m^2)

(b) Point load Q

Figure 69: Imposed loads symmetric structure

D.2 Wind load

The roof is subdivided in the different areas that have different pressure coefficients, which are shown in Figure 13. The pressure and suction on the side of the roof are simply applied to the edges of the square. The friction on the roof (F_{fr}) is again calculated according to Equation 2. The wind friction is again applied as a point load in the middle of the roof. The application of the different wind loads can be seen in Figure 70.

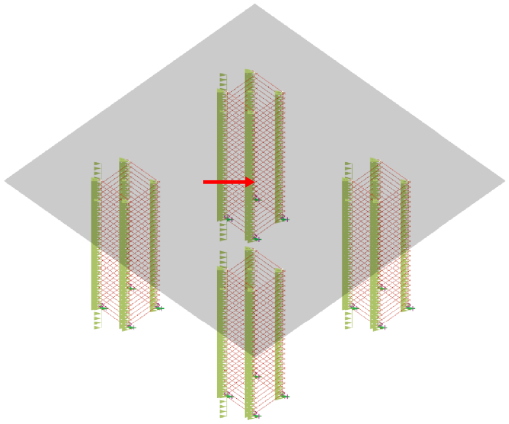

(a) Wind pressure and suction on columns and the side of the roof

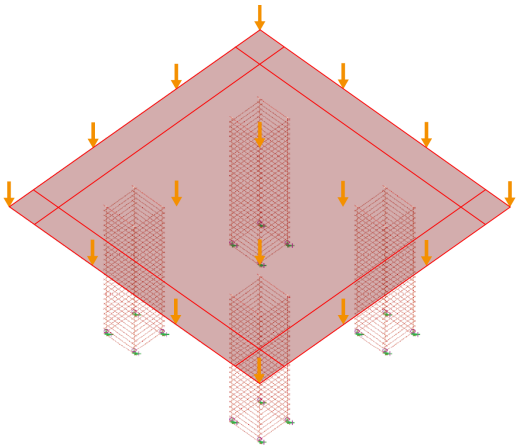

(b) Wind pressure and suction roof (varies per zone)

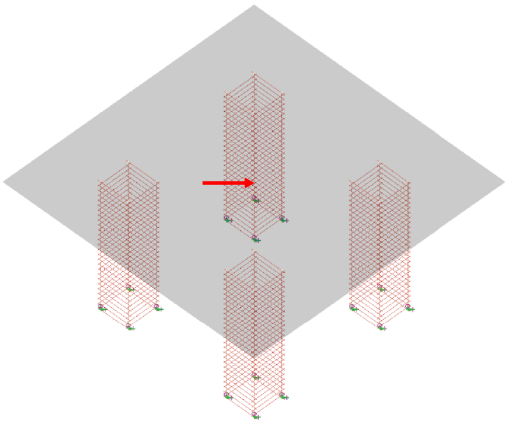

(c) Wind friction

Figure 70: Wind loads symmetric structure

D.3 Snow load

The snow load is applied on the full roof area, which can be seen in Figure 71.

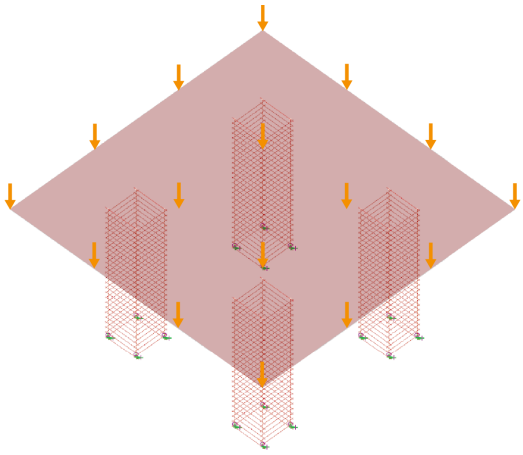

Figure 71: Snow load symmetric structure

E Screw calculations

- Pull-out strength $f_{ax,k}$ is calculated according to Equation 24 (NEN-EN 1995-1-1:2005, section 8.7.2).

$$f_{ax,k} = 0.52 d^{-0.5} l_{ef}^{-0.1} \rho_k^{0.8} = 17.6\, N/mm^2 \tag{24}$$

- Factor k_d is calculated according to Equation 25 (NEN-EN 1995-1-1:2005, section 8.7.2).

$$k_d = min(d/8, 1) = 0.625 \tag{25}$$

- Pull-through strength $f_{head,k}$ for the SPAX screws is calculated according to Equation 26 (SPAX, 2017).

$$f_{head,k} = 27 - d_h = 17.3\, N/mm^2 \tag{26}$$

- The characteristic embedment strength parallel to the grain $f_{h,1,k}$ and perpendicular to the grain $f_{h,2,k}$ without predrilled holes are calculated according to Equation 27 (NEN-EN 1995-1-1:2005, section 8.3.1).

$$f_{h,1,k} = f_{h,2,k} = 0.082 \rho_k d^{-0.3} = 17.7\, N/mm^2 \tag{27}$$

- The characteristic yield moment $M_{y,Rk}$ is calculated according to Equation 28 (NEN-EN 1995-1-1:2005, section 8.3.1).

$$M_{y,Rk} = 0.45 f_{uk} d^{2.6} = 23.6e3\, Nmm \tag{28}$$

  In which:
  f_{uk} = ultimate characteristic tension strength screw (grade 8.8) = 800 N/mm^2

- The shear capacity of the connection of the corner brackets with two times two 5x40 screws is calculated according to Equation 29. The steel bracket is a thin bracket because its thickness is less than $0.5d$ (NEN-EN 1995-1-1:2005, section 8.2.3).

$$F_{v,Rk} = min \begin{cases} 0.4 f_{h,k} t_1 d & (a) \\ 1.15\sqrt{2 M_{y,Rk} f_{h,k} d} + \frac{F_{ax,Rk}}{4} & (b) \end{cases} = 2.13\, kN \tag{29}$$

F Extra optimization results

The wind surface area of the symmetrical structure for every wind direction can be seen in Table 33. The reaction forces for optimization Load Combination 3 are given in Table 34. It can be seen that the maximum surface area (thus horizontal reaction force) of the optimized column is slightly smaller that the straight columns, however this difference is negligible. The minimal vertical reaction force of the optimized column is slightly smaller than the straight columns.

Table 33: Comparison wind surface area columns symmetrical structure

	Wind surface area $[m^2]$				
	x	**xy**	**y**	**-xy**	**Total**
0	5.39	7.62	5.39	7.62	26.02
45	7.62	5.39	7.62	5.39	26.02
Optimized	7.60	5.66	7.61	5.66	26.51

Table 34: Reaction forces symmetrical structure (Load Combination 2.3)

		Reaction force [kN]												
		1			**2**			**3**			**4**			**Total**
		x	**y**	**z**	**x**	**y**	**z**	**x**	**y**	**z**	**x**	**y**	**z**	**y**
0	**C1**	-0.01	-0.42	0.37	-0.01	-0.42	3.64	0.00	-0.42	0.35	0.00	-0.42	3.62	-1.67
	C2	0.00	-0.42	3.84	0.00	-0.42	0.56	0.01	-0.43	3.87	0.00	-0.42	0.57	-1.70
	C3	0.00	-0.42	3.85	0.00	-0.42	0.56	-0.01	-0.42	3.86	0.00	-0.42	0.57	-1.69
	C4	0.00	-0.42	0.37	0.01	-0.42	3.64	0.00	-0.42	0.35	0.00	-0.42	3.62	-1.67
	Total													-6.73
45	**C1**	-0.01	-0.56	-1.11	0.02	-0.58	1.88	-0.02	-0.58	1.93	0.00	-0.61	5.17	-2.34
	C2	0.00	-0.58	5.38	-0.01	-0.59	2.30	0.01	-0.59	2.25	0.00	-0.59	-0.92	-2.35
	C3	0.00	-0.58	5.38	0.01	-0.59	2.30	-0.01	-0.59	2.25	0.00	-0.59	-0.92	-2.35
	C4	0.01	-0.56	-1.11	-0.02	-0.58	1.88	0.02	-0.58	1.93	0.00	-0.61	5.17	-2.34
	Total													-9.36
Opt	**C1**	0.01	-0.54	-1.07	0.05	-0.57	2.13	-0.06	-0.59	1.94	0.00	-0.64	4.88	-2.34
	C2	0.00	-0.62	5.06	0.05	-0.59	2.28	-0.03	-0.57	2.46	-0.01	-0.56	-0.89	-2.34
	C3	0.00	-0.62	5.06	-0.05	-0.59	2.28	0.03	-0.57	2.46	0.01	-0.56	-0.89	-2.34
	C4	-0.01	-0.54	-1.07	-0.05	-0.57	2.13	0.06	-0.59	1.94	0.00	-0.64	4.88	-2.34
	Total													-9.35

G Unity Checks

G.1 Column beams

The timber beams in the column are checked in compression 0° (Equation 30), compression 90° (Equation 31), tension 0° (Equation 32), bending in y and z (Equation 33), torsion (Equation 34), shear (Equation 35), the combination of compression and bending in y and z (Equation 36) and the combination of tension and bending in y and z (Equation 37) (NEN-EN 1995-1-1:2005, section 6).

The UC with the combination of tension and shear in the joint is checked for every ULS load case individually. The total shear load is calculated as the resultant force of the shear in z and y.

$$UC_{c,0} = \frac{\sigma_{c,0,d}}{f_{c,0,d}} = 0.02 \tag{30}$$

$$UC_{c,90} = \frac{\sigma_{c,90,d}}{k_{c90} f_{c,90,d}} = 0.54 \tag{31}$$

$$UC_{t,0} = \frac{\sigma_{t,0,d}}{f_{t,0,d}} = 0.02 \tag{32}$$

$$UC_m = k_m \frac{\sigma_{m,d,1}}{f_{m,d}} + \frac{\sigma_{m,d,2}}{f_{m,d}} = 0.22(y),\ 0.17(z) \tag{33}$$

$$UC_v = \frac{\tau_d}{f_{v,d}} = 0.51 \tag{34}$$

$$UC_{tor} = \frac{\tau_{tor,d}}{k_{shape} f_{v,d}} = 0.00 \tag{35}$$

$$UC_{c,m} = (\frac{\sigma_{c,0,d}}{f_{c,0,d}})^2 + k_m \frac{\sigma_{m,d,1}}{f_{m,d}} + \frac{\sigma_{m,d,2}}{f_{m,d}} = 0.22(y),\ 0.17(z) \tag{36}$$

$$UC_{t,m} = (\frac{\sigma_{t,0,d}}{f_{t,0,d}}) + k_m \frac{\sigma_{m,d,1}}{f_{m,d}} + \frac{\sigma_{m,d,2}}{f_{m,d}} = 0.24(y),\ 0.19(z) \tag{37}$$

In which:
k_{c90} = factor for load combination and splitting = 1.0
k_m = factor for rectangular cross section = 0.7
k_{shape} = factor for shape in torsion = min(1+0.05*(b/h), 1.3) = 1.08

G.2 Screw connection

The screwed connection is checked for tension (Equation 38), shear (Equation 39) and the combination of tension and shear (Equation 40) (NEN-EN 1995-1-1:2005, section 8).

$$UC_{ax,screw} = \frac{F_{ax,Ed}}{F_{ax,Rd}} = 0.54 \tag{38}$$

$$UC_{v,screw} = \frac{F_{v,Ed}}{F_{v,Rd}} = 0.84 \tag{39}$$

$$UC_{ax,v,screw} = (\frac{F_{ax,Ed}}{F_{ax,Rd}})^2 + (\frac{F_{v,Ed}}{F_{v,Rd}})^2 = 1.00 \tag{40}$$

G.3 Pretensioned cable

The cable is checked in tension (Equation 41).

$$UC_{t,cable} = \frac{F_{t,cable,Ed}}{\frac{F_{bl}}{\gamma_{M2}}} = 0.26 \tag{41}$$

In which:
$F_{bl,d}$ = breaking load of the cable (6x19 FC 1770, d=8mm) = 37 kN (Eurocable, n.d.)
γ_{M2} = material factor steel = 1.25

G.4 CLT roof

The Unity Checks on the roof for the stress in the face and the shear are given in Equation 42 and 43. In this case the calculation of the design strength is done with a partial factor γ_M of 1.25 (Glulam) and a modification k_{mod} of 0.4 (CC3, permanent).

$$UC_{face,roof} = \frac{\sigma_{face,roof}}{f_{face,roof,Rd}} = 0.44 \tag{42}$$

$$UC_{v,roof} = \frac{t_{roof}}{f_{v,roof,Rd}} = 0.38 \tag{43}$$

H Screw machine options

Table 35: Screw machine options

Brand	Type	Form	Weight [kg]	Torque [Nm]	RPM	Drive	Price
Makita	DF001DW 3,6V Li-Ion accu schroef-/boormachine	Axial/L	0.36	6	220	3.6 V	€ 55.36
Bosch	Accu schroefmachine PushDrive 3,6V	Axial	0.3	? to 5	360	3.6 V	€ 59.99
Rodac	10133300A Luchtratel super mini 1/4	Axial	0.45	34	260	6.3 bar	€ 83.00
Bosch	GO Professional	Axial	0.3	? to 5	360	3.6 V	€ 85.99
Bosch	Professional Haakse accuboormachine	Axial/L	1.2	? to 11	0 to 1300	10.8 V	€ 101.33
Milwaukee	C12 RAD-0 12V accu haakse boor-/schroefmachine	L	0.9	? to 12	0 to 800	12 V	€ 101.64
Makita	DF012DSE Accu-knikschroefmachine 7.2 V	Axial/L	0.53	? to 3.6/5.6	0-200/0-650	7.2 V	€ 119.83
Proxxon	29840 Accu-knikschroefmachine 10.8 V 2.6 Ah Li-ion	Axial/L	0.6	0.25 to 5	0 to 750	10.8 V	€ 128.10
RS Pro	APT408 Straight Air Screwdriver	Axial	1.1	? to 10/14/17	1700	6.2 bar	€ 137.93
Prevost	Straight Air Screwdriver	Axial	1.3	5 to 13	1800	6.2 bar	€ 173.08
Sumake	Schroevendraaier L/R, 750 rpm, 1-9 Nm	Axial	0.8	1 to 9	750	6-8 bar	€ 175.00
Makita	DF012DSE 7.2V Electric Screwdriver, Euro Plug	Axial	0.55	? to 5.6	200/650	7.2 V	€ 183.00
Rodcraft	Rc4770 Schroevendraaier Recht	Axial	1.1	2 to 6	2000	6.3 bar	€ 219.00
Abac	Schroefmachine recht Pro	Axial	1.2	3 to 8	1700	6.3 bar	€ 226.80
Spedaire	21AA81 Luchtschroevendraaier	Axial	1.25	3.4 to 7.9	1800	6.2 bar	€ 264.00
Senco	SEN612C 800 rpm push-in	Pistol	1.2	16.4	800	6.2-8 bar	€ 297.52
Würth	PNEUMATISCHE AXIALE SCHROEVENDRAAIER	Axial	1.2	2.2 to 10	0 to 1800	6.3 bar	€ ±300
Sam	Schroevendraaier recht (out of stock)	Axial	1.4	? to 10	0 to 1800	6.5 bar	€ 409.00
Senco	SEN611C, 800 rpm push-in instelbare koppeling	Pistol	1.2	? to 10.7	800	6.2 bar	€ 437.19
ASG	HP65 (does not deliver to NL)	Axial	0.8	2.9 to 14.1	300	6.2 bar	€ 450.77
Chicago Pneumatic	CP2621 Industrial Push Start Air Screwdriver	Axial	0.8	0.8 to 6.5	1000	?	€ 460.65
Senco	SEN610C, 1800 rpm push-in instelbare koppeling	Pistol	1.1	? to 7.9	1800	6.2 bar	€ 491.74
Sumake	Air Torque Screwdriver FP075	Axial	0.88	1.2 to 7.3	1000	5.9 bar	€ 696.48
Rodac	RC3460 Schroevendraaier 550 rpm Push Start	Axial	0.79	1.5 to 9.5	550	6.3 bar	€ 679.00
Sumake	Air Torque Screwdriver FL110	Axial	0.9	2.9 to 10.8	550	5.9 bar	€ 732.15
NITTO KOHKI	DLV70A06P-ABK	Axial	0.87	3.8 to 7.0	650	230 V	€ 894.00
Desoutter	SC2-065-2RM500-S4Q	Axial	0.64	3 to 6.5	500	6.3 bar	€ 1,502.41
Ingersoll Rand	41SC10PSQ4-EU or 41SC17LTQ4-EU	Axial	1.4	1.1 to 9	1000	?	€ 1,750.00
NITTO KOHKI	DLV70S06P-AYK	Axial	0.86	3.8 to 7.0	280 to 650	DC40V	€ 1,803.80
Deprag	346-738-31 and 406109C	Axial	1.6	2 to 9	1400	6.3 bar	€ 2,665.00
OnRobot	Screwdriver	Axial	2.5	0.15 to 5	340	24 V	€ 10,850.00
MyTorq	Corded electric screwdriver MYR/MYR-TR 0309L/P	Axial	1.03	3 to 9	900	40 V	?
Sumake	EA-BAN990P/C6	Axial	1.2	3 to 9	800	DC40V	?
Mountz	MDA3211-A Robotic Screwdriver	Axial	1	1 to 8.8	50 to 690	DC 38 V	?
Kuani	KI-35005-STUA (does not deliver to NL)	Axial	1	1.5 to 10.5	480/800/1700	6.2 bar	?

I CAD files

I.1 Final screw holder

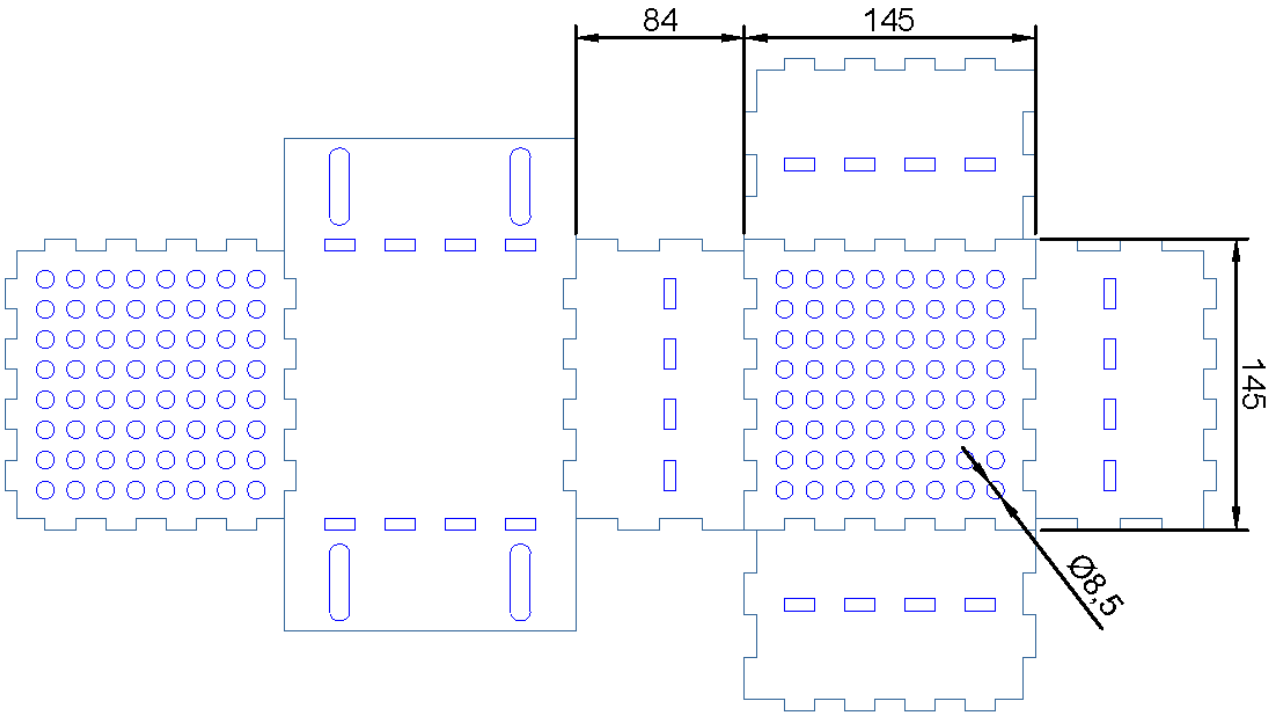

Figure 72: Screw holder

I.2 Sensor bracket

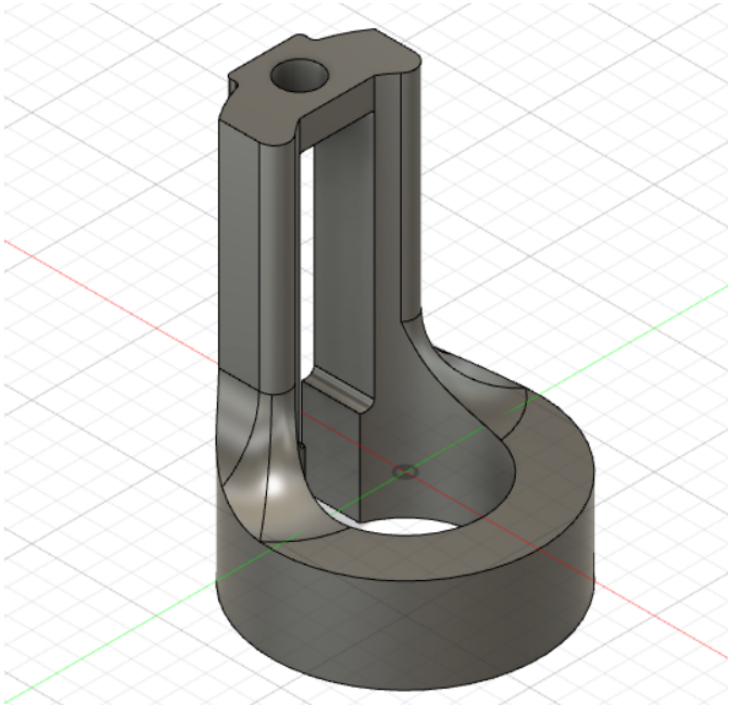

Figure 73: Sensor bracket

I.3 Robot positions

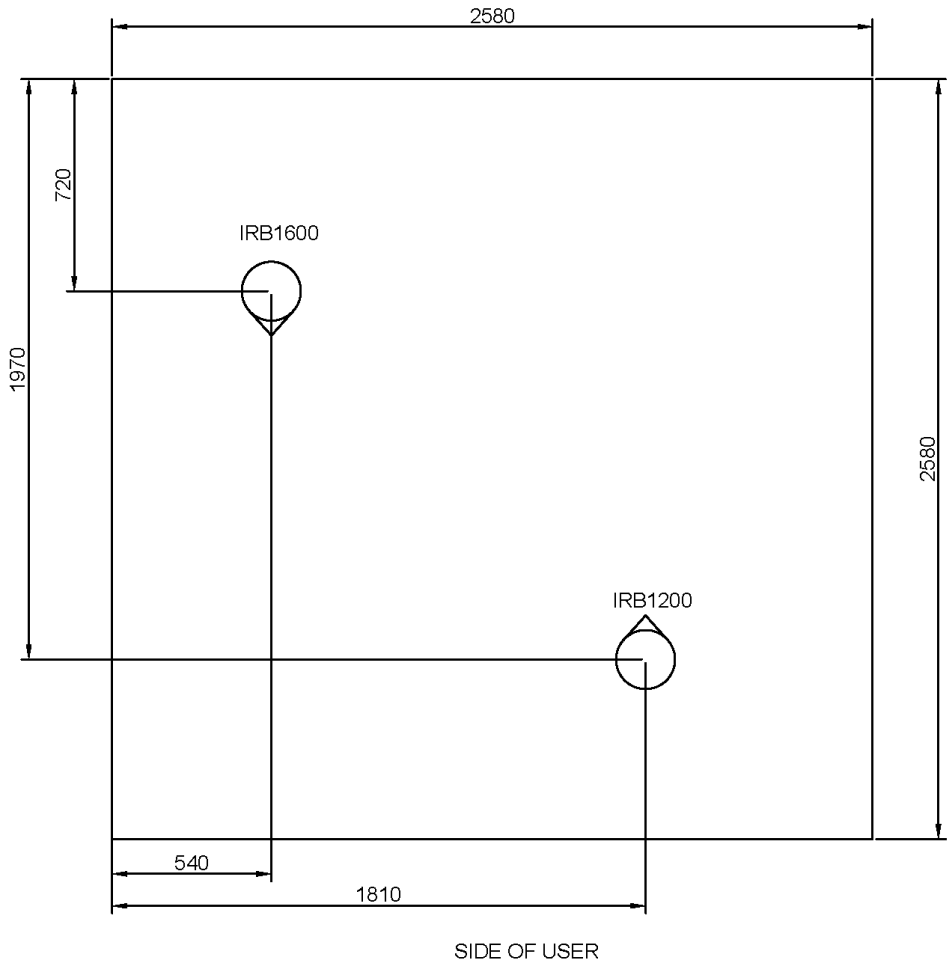

Figure 74: Robot positions

Figure 75: Test screw pick up station for different screw sizes

J Grasshopper script

J.1 Design

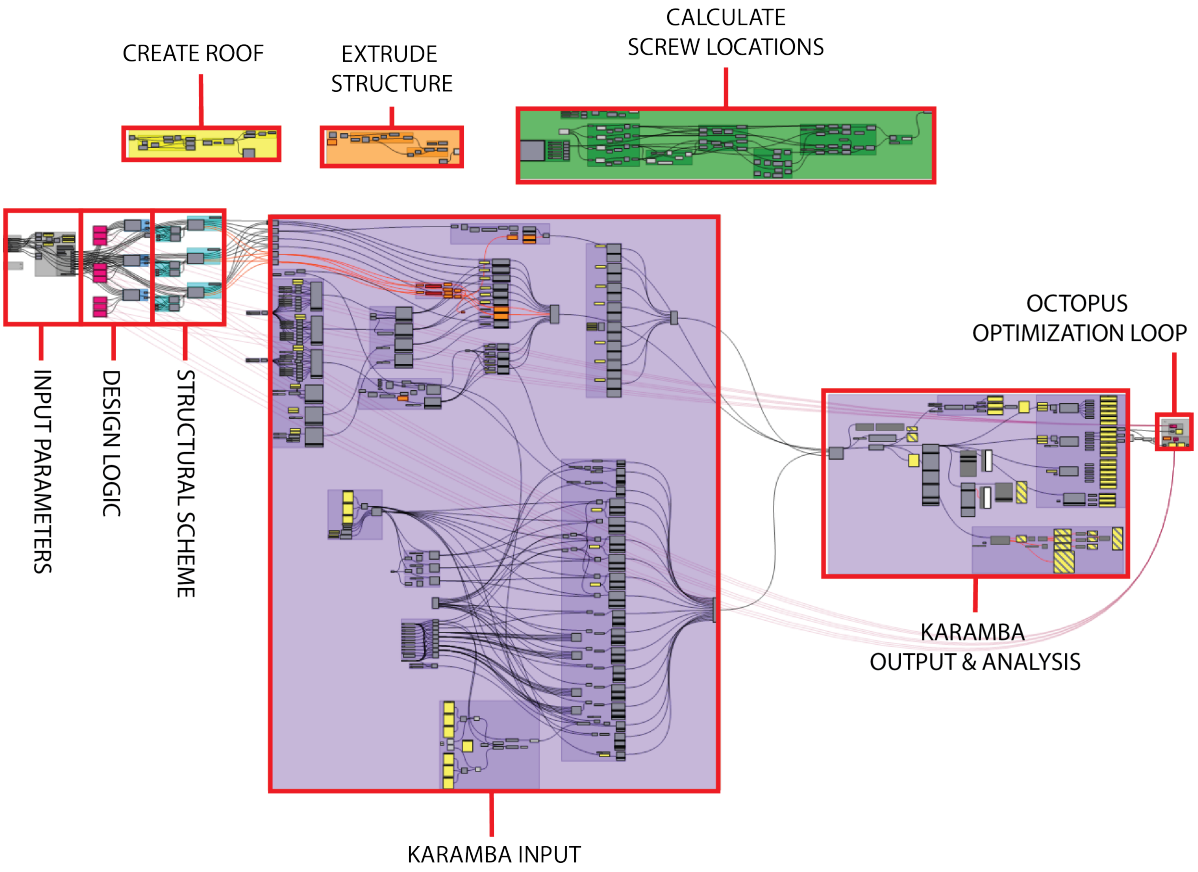

Figure 76: Overview design

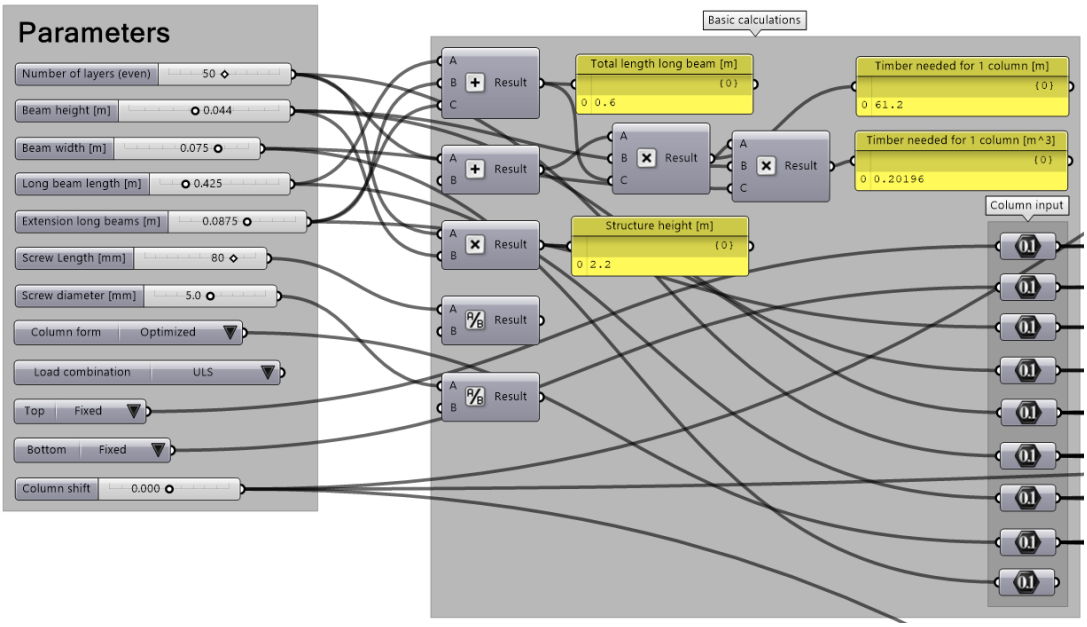

Figure 77: Input parameters

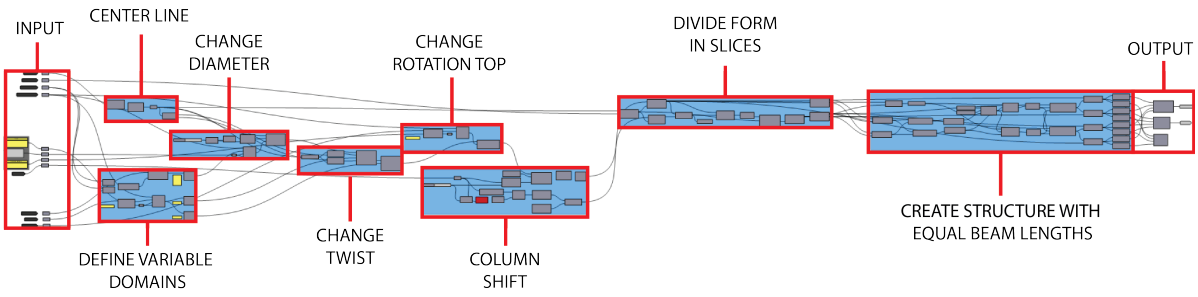

Figure 78: Design logic

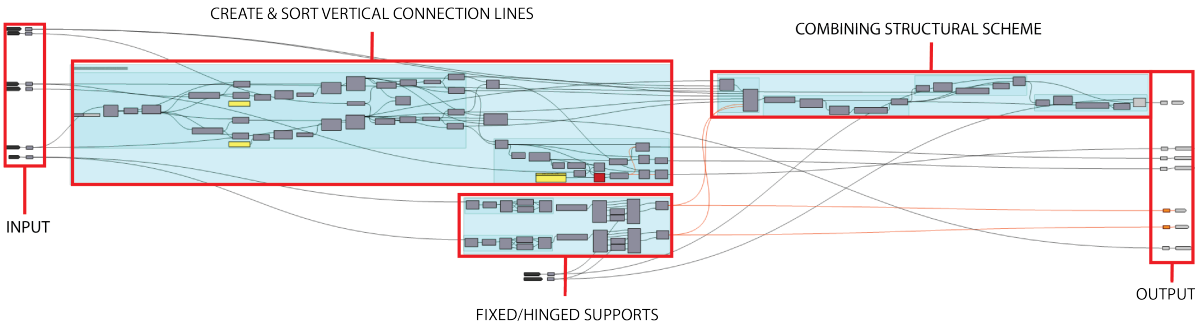

Figure 79: Structural scheme

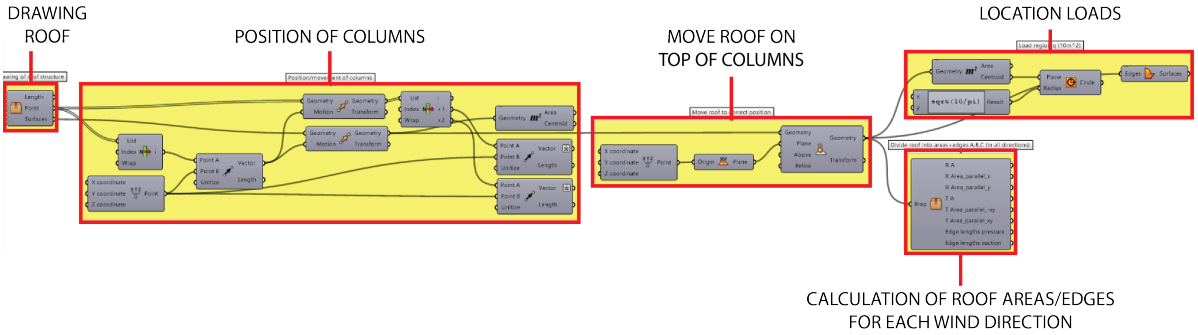

Figure 80: Create roof

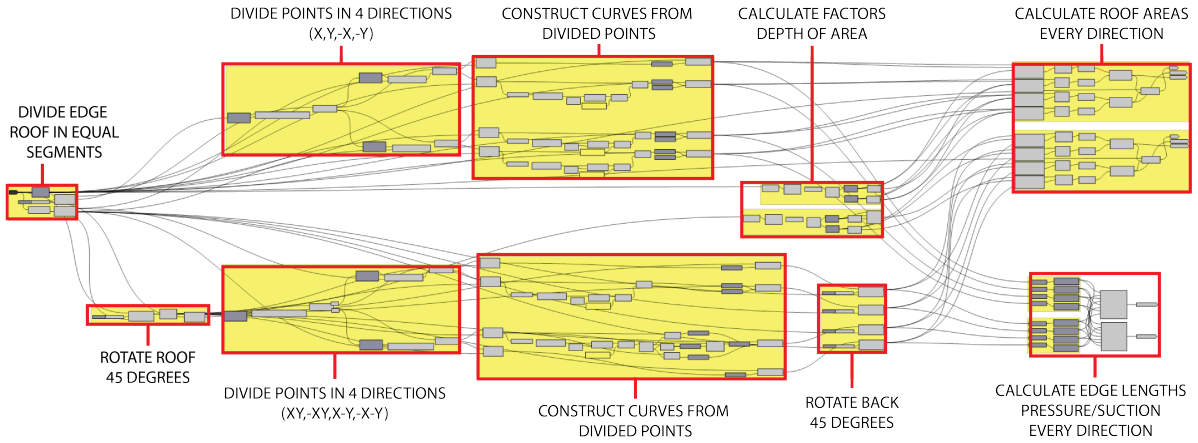

Figure 81: Calculation of roof areas/edges for each wind direction

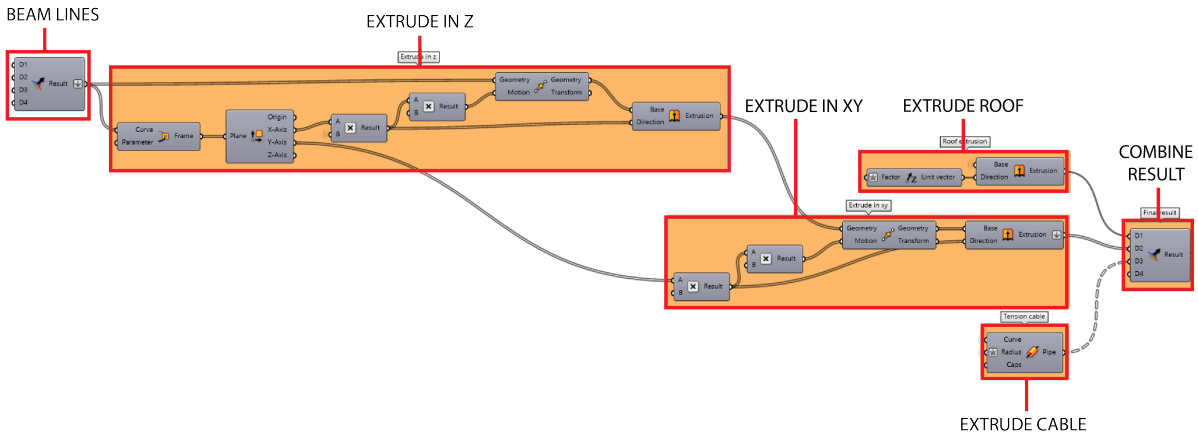

Figure 82: Extrude structure

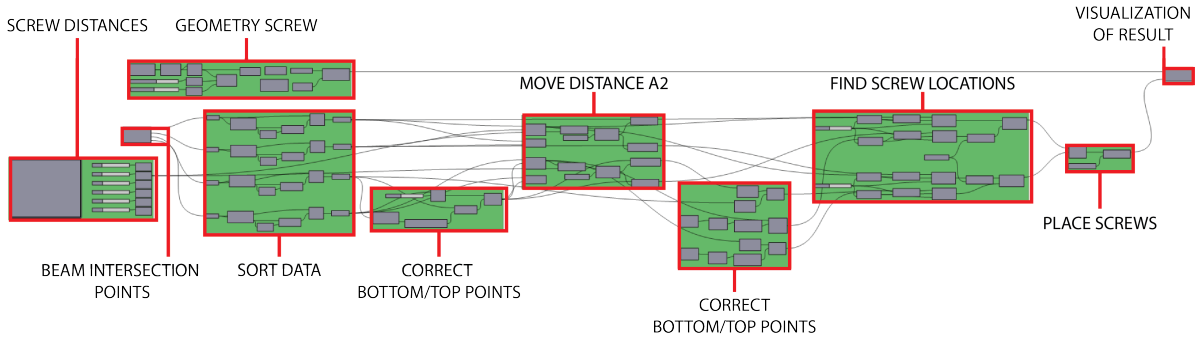

Figure 83: Calculate screw locations

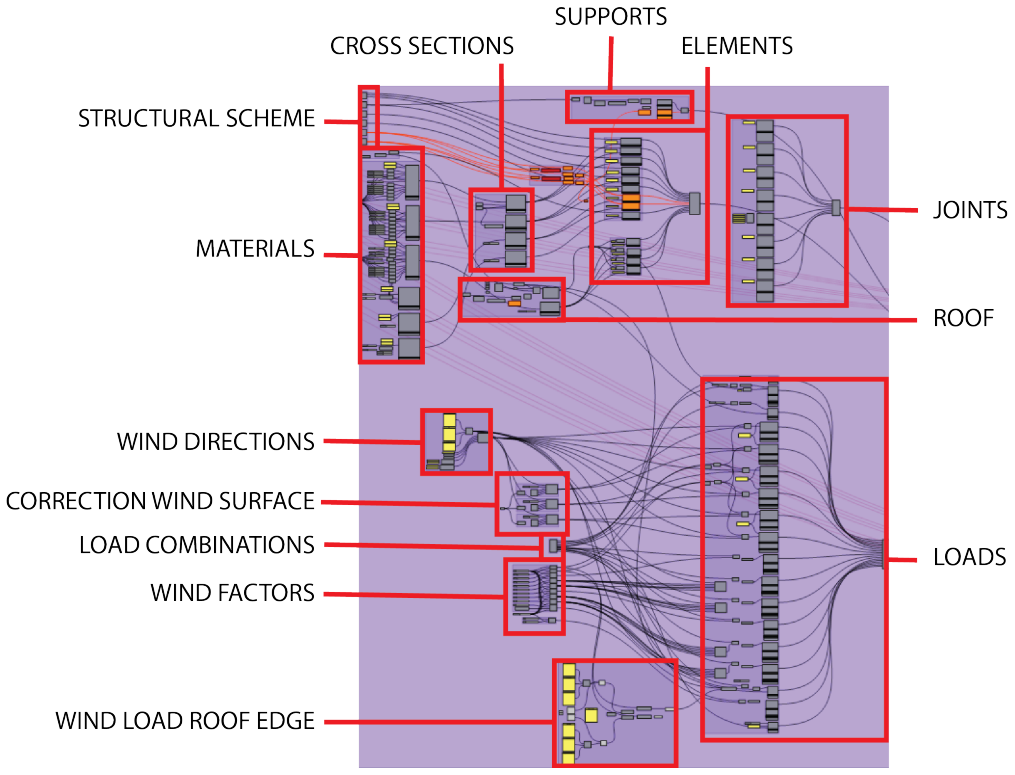

Figure 84: Karamba input

J.2 Assembly

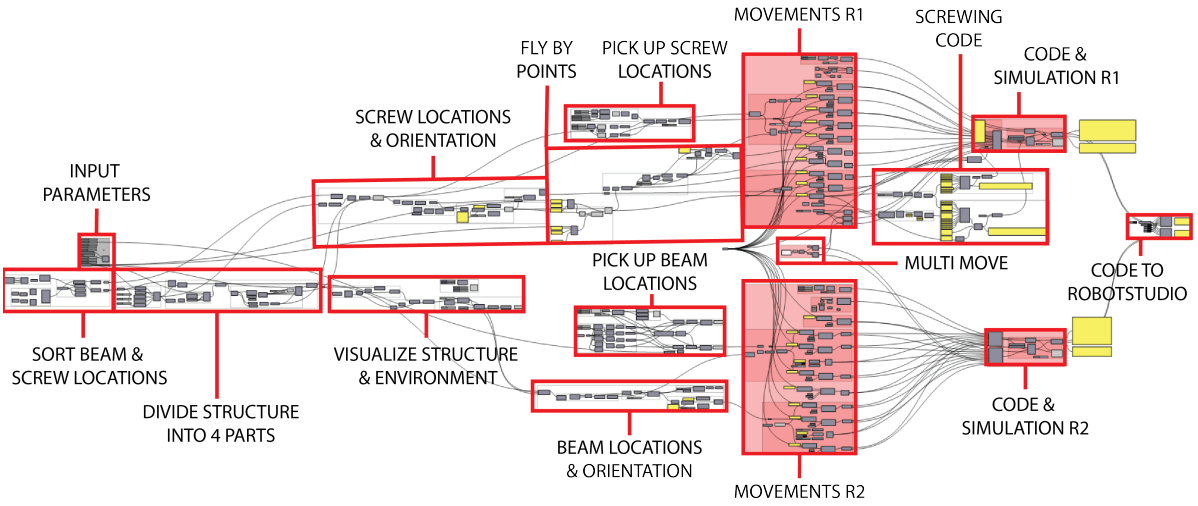

Figure 85: Assembly overview

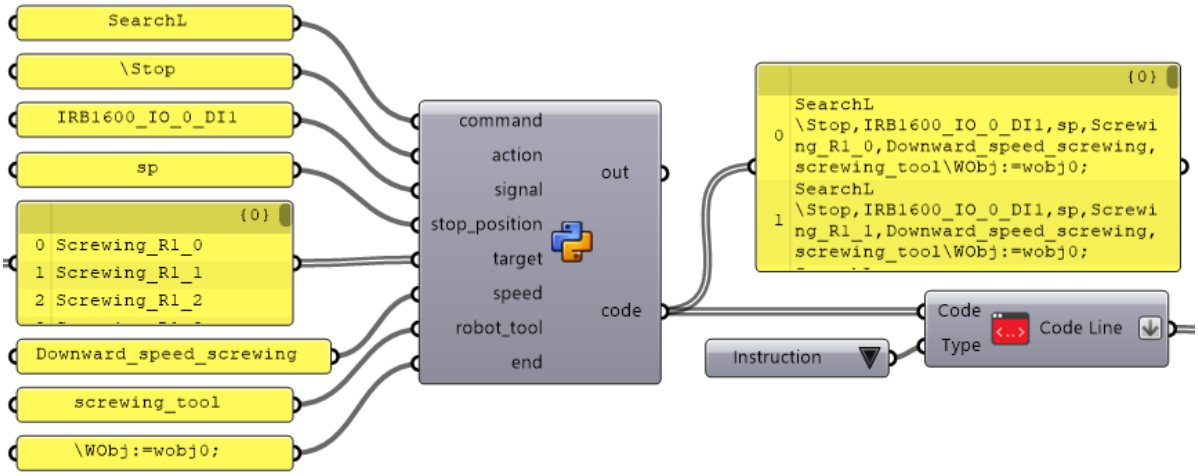

Figure 86: Screwing code 1 (move the "screwing_tool" linearly with velocity "downward_speed_screwing" to point "Screwing_R1", until signal "IRB1600_IO_0_DI1" changes)

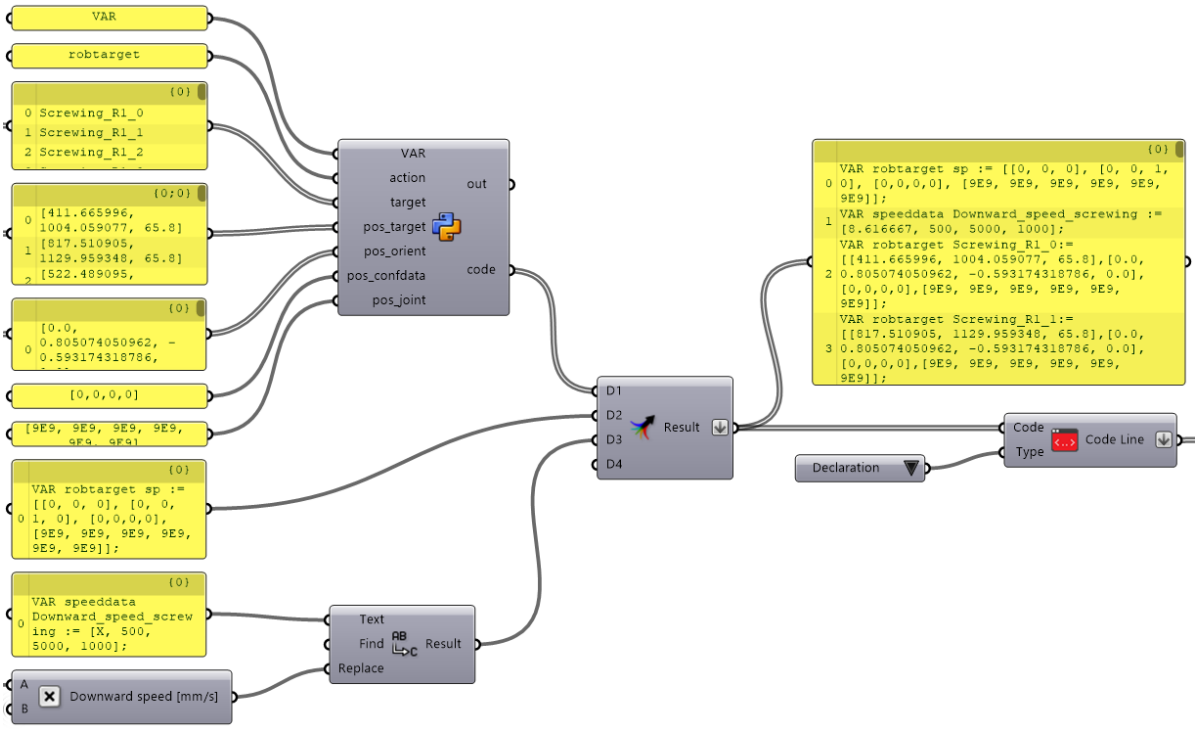

Figure 87: Screwing code 2 (defining screwing robot targets and downward speed)

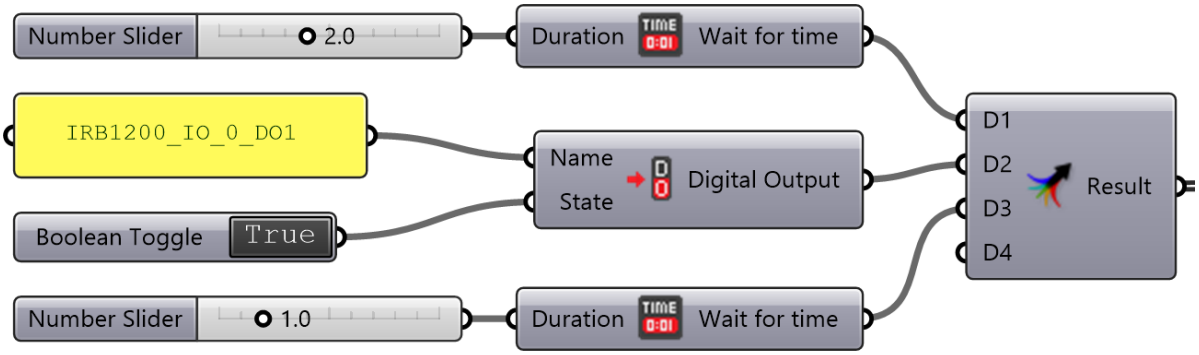

Figure 88: Closing gripper

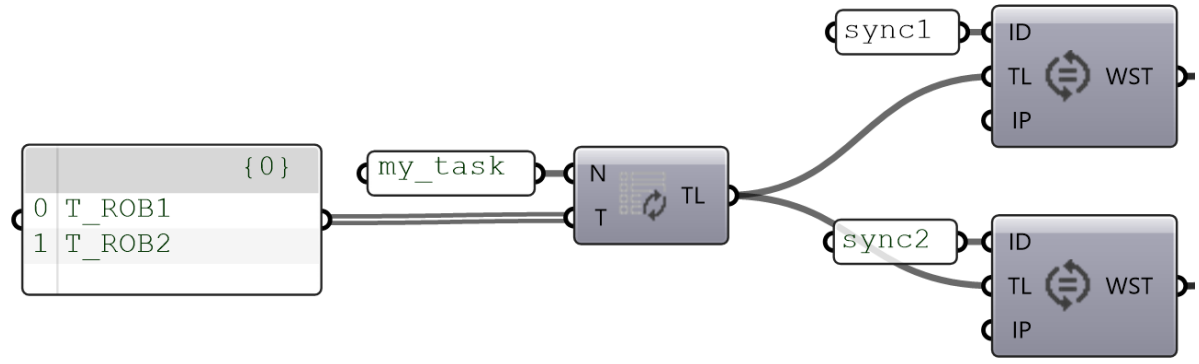

Figure 89: Multi move synchronization points

K Matlab script

```
clear all; clc;
%% Input variables (C24)
f_mk = 24; % [N/mm^2] Characteristic bending strength
f_t0k = 14.5; % [N/mm^2] Characteristic tension strength 0 degrees
f_t90k = 0.4; % [N/mm^2] Characteristic tension strength 90 degrees
f_c0k = 21; % [N/mm^2] Characteristic compression strength 0 degrees
f_c90k = 2.5; % [N/mm^2] Characteristic compression strength 90 degrees
f_vk = 4; % [N/mm^2] Characteristic shear strength

E_m0mean = 11000; % [N/mm^2] Mean modulus of elasticity
E_m0k = 7400; % [N/mm^2] 5 percentile modulus of elasticity
E_m90mean = 370; % [N/mm^2] Mean modulus of elasticity 90 degrees
G_mean = 690; % [N/mm^2] Mean shear modulus

rho_k = 350; % [kg/m^3] 5 percentile density
rho_mean = 420; % [kg/m^3] Mean density

d = 5; % [mm] Diameter fastener
d_h = 9.7; % [mm] Diameter fastener washer head (9.7 for 5mm, 11.3 for 5mm washer head, 11.6 for 6mm)
l_s = 80; % [mm] Screw length
screw_grade = [8,8]; % Screw grade
f_uk = screw_grade(1)*100; % [N/mm^2] Ultimate characteristic strength screw
f_yk = f_uk*screw_grade(2)/10; % [N/mm^2] Yield strength screw

h = 44; % [mm] Height beam
b = 69; % [mm] Width beam
t1 = h; % [mm] Timber thickness or penetration depth
t2 = l_s-h; % [mm] Timber thickness or penetration depth
t_min = 6*d; % [mm] Minimum penetration depth

I = (1/12)*b*h^3; % [mm^4] Moment of inertia
J = (b*h/12)*(b*h^2 + h*b^2); % [mm^4] Polar moment of inertia

%% Factors
gamma_M = 1.3; % Partial factor solid timber
%k_mod = 0.8; % Solid timber, short term action, service class 2
k_mod = 1.1; % Solid timber, instantanious action, service class 2
k_def = 0.8; % Solid timber, service class 2
k_def1 = 0.8; % Solid timber, service class 2
k_def2 = 2; % CLT, service class 3
k_def_combi = 2*sqrt(k_def1*k_def2); % Deformation factor combination timber + CLT
k_h = min((600/h)^0.1 , 1.1); % Height factor
k_m = 0.7; % Factor rectangular cross section
k_c90 = 1; % Factor for load combination and splitting
k_shape = min(1+0.05*(b/h),1.3); % Factor for shape in torsion

psi_0 = 0; % Factor load combination variable loads
psi_21 = 0; % Factor load combination quasi-permanent loads

%% Calculation of design values
f_md = k_mod*(f_mk/gamma_M); % [N/mm^2] Characteristic bending strength
f_t0d = k_mod*(f_t0k/gamma_M); % [N/mm^2] Characteristic tension strength 0 degrees
f_t90d = k_mod*(f_t90k/gamma_M); % [N/mm^2] Characteristic tension strength 90 degrees
f_c0d = k_mod*(f_c0k/gamma_M); % [N/mm^2] Characteristic compression strength 0 degrees
f_c90d = k_mod*(f_c90k/gamma_M); % [N/mm^2] Characteristic compression strength 90 degrees
f_vd = k_mod*(f_vk/gamma_M); % [N/mm^2] Characteristic shear strength

E_d = E_m0mean/gamma_M; % [N/mm^2] Design modulus of elasticity
G_d = G_mean/gamma_M; % [N/mm^2] Design shear modulus
E_m0mean_fin = E_m0mean/(1+k_def); % [N/mm^2] Mean modulus of elasticity with load duration correction
G_mean_fin = G_mean/(1+k_def); % [N/mm^2] Mean shear modulus with load duration correction

%% Input Karamba values
Karamba_N_t0 = 648; % [N] Karamba max tension 0 degrees
Karamba_N_t90 = 744; % [N] Karamba max compression 0 degrees
Karamba_N_c0 = 839; % [N] Karamba max tension 0 degrees
Karamba_N_c90 = 5449; % [N] Karamba max compression 0 degrees
Karamba_V = 5243; % [N] Karamba max shear z
Karamba_Mt = 39000; % [Nmm] Karamba max bending t
Karamba_My = 89000; % [Nmm] Karamba max bending y
Karamba_Mz = 15000; % [Nmm] Karamba max bending z

sigma_t0d = Karamba_N_t0/(b*h); % [N/mm^2] Karamba tension stress 0 degrees
sigma_t90d = Karamba_N_t90/(b*b); % [N/mm^2] Karamba tension stress 90 degrees
sigma_c0d = Karamba_N_c0/(b*h); % [N/mm^2] Karamba compression stress 0 degrees
sigma_c90d = Karamba_N_c90/(b*b); % [N/mm^2] Karamba compression stress 90 degrees
sigma_myd = (Karamba_My*0.5*h)/I; % [N/mm^2] Karamba bending stress y
sigma_mzd = (Karamba_Mz*0.5*h)/I; % [N/mm^2] Karamba bending stress z
tau_d = Karamba_V/(b*h); % [N/mm^2] Karamba shear stress
tau_tor_d = (Karamba_Mt*0.5*b)/J; % [N/mm^2] Karamba torsion stress

%% Unity checks timber
UC_t0 = sigma_t0d/f_t0d % UC tension 0 degrees
UC_t90 = sigma_t90d/f_t90d % UC tension 0 degrees
UC_c0 = sigma_c0d/f_c0d % UC compression 0 degrees
UC_c90 = sigma_c90d/(k_c90*f_c90d) % UC compression 90 degrees
UC_m1 = (sigma_myd/f_md) + k_m*(sigma_mzd/f_md) % UC bending 1
UC_m2 = k_m*(sigma_myd/f_md) + (sigma_mzd/f_md) % UC bending 2
UC_v = tau_d/f_vd % UC shear
UC_tor = tau_tor_d/(k_shape*f_vd) % UC torsion
UC_t0_m1 = (sigma_t0d/f_t0d) + (sigma_myd/f_md) + k_m*(sigma_mzd/f_md); % UC bending + tension 1
UC_t0_m2 = (sigma_t0d/f_t0d) + k_m*(sigma_myd/f_md) + (sigma_mzd/f_md); % UC bending + tension 2
UC_c0_m1 = (sigma_c0d/f_c0d)^2 + (sigma_myd/f_md) + k_m*(sigma_mzd/f_md); % UC bending + compression 1
UC_c0_m2 = (sigma_c0d/f_c0d)^2 + k_m*(sigma_myd/f_md) + (sigma_mzd/f_md); % UC bending + compression 2

```

```
%% Calculation of max forces
F_mk = (f_mk*I)/(0.5*h); % [Nmm] Max characteristic bending force
F_md = (f_md*I)/(0.5*h); % [Nmm] Max design bending force
F_t0k = f_t0k*h*b; % [N] Max characteristic tension force 0 degrees
F_t0d = f_t0d*h*b; % [N] Max design tension force 0 degrees
F_t90k = f_t90k*b*b; % [N] Max characteristic tension force 90 degrees
F_t90d = f_t90d*b*b; % [N] Max design tension force 90 degrees
F_c0k = f_c0k*h*b; % [N] Max characteristic compression force 0 degrees
F_c0d = f_c0d*h*b; % [N] Max design compression force 0 degrees
F_c90k = f_c90k*b*b; % [N] Max characteristic compression force 90 degrees
F_c90d = f_c90d*b*b; % [N] Max design compression force 90 degrees
F_vk = f_vk*h*b; % [N] Max characteristic shear force
F_vd = f_vd*h*b; % [N] Max design shear force

%% Calculation pull out strength screw
n_ef = 1; % Number of screws
l_ef = t2; % [mm] Penetration depth of screw thread
k_d = min(d/8,1); % Factor
A_s = (1/4)*pi*d^2; % [mm^2] Area of screw
alpha2 = 90; % [degrees] Angle screw with timber
%f_axk = 14; % [N/mm^2] Characteristic pull out strength screw --> SPAX value
f_axk = 0.52*d^(-0.5)*l_ef^(-0.1)*rho_k^(0.8); % [N/mm^2] Characteristic pull out strength screw
%f_axk = 20*10^(-6)*rho_k^2; % [N] Characteristic pointside withdrawal strength nail
f_headk = 27-d_h; % [N/mm^2] Characteristic pull through strength screw (d_h<16mm) --> SPAX value
%f_headk = 70*10^(-6)*rho_k^2; % [N] Characteristic headside pull through strength nail
f_tensk = 4900; %4900 for d=5, 7100 for d=6 [N/mm^2] Characteristic tensile resistance screw (d=5mm)
    --> SPAX value

F_axrk1 = (n_ef*f_axk*d*l_ef*k_d)/(1.2*(cos(alpha2)^2)+(sin(alpha2)^2)); % [N] Characteristic axial
    withdrawal capacity of the screw
F_axrk2 = n_ef*f_headk*(d_h^2)*((rho_k/350)^0.8); % [N] Characteristic axial pull through capacity of
    the screw
F_axrk3 = n_ef*f_tensk; % [N] Characteristic axial strength of the screw
F_axrk = min([F_axrk1,F_axrk2,F_axrk3]);
F_axrd = k_mod*(F_axrk/gamma_M); % [N] Design axial withdrawal capacity screw

%% Calculation load-carrying capacity connection
M_yrk = 0.45*f_uk*d^2.6; % [Nmm] Characteristic fastener yield moment
k_90 = 1.35+0.015*d; % For softwoods
%k_90 = 0.90+0.015*d; % For hardwoods
f_h0k = 0.082*rho_k*d^(-0.3); % [N/mm^2] Characteristic embedment strength in timber 0 degrees (
    without predrilled holes)
%f_h0k = 0.082*rho_k*(1-0.01*d); % [N/mm^2] Characteristic embedment strength in timber 0 degrees (
    with predrilled holes)
f_h90k = f_h0k/(k_90*sin(90)^2+cos(90)^2); % [N/mm^2] Characteristic embedment strength in timber 90
    degrees
f_h1k = f_h0k; % Determine orientation timber in connection
f_h2k = f_h0k; % Determine orientation timber in connection
beta = f_h2k/f_h1k; % Ratio between embedment strength of the members

% Eurocode formulas
F_vrk_a = f_h1k*t1*d;
F_vrk_b = f_h2k*t2*d;
F_vrk_c = (f_h1k*t1*d)/(1+beta) * sqrt(beta + 2*beta^2*(1+(t2/t1)+(t2/t1)^2) + (beta^3)*((t2/t1)^2) -
    (beta*(1+(t2/t1)))) + (F_axrk/4);
F_vrk_d = 1.05*(f_h1k*t2*d/(2+beta)) * (sqrt(2*beta*(1+beta) + (4*beta*(2+beta)*M_yrk)/(f_h1k*d*t1^2))
    - beta) + (F_axrk/4);
F_vrk_e = 1.05*(f_h1k*t2*d/(1+2*beta)) * (sqrt(2*(beta^2)*(1+beta) + (4*beta*(1+2*beta)*M_yrk)/(f_h1k*
    d*t2^2)) - beta) + (F_axrk/4);
F_vrk_f = 1.15*sqrt((2*beta)/(1+beta)) * sqrt(M_yrk*f_h1k*d) + (F_axrk/4);

F_vrk = min([F_vrk_a,F_vrk_b,F_vrk_c,F_vrk_d,F_vrk_e,F_vrk_f]); % [N] Characteristic strength per
    shear plane per fastener
F_vrd = k_mod*(F_vrk/gamma_M); % [N] Design strength per shear plane per fastener

%% Unity checks screws
F_axed = 744; % [N] Axial load on screws
F_vedz = 1208; % [N] Shear load on screw in z
F_vedy = 672; % [N] Shear load on screw in y
F_ved = sqrt(F_vedz^2 + F_vedy^2); % [N] Shear load on screws
UC_s_ax = F_axed/F_axrd % Unity check screw loaded axial
UC_s_v = F_ved/F_vrd % Unity check screw loaded shear
UC_s_ax_v = (F_axed/(F_axrd))^2+(F_ved/(F_vrd))^2 % Unity check screw loaded axial and shear

%% Calculation edge & screw distances --> not predrilled, rho_k<420, d>=5mm!
alpha = 0; % [degrees] Angle of loading
a1 = (5+7*(cos(alpha)))*d; % [mm] Spacing parallel to grain
a2 = 5*d; % [mm] Spacing perpendicular to grain
a3t = (10+5*(cos(alpha)))*d; % [mm] Distance loaded end
a3c = 10*d; % [mm] Distance unloaded end
a4t = (5+5*(sin(alpha)))*d; % [mm] Distance loaded edge
a4c = 5*d; % [mm] Distance unloaded edge

%% Deformation
u_instG =    [-0.12-0.06;-0.65+0.23;-0.61-2.92];%[-0.06-0.05;-0.31+0.17;-0.44-2.16]; % [mm] x,y,z
    Deformation permanent load G
u_instLC1 = [-0.14;-1.03;-0.75];%[-0.13;-0.81;-1.00]; % [mm] x,y,z Deformation variable load LC1
u_instLC2 = [-8.31;-1.03;-0.15];%[-4.56;-0.82;-0.59]; % [mm] x,y,z Deformation variable load LC2
u_instLC3 = [-0.04;-0.57;-0.43];%[-0.08;-0.59;-0.76]; % [mm] x,y,z Deformation variable load LC3
u_fin = u_instG.*(1+k_def_combi) + u_instLC1.*(1+psi_21*k_def_combi) + u_instLC2.*(psi_0 + psi_21*
    k_def_combi)+ u_instLC3.*(psi_0 + psi_21*k_def_combi); % [mm] Final deformation

%% Other calculations
K_ser = (rho_mean^(1.5))*d*(1/23); % [N/mm] Connection stiffness screws

%% Steel cable
F_t_cable_ED = 7560; % [N] Tension in cable
F_bl_cable = 37000; % [N] Breaking load cable
```

```
gamma_M2s = 1.25; % Partial factor steel
UC_cable = gamma_M2s*(F_t_cable_ED/F_bl_cable); % Unity check tension cable

%% CLT Roof
M_roof_ED = 1860056; % [Nmm] Maximum moment in roof
V_roof_ED = 56300; % [N] Maximum shear in roof

gamma_MGL = 1.25; % Partial factor Glulam
k_modGL = 0.4; % Factor Glulam (CC3, permanent)
h_roof = 130; % [mm] Height roof
b_roof = 2000; % [mm] Height roof
z = h_roof/2; % [mm] Distance roof mid to edge
E_meanGL = 110000; % [N/mm^2] E mean Glulam
E_face = E_meanGL/gamma_MGL; % [mm] E face Glulam
EI_eff = 5.202*10^12; % [Nmm^2] EI effective Glulam (see excel)
A_GL = h_roof*b_roof; % [mm^2] Area Glulam

sigma_face_roof = (M_roof_ED*z*E_face)/EI_eff; % [N/mm^2] Maximum stress in face roof
t_max_roof = (3*V_roof_ED)/(2*A_GL); % [N/mm^2] Maximum shear stress in roof

f_roof_face_RD = 14.5; % [N/mm^2] Strength face roof
f_roof_shear_RD = 2.7; % [N/mm^2] Strength shear roof

UC_roof_face = gamma_MGL*sigma_face_roof/(k_modGL*f_roof_face_RD); % Unity check roof face
UC_roof_shear = gamma_MGL*t_max_roof/(k_modGL*f_roof_shear_RD); % Unity check roof shear

%% Corner anchors
t1_ca = 30; % [mm] Screw depth in corner anchor
F_ca_vrk_a = 0.4*f_h1k*t1_ca*d;
F_ca_vrk_b = 1.15*sqrt(2*M_yrk*f_h1k*d) + (F_axrk/4);
F_ca_vrk = 2*min(F_ca_vrk_a,F_ca_vrk_b); % [N] Shear capacity thin steel plate (d_plate=<0.5d)
```